CR-137477

COLLEGE
OF
ENGINEERING

VIRGINIA
POLYTECHNIC
INSTITUTE AND
STATE
UNIVERSITY

**BLACKSBURG,
VIRGINIA**

College of Engineering
Virginia Polytechnic Institute and State University
Blacksburg, Virginia 24061

VPI-E-74-26

A METHOD FOR THE MEASUREMENT AND

THE STATISTICAL ANALYSIS OF

ATMOSPHERIC TURBULENCE

H. W. Tieleman* and S. C. Tavoularis**

DEPARTMENT OF ENGINEERING SCIENCE & MECHANICS

October 1974

*Associate Professor
**Graduate Research Assistant
  Engineering Science & Mechanics Department
  Virginia Polytechnic Institute & State University
  Blacksburg, Virginia 24061

ABSTRACT

The instantaneous values of output voltages representing the wind velocity vector and the temperature at different elevations of the 250-foot meterological tower located at NASA Wallops Flight Center are provided with the three dimensional split-film TSI Model 1080 anemometer system. The output voltages are sampled at a rate of one every 5 milliseconds, digitized and stored on digital magnetic tapes for a time period of approximately 40 minutes, with the use of a specially designed data acquisition system. A new calibration procedure permits the conversion of the digital voltages to the respective values of the temperature and the velocity components in a Cartesian coordinate system connected with the TSI probe with considerable accuracy.

Each data-sample is divided into 58 blocks consisting of 8192 data points each. Stationarity of the time histories is checked by inspecting the variation of the block-means and with the use of a statistical test. The velocity components are transformed into the mean wind oriented coordinate system so that the longitudinal, lateral and vertical wind components are obtained. Mean values, variances and covariances in each data-block are first calculated and then averaged to produce the respective sample-means, variances and covariances.

Power, cross, coincidence and quadrature spectra of the wind components and the temperature are obtained with the use of the fast Fourier transform. The cosine taper data window and ensemble and frequency smoothing techniques are used to provide smooth estimates of the spectral functions.

TABLE OF CONTENTS

LIST OF FIGURES

LIST OF TABLES

LIST OF SYMBOLS

A	Sensor rod A
A_q	Quantity used at the qth step of the FFT
A^i	Any statistical quantity referred to the ith block of data
B	Sensor rod B
C	Sensor rod C
C	Constant in the expression for the sensor-yaw angle (2.4.15)
$CF_{\alpha i}$	Temperature correction factor for the heat transfer expression (2.4.2); $\alpha = A,B,C$, $i = 1,2$
C_{T1}, C_{T2}	Coefficients in the temperature expression (2.4.18)
C_{xy}	Coincidence spectral density function
c_p	Coefficient of specific heat under constant pressure
D	Constant in the heat transfer-effective cooling velocity relation (2.4.11)
$E_{\alpha i}$	Bridge voltage of the film; $\alpha = A,B,C$, $i = 1,2$
f	Frequency
G_x	Power spectral density function
G_{xy}	Cross-spectral density function
H_j	Total heat flux vector
$h_1, h_2, \ldots$	Binary coefficients in expression 4.3.3
Im	Imaginary part of a complex quantity
$j_1, j_2, \ldots$	Binary coefficients in expression 4.3.4
$K_{\alpha i}$	Film constant at the heat transfer expression (2.4.2);

$\alpha = A,B,C$, $i = 1,2$

k	Thermal conductivity coefficient of the air
k_{α}	Constant in the effective-cooling velocity expression (2.4.12); $\alpha = A,B,C$
k_{av}	Constant in the expression for the standard velocity (2.4.14)
k_q	Quantity used in the FFT, defined in equation 4.3.16
ℓ	Length of frequency intervals in frequency smoothing
M	Total number of data blocks
N	Number of data in each block
N_q	Quantity used in the FFT, defined in equation 4.3.15
n	Exponent in the heat transfer-effective cooling velocity relation (2.4.11)
p	Exponent of 2, so that $N = 2^p$
p	Atmospheric pressure
p_o	Undisturbed atmospheric pressure
p'	Deviation from the undisturbed pressure
p''	Pressure fluctuation
P_s	Standard atmospheric pressure (29.92 in Hg)
Q_{α}	Heat convected from the sensors; $\alpha = A,B,C$
Q_{xy}	Quadrature spectral density function
R_{α}	Ratio of the two film voltages of each sensor rod at zero sensor-pitch angle; $\alpha = A,B,C$
R	Total number of reverse arrangements
R_c	Cable resistance
Re	Real part of a complex quantity

R_f	Film resistance
R_x	Autocorrelation function
R_{xy}	Cross-correlation function
r_q	Quantity used in the FFT, defined in equation 4.3.7
T	Temperature
T	Time interval
T_o	Undisturbed temperature
T'	Deviation from the undisturbed temperature
T_a	Ambient temperature
T_c	Cable temperature
T_f	Film temperature
T_s	Standard atmospheric temperature (530° R)
t	Time
U	Actual velocity magnitude
U_1, U_2, U_3	Velocity components in any Cartesian system
U_A, U_B, U_C	Velocity components in the sensor oriented coordinate system
U_{es}	Standard effective-cooling velocity
U_s	Standard velocity magnitude
u	Longitudinal velocity component
u_1, u_2, u_3	Fluctuations of the velocity components in any Cartesian system
$V_{\alpha i}$	0 to 5 output voltage of the anemometer; $\alpha = A,B,C$, $i = 1,2$
V_s	Standard velocity magnitude measured with Pitot-tube
V_T	0 to 5 output voltage of the thermocouple
v	Lateral velocity component

W	Exponential term in equation 4.3.2
W	Fourier transform of the data-window function
w	Data window function
w	Vertical velocity component
$X(f)$	Fourier transform of a time function
$X(f,T)$	Finite Fourier transform of a time history
X_r	Discrete Fourier transform of a discrete time history
X_r^*	Complex conjugate of the Fourier transform
$x(t)$	Any function of time
x_i	Discrete time history
$\bar{x}$	Mean value of a discrete time history
$\overline{x^2}$	Variance of a discrete time history
$\{x^k(t)\}$	Notation for a time series
$\overline{xy}$	Covariance of two discrete time histories
α	Probe-pitch angle
α_{cu}	Temperature coefficient of resistivity of copper
α_f	Temperature coefficient of resistivity of the film
β	Probe-yaw angle
γ_{xy}^2	Coherence function
Δf	Frequency increment
ΔR_c	Change in cable resistance from the TSI calibration temperature to the operation temperature
Δt	Time increment
δ	Delta function
δ_{ij}	Kronecker's delta

θ	Fluctuation of temperature
θ_{xy}	Phase angle of the cross-spectral density function
μ	Dynamic viscosity coefficient of the air
μ_x	Mean value of a sample function
π	3.14159
ρ	Air density
ρ_o	Undisturbed density of the air
ρ'	Deviation from the undisturbed density of the air
ρ''	Fluctuation of the density of the air
σ_x	Standard deviation of a sample function
σ_x^2	Variance of a sample function
σ_{xy}^2	Covariance of two sample functions
τ_{ij}	Total stress tensor
ϕ_α	Sensor-yaw angle; α = A,B,C
X_i	Fluctuating component of a discrete time history
ψ_x^2	Mean square value of a sample function

Subscripts

A,B,C	Reference to the three sensor rods
1,2	Reference to the two films on the same sensor rod
s	Reference to standard conditions
q	Reference to the qth step of the FFT

Superscripts

cold	Reference to the TSI standard conditions

m   Reference to the cable resistance measurement conditions

n   Reference to the nth block of data

o   Reference to the TSI calibration conditions

−   Reference to an average value

^   Reference to a smooth spectral estimate

CHAPTER I

BASIC CHARACTERISTICS OF THE ATMOSPHERIC BOUNDARY LAYER

1.1 Description of the Lower Atmosphere

The lower part of the atmosphere of the earth forms a boundary layer with a thickness of several hundred meters. The flow in the atmospheric boundary layer is typically turbulent, as a result of the combined action of shear stresses, Coriolis forces and buoyancy forces. The knowledge of the internal structure of the atmospheric boundary layer is of great importance for a large number of modern human activities, such as weather prediction, building and bridge construction, launching of aircrafts and missiles, telecommunications and air pollution control.

The atmospheric boundary layer can conveniently be divided in smaller regions with their own particular properties.

1. The "molecular boundary layer" is located closest to the ground, with a thickness of the order of one millimeter. In this region, molecular properties have a strong influence on the flow.

2. The "surface boundary layer" extends up to a height between 20 and 60 meters, depending on the conditions. It is defined as the region where the shear stress does not vary significantly with height, so that it can be considered as constant. In the surface boundary layer, it is mainly the surface rough.ess and the density stratification that determine the flow, while the Coriolis forces are negligible.

1

3. The upper part of the atmospheric boundary layer, often called the "Ekman layer," extends usually up to approximately 500 meters. In this layer, the surface conditions are of minor importance while the Coriolis forces cannot anymore be neglected.

Above the atmospheric layer, the "free atmosphere" is located, where the air flow can be considered as inviscid and is a result of ine tial, Coriolis and pressure gradient forces.

1.2 The Governing Equations

The air in the surface boundary layer and the lower part of the Ekman layer can be considered as a compressible Newtonian fluid in a uniform gravitational nonrotating field. Let p_o, T_o and ρ_o be the undisturbed pressure, temperature and density of the air at a certain height and p', T' and ρ' the respective instantaneous deviations of pressure, temperature and density, which can be reasonably assumed small, compared to p_o, T_o and ρ_o. Let also U_i, where $i = 1,2,3$, be the air velocity components in a Cartesian system $x_1 x_2 x_3$, where the x_3 axis is vertical. Since the flow is turbulent, it is convenient to consider all quantities as consisting of a mean component and a fluctuating component, as follows

$$U_i = \overline{U}_i + u_i \quad ,$$
$$T' = \overline{T}' + \theta \quad ,$$
$$p' = \overline{p}' + p'' \quad , \tag{1.2.1}$$
$$\rho' = \overline{\rho}' + \rho'' \quad .$$

For short time periods, usually not exceeding one hour, the air flow can also be considered as steady and stationary. Steadiness of

the flow implies that all mean quantities are independent of time, while stationarity of the flow implies that all statistical quantities are independent of time.

Making use of all the previously discussed assumptions, one can write the general equations for the mean motion of the air in the surface boundary layer and the lower part of the Ekman layer in the following form.

Equation of continuity

$$\overline{U}_{i,i} = 0 \qquad \text{(1.2.2)}$$

Momentum equation

$$\rho_o \overline{U}_j \; \overline{U}_{i,j} = -\overline{p}'_{,i} + \mu \; \overline{U}_{i,jj} - \rho_o \; \overline{u_i u_j}_{,j} \qquad \text{(1.2.3)}$$

Energy equation

$$c_p \rho_o \; \overline{T}'_{,i} \; \overline{U}_i = k \; \overline{T}'_{,ii} - c_p \rho_o \; \overline{\theta_{,i} u_i} \qquad \text{(1.2.4)}$$

The dynamic viscosity, μ, the thermal conductivity, k, and the specific heat coefficient under constant pressure, c_p, of the air are assumed to be constant throughout the entire region considered.

The above equations of mean motion for turbulent flow may acquire a form similar to the equations of motion for laminar flow with the introduction of a total stress tensor, τ_{ij}, and a total heat flux vector, H_j, defined respectively as

$$\tau_{ij} = -\overline{p}' \; \delta_{ij} + \mu(\overline{U}_{i,j} + \overline{U}_{j,i}) - \rho_o \; \overline{u_i u_j} \qquad \text{(1.2.5)}$$

and

$$H_j = -k \; \overline{T}'_{,j} + c_p \rho_o \; \overline{\theta u_j} \qquad \text{(1.2.6)}$$

Compared to the respective quantities for laminar flow, the above

introduced stress tensor and heat flux vector contain the additional stresses $-\rho_o \overline{u_i u_j}$ (called Reynolds stresses) and the additional heat flux components $c_p \rho_o \overline{\theta u_j}$ respectively.

The exact solution of the equations of motion in the atmospheric boundary layer, due to their complicated form, presents enormous difficulties. It has also been recognized that the usual mathematical analysis does not possess the capability for a clear description of the turbulent flow and, therefore, statistical and spectral analysis have to be used. Statistical and spectral properties have the additional advantage of being experimentally reproducible, so that an experimental verification of related theoretical achievements is possible.

1.3 The Measurement of Atmospheric Turbulence

The properties of the lower part of the atmospheric boundary layer, up to a height of approximately 150 meters, are usually measured with instruments placed on meteorological towers or other tall structures, while for higher altitudes meteorological baloons and low-flying airplanes can be used. During the last five years, a considerable amount of atmospheric measurements, mostly from meteorological towers, has been gathered and several important conclusions have been derived from these experiments. A discussion of some of these tower measurements can be found in the references 6, 7, 17 and 26. However, these research programs have been limited in scope in the sense that none of them provided a complete and multi-point set of measurements at reasonably high frequencies. Either the vertical velocity component or the fluctuating

temperature are missing or measurements are made with instruments whose frequency response is limited.

Therefore, it is the objective of this research program to make a complete and extensive set of measurements of the three velocity components and the temperature in the lower atmosphere. This will allow the determination of the various statistical quantities of the velocity and temperature fluctuations, including the vertical momentum flux and vertical heat transfer, which are of main importance.

In order to achieve the above requirements, measurements of the wind velocity components and the temperature were made at different elevations of the 250-foot meteorological tower located at NASA Wallops Flight Center. As measuring instrument, the TSI three-dimensional split-film anemometer was selected, which provides a satisfactory accuracy and a high frequency response for the velocity and temperature measurements.

The data obtained from the measuring instruments could be processed either in analog or in digital form. The recent development of high-speed digital computers and the invention of effective digital data-processing techniques permitted the fast and efficient calculation of the desired statistical quantities from digital records of data. Therefore, a data-acquisition system was designed, by the use of which the analog signals produced by the anemometers were sampled, digitized and stored on digital magnetic tapes. These magnetic tapes were further processed in digital computers. Computer programs, based on the latest developments of the digital data-analysis, were used to provide all desired statistical quantities, such as mean values, variances and covariances, turbulence intensities and power and cross-spectral density functions.

CHAPTER II

INSTRUMENTATION AND CALIBRATION PROCEDURES

2.1 The TSI 1080 Three-Dimensional Split-Film Anemometer System

The TSI (Thermo-Systems Inc.) Model 1080 Anemometer provides volt-
age measurements, from which the instantaneous velocity vector and the
temperature at a certain point in moving air can be calculated. The
TSI 1080 system consists of the following components:

1. The Probe (Model 1296E), consisting of three sensor rods for
a total of six hot film anemometers and one thermocouple. The probe
will be described in detail in section 2.2.

2. One Control Circuit (Model 1053BP6T) for each probe, controlling
the six films and the amplifier of the thermocouple. The front panel
of the control circuit contains the pin jacks for the bridge-voltage
outputs, the 0-5 volt outputs and the thermocouple output. In addition,
it contains the balance potentiometers to ensure same temperature of
adjacent films and the zero and gain adjustments for the thermocouple
amplifier and the 0-5 volt outputs.

3. One Voltage Regulator (Model 1051F), supplying regulated +19
volts and -19 volts to six control circuits.

4. One Chassis (Model 1045G6) for six control circuits.

5. One "Rough" Power Supply (Model 1051FTR), with a capability
to supply 8 regulators with ±24 volts DC and 110 volts AC.

For further information on the anemometer and its operation,

6

one is referred to the Operating and Service Manual for Model 1080

Total Vector Anemometer by Thermo Systems Inc.

2.2 The Probe

A schematic drawing of the TSI Model 1296E Probe is provided in figure 1. Its main parts are the three sensors, the thermocouple, the supporting structure, the protective shield, the pneumatic cylinder and valve, the mounting flange, the electrical leads and the cable connector.

The three sensor rods are mounted mutually perpendicular to form a Cartesian coordinate system as shown in figure 2. A thin platinum film of approximately 1000 angstrom thickness and 0.080 inch long is placed on a 0.2 inch long, 0.006 inch diameter cylindrical quartz rod. A thin coat of quartz over the film is used to provide environmental protection. The platinum film on each rod consists of two segments, separated from each other by two longitudinal splits 180 degrees apart. The orientation of the splits on each sensor rod is such that it allows the determination of the octant in which the instantaneous velocity vector is located. For minimum support interference the three sensor rods are mounted at only one end to a long and thin supporting structure.

A copper-constantan thermocouple is mounted close to the sensors and measures ambient temperature with a maximum frequency response of 25 hertz.

The three sensors and the thermocouple are protected, while not in use, by an aluminum shield which can be placed over the sensors

and retracted pneumatically. Due to difficulties in supplying proper air pressure at the sonic orifices when the probes are mounted on a tall meteorological tower, the sensors are balanced at the no-flow condition. A weak air stream is continuously supplied through the shield, in order to keep the sensors free of contamination while not in operation.

Six TSI 1296E probes were mounted on the NASA Wallops Island 250-foot meteorological tower at the 30, 50, 100, 150, 200 and 250-foot levels. All probes are mounted in a vertical plane which also contains the axis of the tower. The maximum horizontally-measured distance between the two probes at the 30 and 250-foot levels is approximately 13 feet. Each probe is mounted with its axis in a horizontal direction, on a rotor that is controlled from the instrumentation trailer and can be rotated about a vertical axis to obtain any position between 0 and 360 degrees, with an accuracy of about ± 1 degree. The rotor is supported by an 8 feet long boom, mounted perpendicular to the south face of the 250-foot meteorological tower.

2.3   The Data Acquisition System

The Data Acquisition System was designed to provide simultaneous digitized data from one to thirteen TSI 1080 anemometer systems, sampled at a rate of 200 samples per second, for a time duration of approximately 40 minutes. All necessary equipment and controls are fixed in an instrumentation trailer placed under the tower. The system consists of two main parts with separated operation: a) the multiplexing and analog recording system, shown in figure 4 and b) the

demultiplexing, digitizing and digital recording system, shown in figure 5.

Each anemometer provides seven analog voltages: one from the thermocouple and six from the hot films of each probe. All voltages are in the range of 0-5 volts. Each voltage is frequency modulated by a voltage-controlled oscillator (Data-Control Systems Inc., Model GOV-5C), each with a different center frequency. For the outputs of each anemometer there is one set of voltage-controlled oscillators with center frequencies of 8, 12, 16, 20, 24, 28, and 32 kilohertz respectively. All voltage-controlled oscillators operate at a deviation from their center frequency of ± 1 kilohertz for a maximum voltage input ± 5 volts. The seven frequency modulated signals together with a reference signal of 100 kilohertz produced by a reference oscillator are summed by a Summing Amplifier (Data-Control Systems Inc., Model GAS-5), to produce one single multiplexed signal of approximately 3 volts peak-to-peak.

The six multiplexed signals from the six anemometers are simultaneously recorded on six separate channels of a 14-channel analog tape recorder (Bell and Howell, Model VR3700B). The time-of-day, provided by a time-of-day Generator (Hermes Electronics Co.) in NASA fast serial time code and monitored by a remote display (Itek Electro-Products Co., Model 2124C), is recorded on the fourteenth channel of the analog tape recorder.

The demultiplexing, digitizing and digital recording system can handle data from one anemometer, i.e. one channel of the analog

tape at a time. The analog tape is played back and the multiplexed signal from the desired channel is demultiplexed to its seven components by passing through seven discriminators (Data-Control Systems, Inc., Model GFD-16). The center frequency of each discriminator corresponds to the center frequency of one of the voltage controlled oscillators and each discriminator produces an output voltage of ±5 volts. A reference discriminator senses any deviation in the reference frequency of 100 kilohertz caused by fluctuations in the tape speed of the analog tape recorder, and corrects the output of the other seven discriminators with a feedback procedure.

The six outputs corresponding to the six anemometer bridge voltages are each passed through a low-pass filter (VTC Model LMI-100), which removes any frequency component over 100 hertz. This is necessary in order to avoid aliasing (distortion) of the velocity spectra at frequencies below 100 hertz. The thermocouple output need not be filtered since it does not contain frequencies higher than 25 hertz.

The seven analog voltages are fed to the multiplexing analog-to-digital converter (DEC Model ADO1-D). It converts an analog signal to an 11-bit (plus sign) digital word with a time of 5 micro-seconds. The total scan, settling and conversion time for one sample of seven voltages is 50 microseconds, which is approximately 1% of the time interval between two samples.

The recorded time-of-day is converted to a 32-bit binary coded decimal signal by a serial-to-parallel converter (Hermes Electronics

Co.). This converter is interfaced with the computer by a Digital Equipment Corporation custom-designed interface.

The Computer (DEC Model PDP 11/20) controls the multiplexing analog-to-digital converter and the digital tape recorder (DEC Model TR06-FB) through a tape transport controller (DEC Model TB68-C). The computer is programmable in DEC PAL-11 assembly language and has an 8K memory of 16-bit-words. Input and output to the computer is obtained through a teletypewriter.

The conversion starts at a time-of-day prescribed by the operator to assure correlated data for the different anemometers. Then the analog-to-digital converter performs successive scans and conversion of the seven analog voltages into two-byte words at a rate of one scan every 5 milliseconds. These words are stored in one of the four buffers of the computer. When the buffer, having a capacity of 209 scans or 2926 bytes, is filled with data, it is dumped on a 9-track digital magnetic tape. A total of 2298 blocks or 480,282 data points make up one sample of data, extended over a time period of approximately 40 minutes.

2.4 Conversion of the Output Signals into the Actual Quantities

A detailed discussion of the theory of operation of hot-wire and hot-film anemometers can be found in the references 15 and 22. This report is limited to a discussion of the empirical expressions obtained through the calibration of the probes from which the three velocity components in the sensor-oriented coordinate system can be calculated.

Each one of the six films of the probe is connected in a bridge circuit as shown in figure 6 and operates at a constant temperature. Special care has been taken so that both films of each sensor operate at the same temperature, in order to prevent heat transfer from one film to the other.

The bridge voltage is amplified in a feedback loop to ascertain thermal inertia compensation and is measured to provide the value $E_{\alpha i}$, where the subscript $\alpha = A,B,C$ stands for the ser   rod and the subscript $i = 1,2$ stands for the appropriate film (figure 2 for the exact location and orientation of all six films). The 0-5 volt output circuit is set up so that the bridge voltage for each film can be obtained from the corresponding 0-5 output voltage, $V_{\alpha i}$, with the following expression

$$E_{\alpha i} = 2 \cdot V_{\alpha i} + 3 \ , \ \alpha = A,B,C \ , \ i = 1,2 \qquad . \quad (2.4.1)$$

The heat convected from the electric heated element to the ambient air is proportional to the square of the voltage drop in this element and can be approximated by the following expression

$$Q_{\alpha} = CF_{\alpha 1} \cdot K_{\alpha 1} \cdot E_{\alpha 1}^{2} + CF_{\alpha 2} \cdot K_{\alpha 2} \cdot E_{\alpha 2}^{2}, \quad \alpha = A,B,C \qquad , \quad (2.4.2)$$

where $K_{\alpha 1}$ and $K_{\alpha 2}$ are calibration constants for each film and $CF_{\alpha 1}$ and $CF_{\alpha 2}$ are correction factors to account for cable and ambient temperature changes. According to reference 22, the expression for these correction factors is

$$CF_{\alpha i} = \left[1 + \frac{\Delta R_{c_{\alpha i}}}{R_{f_{\alpha i}}^{0}} \right] \left[\frac{T_{f_{\alpha}}^{0} - T_{a}^{0}}{T_{f_{\alpha i}} - T_{a}} \right] \qquad . \quad (2.4.3)$$

The zero-superscribed quantities refer to the TSI calibration conditions. The change of the cable resistance due to a change in cable temperature from the TSI ambient temperature, $T_a^{\,o}$, is equal to

$$\Delta R_{c_{\alpha i}} = R_{c_{\alpha i}}^{\,o} - R_{c_{\alpha i}} = -R_{c_{\alpha i}}^{\,o} \, \alpha_{cu}^{\,o} (T_c - T_a^{\,o}) \qquad , \qquad (2.4.4)$$

where the temperature coefficient of resistivity for copper, referenced to the temperature $T_a^{\,o}$, can be calculated as

$$\alpha_{cu}^{\,o} = \frac{1}{390.1 + T_a^{\,o}} \qquad . \qquad (2.4.5)$$

If $R_{c_{\alpha i}}^{\,m}$ is the resistance of the cable measured at a temperature, $T_c^{\,m}$, then the cable resistance at TSI ambient temperature can be calculated from the following expression

$$R_{c_{\alpha i}}^{\,o} = R_{c_{\alpha i}}^{\,m} \left[1 + \frac{1}{390.1 + T_c^{\,m}} (T_a^{\,o} - T_c^{\,m}) \right] \qquad . \qquad (2.4.6)$$

The hot-film resistance, $R_{f_{\alpha i}}$, at TSI conditions can be calculated from the measured cold-film resistance, $R_{f_{\alpha i}}^{cold}$, as

$$R_{f_{\alpha i}}^{\,o} = R_{f_{\alpha i}}^{cold} [1 + \alpha_{f_{\alpha i}}^{cold} (T_{f_\alpha}^{\,o} - T_f^{cold})] \qquad , \qquad (2.4.7)$$

where $\alpha_{f_{\alpha i}}^{cold}$ is the measured temperature coefficient of resistivity of the film.

The hot-film resistance at operation conditions in the wind tunnel or in the atmosphere can be obtained from the hot-film resistance at TSI conditions according to the expression

$$R_{f_{\alpha i}} = R_{f_{\alpha i}}^{\,o} + \Delta R_{c_{\alpha i}} \qquad . \qquad (2.4.8)$$

This is due to the fact that the total resistance in the

bridge arm containing the cable and the film must be constant. Therefore, a change in cable resistance causes a change in hot-film resistance and, as a result, changes the operation temperature of the film. The new operation temperature of the film can be calculated from the following expression

$$T_{f_{\alpha i}} = T_{f_\alpha}^o + \frac{\Delta R_{c_{\alpha i}}}{\alpha_{f_{\alpha i}}^{cold} R_{f_{\alpha i}}^{cold}} \qquad . \qquad (2.4.9)$$

In order to be able to use the same empirical expressions when the density of the air changes, all velocities are calculated for standard pressure and temperature of

$$p_s = 14.7 \text{ psia} = 29.92 \text{ in Hg}$$

$$T_s = 530° \text{ R} \qquad .$$

Since the hot-film sensors measure the mass flux, ρU, where ρ is the air density, the standard velocity U_s, can be obtained with use of the equation of state as follows

$$U_s = U \cdot \frac{p}{p_s} \cdot \frac{T_s}{T_a} \qquad . \qquad (2.4.10)$$

When the hot film is heated in flowing air, the heat convected from the film to the air depends on the velocity magnitude as well as the angle of attack, ϕ. The effective cooling velocity, U_e, is defined as the normal velocity that would produce the same amount of cooling from the film, as produced by the actual velocity, U, at a particular angle of attack, ϕ. The standard effective-cooling velocity, U_{es}, can be obtained from the heat transfer, Q_α,

through an expression of the following form

$$\frac{Q_\alpha}{T_{f_\alpha}^o - T_{a_\alpha}^o} = D \cdot U_{es_\alpha}^n \qquad , \qquad (2.4.11)$$

where the constants D and n are to be obtained through calibration
of the probes. In order to obtain identical calibration curves (heat
transfer versus standard effective-cooling velocities) for all three
sensors on the same probe, the calibration constants $K_{\alpha i}$ need to be
adjusted.

According to reference 8, the standard effective-cooling velocities
are related to the magnitude of the standard velocity, U_s, and the
angle of attack, ϕ, by the expression

$$U_{es_\alpha}^2 = U_s^2(\cos^2\phi_\alpha + k_\alpha \sin^2\phi_\alpha) \quad , \quad \alpha = A,B,C \qquad , \qquad (2.4.12)$$

where the constants k_A, k_B, k_C are of the order of 0.1 and have to be
determined through calibration. The three sensor-yaw angles ϕ_A, ϕ_B
and ϕ_C have the following trigonometric relationships

$$\sin^2\phi_A + \sin^2\phi_B + \sin^2\phi_C = 1$$

and $\hspace{11cm}$ (2.4.13)

$$\cos^2\phi_A + \cos^2\phi_B + \cos^2\phi_C = 2 \qquad .$$

Assuming that identical values of k_α exist for all three
sensors and using the above trigonometric relationships, one obtains
the magnitude of the standard velocity in terms of the standard
effective-cooling velocities of the three sensors, as follows

$$U_s^2 = \frac{U_{es_A}^2 + U_{es_B}^2 + U_{es_C}^2}{k_{av}} \qquad , \qquad (2.4.14)$$

where the constant k_{av} is of the order of 2.1. Now the sensor-yaw angles can be calculated from

$$|\phi_\alpha| = \arcsin \left[\frac{1 - \left(C_\alpha \dfrac{U_{es}}{U_s} \right)^2}{1 - k_\alpha} \right]^{\frac{1}{2}} \qquad , \qquad (2.4.15)$$

where the coefficients C_A, C_B, C_C are the reciprocal of the respective maximum values of U_{es_α}/U_s at zero sensor-yaw angle. Ideally, the values of these coefficients should be equal to one, but due to experimental errors and errors in curve fitting they may deviate a small amount from unity.

The sign of each angle can be determined by comparing the ratio of the voltages of the two films of some other sensor to the ratio, R, of the voltages of the same two films, when the velocity vector lies in the plane of their split. Hence,

$$\phi_A > 0 \quad \text{when} \quad E_{C1}/E_{C2} > R_C \qquad ,$$
$$\phi_B > 0 \quad \text{when} \quad E_{A1}/E_{A2} > R_A$$

and

$$\phi_C > 0 \quad \text{when} \quad E_{B1}/E_{B2} > R_B \qquad .$$

The actual velocity components in the sensor-oriented coordinate system will be calculated by the equations

$$U_\alpha = U \sin\phi_\alpha \quad , \quad \alpha = A,B,C \qquad , \qquad (2.4.16)$$

where the actual velocity magnitude, U, is calculated from the standard-

velocity magnitude, U_s, by

$$U = U_s \cdot \frac{P_s}{p} \cdot \frac{T_a}{T_s} \qquad . \qquad (2.4.17)$$

The ambient temperature can be calculated from the output voltage of the thermocouple, according to the following linear expression

$$T_a = C_{T1} \cdot V_T + C_{T2} \qquad , \qquad (2.4.18)$$

where the values of the constants C_{T1} and C_{T2} are determined through calibration of the thermocouple. It is assumed that the thermocouples are not affected by the heat convected from the hot films.

2.5 Calibration of the Anemometers

It was concluded in reference 22 that the data analysis suggested by TSI does not possess the required accuracy. Therefore, a new method based on new calibration procedures was developed. It was also concluded that accurate measurements with the TSI 1296E probe are only obtained when the mean velocities are in a direction nearly-parallel to the axis of the probe. This can be made possible for the tower measurements by rotating the probe, until it is approximately in the mean wind direction. If during the measurement period of 40 minutes the mean wind would change direction appreciably, the data would be discarded as being non-stationary.

The calibration of the split-film sensors was carried out in the low-speed Aerolab wind tunnel, located in the Quality Verification and Calibration Facility at NASA, Wallops Flight Center.

The test section dimensions are 32 inches (height) by 45 inches
(width) by 48 inches (length). The air flow is produced by a three-
blade variable pitch propeller, moved by a 1160 RPM / 50 HP con-
stant speed electric motor. Temperature and air speed in the test
section are measured with an electronic thermometer (Atkins H-51)
and two electronic manometers (CGS Models 1015 and 1014A) respec-
tively. Their outputs, together with the six voltages from the
TSI anemometers are scanned, digitized and averaged for a period
of approximately 2 seconds. The data acquisition system is con-
trolled by a HP 9810A programmable calculator and a HP 2570A
coupler/controller. The average values of the temperature, the
standard velocity and the six bridge voltages from the TSI anemo-
meter are printed on paper tape.

The probe was mounted on a vertical support and could be
rotated in a horizontal plane at any probe-yaw angle, β, while
the probe-pitch angle, α, was held equal to zero. Rotation of
90 degrees of the probe on the support offered the possibility
of varying the pitch angle, α, while keeping the probe-yaw angle,
β, equal to zero. Three sets of data, each for 13 different flow
velocities between 3.5 and 50 feet per second were first taken,
with the probe in such a position that one sensor at a time was
perpendicular to the flow. From the geometry of the sensor array
it can be seen that A is perpendicular to the flow when α = -35.26
degrees and β = 0 degrees, B is perpendicular to the flow when
α = 0 degrees and β = 39.25 degrees and C is perpendicular to the

flow when $\alpha = 0$ degrees and $\beta = -39.25$ degrees. Nine more sets of data, each for five air velocities between 6 and 35 feet per second, were also taken for $\alpha = 0$ and $\beta = 0$, ± 10, ± 20, ± 30 and ± 50 degrees.

The data required for the calculation of the temperature correction factors for each film as given by equation 2.4.3 are obtained from the following measurements. The resistance of the cold films, $R_{f_{\alpha i}}^{cold}$, at ambient temperature T_f^{cold}, as well as the cable resistances, $R_{c_{\alpha i}}^m$, at temperature T_c^m, are measured with a precision digital volt-ohm-meter (Fluke Model 8200A). The temperature coefficient of resistivity of the films, $\alpha_{f_{\alpha i}}^{cold}$, is calculated from measuremer. s in the thermal-chamber, also located in the Quality Verification and Calibration Facility.

The different constants that are necessary for the calculation of the velocity components will now have to be determined from the above measurements. First, the rate at which heat is convected from each sensor when it is perpendicular to the flow is calculated, by making use of the equation 2.4.2 and using values suggested by TSI as a first approximation for the constants $K_{\alpha i}$. Then the heat fluxes for the three sensors are plotted versus the standard velocities and the values of $K_{\alpha i}$ are adjusted, so that the data collapse to one single curve.

The next step is to determine the proper coefficient D and exponent n in the expression 2.4.11, which will fit the experimental data. It has been found that not one single set of values for D and n will describe the calibration curve adequately. The

calibration curve has to be divided into three ranges with different values of D and n in each range.

Once the heat flux versus effective cooling-velocity relation has been established, the standard cooling velocities, U_{es} , can be calculated for different sensor-yaw angles. Accepting that an expression of the form of 2.4.14 exists, an average value of the coefficient k_{av} can be obtained, for which the probe is expected to operate most of the time. The value of the standard velocity magnitude, V_s, is obtained from the measurement of the dynamic pressure by a Pitot-static tube in the wind tunnel.

The final step is to determine the constants for the expression 2.4.15, which yield the magnitudes of the sensor-yaw angles. These constants for sensors B and C are obtained by fitting a curve of the form 2.4.15 to the calibration data, obtained by plotting of the velocity ratios U_{es}/U_s versus the respective sensor-yaw angles. In order to obtain the yaw angle for sensor A, use is made of the trigonometric relationship 2.4.13.

The copper-constantan thermocouple is independently calibrated. First the zero and gain potentiometers were set up approximately, so that an output-voltage range of 0 to 5 volts DC corresponds to a temperature range of 0 to 200 degrees Fahrenheit. Then the thermocouple was placed in ther thermal-chamber and measurements of the output voltage were taken for temperatures in the range from 20 to 100 degrees Fahrenheit. Fitting the so obtained data to a straight line permits the calculation of the values of the constants in the expression 2.4.18.

As an example of the above calibration procedure and its accuracy, the calibration constants and the observed calibration errors are provided for the TSI #1193 Anemometer, which was placed in the 100-foot level of the meteorological tower. The experimental values of U_{es}/U_s and the semi-empirical relation of the form of equation 2.4.15 are plotted versus the sensor-yaw angle, ϕ, in figure 7 for sensor B and in figure 8 for sensor C. The calibration curve for the heat flux versus the standard effective cooling velocity for all three sensors is shown in figure 9. All necessary calibration constants are provided in table I. Finally, the observed calibration error in the calculation of the velocity components versus sensor-yaw angle is shown in figure 10 and the error in the calculation of the velocity magnitude versus the probe-yaw angle is shown in figure 11.

CHAPTER III

STATISTICAL ANALYSIS OF THE DATA

3.1 Limitations of Discrete Time Histories

Consider a physical quantity $x(t)$, which shows a random variation with time. Every record, $x^k(t)$, of the output of an instrument measuring the quantity $x(t)$ over a finite time interval is called a time history. Every record of $x(t)$ extending over an infinite time interval is called a sample function. The ensemble of all possible sample functions, that can be recorded if the measurement of $x(t)$ is repeated an infinite number of times, is called time series (or random process or stochastic process) and is denoted as $\{x^k(t)\}$. The assumption of ergodicity permits the derivation of desired information about the entire time series from the analysis of a single arbitrary time history.

In many cases, the continuous output of the measuring instruments is digitized and sampled at some appropriate uniform time increment, Δt, over a total time interval, T. Then the time series which is being measured is represented by the discrete time history, x_i, where by definition

$$x_i = x(i \cdot \Delta t) \quad \text{for} \quad i = 1,2,\ldots,N \qquad (3.1.1)$$

and the total record time, T, is equal to the time increment, Δt, times the number of data points in the sample, N.

The analysis of discrete time histories is subjected to the fol-

22

lowing constraints:

    i)   Sampling of the time series.

    ii) Finite record length.

    iii) Discretization of data.

    iv) Restricted range of data, due to the limited response of the transducer used.

It is required that the effects of these constraints are confined by the use of appropriate techniques.

3.2 Basic Statistical Definitions

Given any sample function of time, $x(t)$, its mean value, μ_x, is defined as

$$\mu_x = \lim_{T \to \infty} \frac{1}{2T} \int_{-T}^{T} x(t)dt \qquad , \qquad (3.2.1)$$

while its mean square value, ψ_x^2, is defined as

$$\psi_x^2 = \lim_{T \to \infty} \frac{1}{2T} \int_{-T}^{T} x^2(t)dt \qquad . \qquad (3.2.2)$$

The average of the squared differences of each value of $x(t)$ from the mean value is called the variance, σ_x^2, defined as

$$\sigma_x^2 = \lim_{T \to \infty} \frac{1}{2T} \int_{-T}^{T} [x(t) - \mu_x]^2 dt \qquad . \qquad (3.2.3)$$

The square root of the variance, σ_x, is called standard deviation.

Given two sample functions, $x(t)$ and $y(t)$, their covariance, σ_{xy}^2, is defined as

$$\sigma_{xy}^2 = \lim_{T \to \infty} \frac{1}{2T} \int_{-T}^{T} [x(t) - \mu_x][y(t) - \mu_y] dt \qquad . \qquad (3.2.4)$$

The dependence of future values of the considered sample functions $x(t)$ or $y(t)$ upon the present values of $x(t)$ is described by the autocorrelation function, $R_x(\tau)$, and the cross-correlation function, $R_{xy}(\tau)$, which are respectively defined as

$$R_x(\tau) = \lim_{T \to \infty} \frac{1}{2T} \int_{-T}^{T} x(t)\, x(t + \tau)dt \quad , \quad (3.2.5)$$

and

$$R_{xy}(\tau) = \lim_{T \to \infty} \frac{1}{2T} \int_{-T}^{T} x(t)\, y(t + \tau)dt \quad . \quad (3.2.6)$$

When a discrete time history, x_i, where $i = 1,2,\ldots,N$ is given, its mean value, $\bar{x}$, is defined as

$$\bar{x} = \frac{1}{N} \sum_{i=1}^{N} x_i \quad . \quad (3.2.7)$$

Then any instantaneous value, x_i, can be considered as the combination of a static or mean component, $\bar{x}$, and a dynamic or fluctuating component, χ_i, so that

$$x_i = \bar{x} + \chi_i \quad . \quad (3.2.8)$$

As a result of the definition of the mean value, it comes out that the mean value of the fluctuating component is equal to zero, i.e. $\bar{\chi} = 0$.

In many cases it is necessary to remove the mean component from the discrete time history and therefore generate a new mean-free time history, which contains only the fluctuating component. This is obtained by subtracting the mean value, $\bar{x}$, from each instantaneous value, x_i, of the original time history.

If x_i, for $i = 1,2,\ldots,N$, is such a mean-free time history, its

variance, $\overline{x^2}$, is given by the expression

$$\overline{x^2} = \frac{1}{N} \sum_{i=1}^{N} x_i^2 \qquad . \qquad (3.2.9)$$

If x_i and y_i are both mean-free time histories, their covariance, $\overline{xy}$, is defined as

$$\overline{xy} = \frac{1}{N} \sum_{i=1}^{N} x_i y_i \qquad . \qquad (3.2.10)$$

The existence of slowly varying mean values in the time histories results in great distortions of their spectral estimates. Therefore, it is good practice to remove the means from the data before proceeding with the spectral analysis. The removal of the means proved necessary for time histories related to atmospheric measurements, such as air velocity, temperature and pressure.

3.3 Partition of Each Sample of Data into Blocks

As described in Chapter II, each sample of data from each TSI 1080 probe consists of four discrete time histories, namely the three velocity components in the sensor oriented coordinate system and the temperature, sampled at a rate of 200 points per second, for a time period of approximately 40 minutes. The total number of data points in each time history is approximately 480,000.

The simultaneous spectral analysis of this number of data points is far beyond the capacity of any available computer. It is therefore necessary that each time history is divided into a number of data blocks and that the statistical and spectral analysis is applied separately to

each block. As will be explained in Chapter 4.3, the most efficient
use of the fast Fourier transform requires that the number of data
points per block is equal to an integer power of 2. After considera-
tion of the capacity of the IBM 370 computer that was used, the number
of data points per block was chosen to be $N = 2^{13} = 8192$. Consequently,
the number of data blocks in each time history had to be taken as $M = 58$,
so that the total number of data in each time history was reduced to
$M \cdot N = 475,136$, corresponding to a time period of approximately 39 min-
utes and 35 seconds.

Assuming that the data sample is stationary, mean quantities, vari-
ances and covariances in each block were first calculated and later
all block means, variances and covariances were averaged to provide the
sample mean values, the sample variances and the sample covariances of
the fluctuations of the three velocity components and the temperature.

3.4 Stationarity Tests

As already mentioned in former chapters, the statistical and spec-
tral analysis is based on the assumption that the time histories are
stationary. Therefore, it is required that this assumption is carefully
checked. This will be done in two ways:

1. By simply inspecting the variation of the block means, the
block standard deviations and the block probe-yaw angles. Large varia-
tions of the mean wind, while large variations of the standard devia-
tions indicate that the frequency structure of the turbulence is vary-
ing with time. The magnitude of the probe-yaw angle, i.e. the angle α

between the longitudinal axis of the probe and the direction of the
horizontal mean wind, will also determine the level of accuracy of the
probe operation, since the most accurate data are obtained when the
probe is directed straight into the mean wind direction.

2. By detecting monotonic trends using the following nonstation-
arity trend test.

If A^i, $i = 1,2,\ldots,M$ represent any of the statistical quantities
calculated in the ith data block, the total number of reverse arrange-
ments, R, is defined as

$$R = \sum_{i=1}^{M-1} \sum_{j=i+1}^{M} R_{ij} \qquad . \qquad (3.4.1)$$

where

$$R_{ij} = \begin{cases} 1 & , \quad \text{if} \quad A^i > A^j \quad , \\ 0 & , \quad \text{if} \quad A^i \leq A^j \quad . \end{cases} \qquad (3.4.2)$$

Assuming a normal distribution for the number of reverse arrange-
ments, there exists a certain interval $[R_1, R_2]$ for the values of R, in
which one can be assured at a certain level of confidence, α, that
the data sample does not show any monotonic trend. For values of R
greater than R_2, a downward trend of the statistical quantity tested
is to be expected, while for values of R smaller than R_1, the data
sample shows an upward trend of the respective statistical quantity.

The limits of the stationarity interval have been calculated in
reference 23 for a total number of blocks, M, between 10 and 100.
For $M = 58$, it was found that at a confidence level, α, equal to 90%,
the lower limit, R_1, is equal to 703 and the upper limit, R_2, is equal

to 949, while at a confidence level 98%, R_1 is equal to 652 and R_2 is equal to 1000.

The stationarity trend test is performed for the block means of the three velocity components, the magnitude of the velocity vector and the probe-yaw angle, as well as the block standard deviations of the three velocity components.

Based on the results f the inspection and the nonstationarity trend test of the block statistical quantities, a decision will be made at this point whether or not to continue the statistical analysis for each one sample of data.

3.5 Coordinate Transformation into the Mean-Wind Oriented Coordinate System

The TSI 1030 anemometers provide the three components U_A, U_B and U_C of the wind velocity vector in the Cartesian system that is formed by the three sensors, as shown in figure 2.

Nevertheless, the velocity components have to be expressed in some coordinate system, which is physically connected with the flow field. For this purpose, the mean-wind oriented coordinate system, with co-ordinate directions x,y and z was introduced. This is a Cartesian system, where the z-axis is vertically upward, the x- and y-axes are horizontal and the sample mean velocity vector has to lie in the x-z plane. Then, by definition, the y-component of the sample mean velocity is zero. On the other hand, since the flow in the atmospheric boundary layer is almost horizontal, it is expected that the z-component of the

sample mean velocity vector will be very small compared to the x-component.

Using geometrical relations between the two coordinate systems, one finds that the transformation will have the following matrix form

$$\begin{Bmatrix} u \\ v \\ w \end{Bmatrix} = \begin{vmatrix} 0.57735\cos\beta & 0.57735\cos\beta-0.70711\sin\beta & 0.57735\cos\beta+0.70711\sin\beta \\ 0.57735\sin\beta & 0.57735\sin\beta+0.70711\cos\beta & 0.57735\sin\beta-0.70711\cos\beta \\ -0.81650 & 0.40824 & 0.40824 \end{vmatrix} \begin{Bmatrix} U_A \\ U_B \\ U_C \end{Bmatrix}$$

$$(3.5.1)$$

where u, v and w are the velocity components in the xyz-system and β is the sample probe-yaw angle, defined as the angle between the axis of the probe and the x-axis, as shown in figure 3.

According to the geometry of the probe, the sample probe-yaw angle can be calculated from the following expression

$$\beta = \arctan\left(1.22475 \, \frac{\overline{U}_C - \overline{U}_B}{\overline{U}_A + \overline{U}_B + \overline{U}_C} \right) \qquad , \qquad (3.5.2)$$

where $\overline{U}_A$, $\overline{U}_B$ and $\overline{U}_C$ are the sample mean values of the velocity components U_A, U_B and U_C respectively.

3.6 Calculation of the Mean Values, Variances and Covariances

After the transformation of the velocity components into the mean-wind oriented coordinate system, the time histories to be analyzed are the temperature, T (in degrees Fahrenheit), the longitudinal velocity component, u, the lateral velocity component, v, and the vertical velo-city component, w (all velocity components are expressed in feet per second). Again as before, each time history is divided into 58 blocks of 8192 data points each.

The sample-mean values are calculated in two steps. First, the block-mean values, $\bar{x}^n$, are calculated from the expression

$$\bar{x}^n = \frac{1}{N} \sum_{i=1}^{N} x_i \qquad (3.6.1)$$

and then all block-means are averaged to produce the respective sample-mean values, $\bar{x}$, as follows

$$\bar{x} = \frac{1}{M} \sum_{n=1}^{M} \bar{x}^n \qquad , \qquad (3.6.2)$$

where x represents any one of the quantities T, u, v or w.

For the calculation of the variances and covariances, it is necessary to use time histories with zero mean values. Therefore, the block-means have to be subtracted from all values in each block and the block-variances, $\overline{x^2}^n$, and sample-covariances, $\overline{xy}^n$, of the time histories represented by x and y, are calculated as

$$\overline{x^2}^n = \frac{1}{N} \sum_{i=1}^{N} (x_i - \bar{x}^n) \qquad (3.6.3)$$

and

$$\overline{xy}^n = \frac{1}{N} \sum_{i=1}^{N} (x_i - \bar{x}^n)(y_i - \bar{y}^n) \qquad . \qquad (3.6.4)$$

The sample-variances, $\overline{x^2}$, and sample-covariances, $\overline{xy}$, are calculated as the average of the respective block-quantities, as follows

$$\overline{x^2} = \frac{1}{M} \sum_{n=1}^{M} \overline{x^2}^n \qquad , \qquad (3.6.5)$$

and

$$\overline{xy} = \frac{1}{M} \sum_{n=1}^{M} \overline{xy}^n \qquad . \qquad (3.6.6)$$

CHAPTER IV

SPECTRAL CALCULATIONS

4.1 Definitions

The nature and properties of a physical system, whose character-
istics are measured as functions of time, are well illustrated with
the spectral density functions in the frequency domain.

A function that describes the general frequency composition of the
measured quantity, $x(t)$, and the relative significance of every frequency
is the power spectral density function, $G_x(f)$. There exist three ways
by which the power spectral density function can be defined.

1. From the direct Fourier transform of the function $x(t)$, accord-
ing to the expression

$$G_x(f) = 2 \cdot \lim_{T \to \infty} \frac{1}{2T} \left| \int_{-T}^{T} x(t) \cdot e^{-i2\pi ft} dt \right|^2 \qquad . \qquad (4.1.1)$$

2. From the Fourier transform of the autocorrelation function, as
follows

$$G_x(f) = 2 \int_{-\infty}^{\infty} R_x(\tau) \cdot e^{-i2\pi ft} d\tau \qquad . \qquad (4.1.2)$$

3. From the mean square value of the output of a sharp band-pass
filter. The filter output, $x(t,f,\Delta f)$, consists of the portion of $x(t)$
that lies in a frequency range with center frequency f and bandwidth Δf.
The power spectral density function is then defined as follows

$$G_x(f) = \lim_{\Delta f \to 0} \frac{1}{\Delta f} \left[\lim_{T \to \infty} \frac{1}{2T} \int_{-T}^{T} x^2(t,f,\Delta f) dt \right] \qquad . \qquad (4.1.3)$$

All three definitions of the power spectral density function are asymptotically equivalent, when applied to stationary time series. The power spectral density function is always a real-valued, non-negative function of frequency. Its complete plot versus frequency is called power spectrum. Since negative frequencies do not possess any physical meaning, the power spectrum extends only in the positive frequency domain.

The joint properties of two functions of time, $x(t)$ and $y(t)$, in the frequency domain, are described by the cross-spectral density function $G_{xy}(f)$. Similar to the power spectral density function, the cross-spectral density function can be defined in three equivalent ways.

1. From the Fourier transform, $Y(f,T)$, of $y(t)$ and the complex conjugate, $X^*(f,T)$, of the Fourier transform of $x(t)$, as follow-

$$G_{xy}(f) = 2 \lim_{T \to \infty} \left[\frac{1}{2T} X^*(f,T) \cdot Y(f,T) \right] \qquad , \qquad (4.1.4)$$

where the finite Fourier transform, $X(f,T)$, of the function $x(t)$ in the interval $(-T,T)$ is defined as

$$X(f,T) = \int_{-T}^{T} x(t) \cdot e^{-i2\pi ft} dt \qquad . \qquad (4.1.5)$$

2. From the cross-correlation function, according to the expression

$$G_{xy}(f) = 2 \int_{-\infty}^{\infty} R_{xy}(\tau) \ e^{-i2\pi ft} d\tau \qquad . \qquad (4.1.6)$$

3. From the product of the output of two band-pass filters, ap-

plied to the functions $x(t)$ and $y(t)$, according to the expression

$$G_{xy}(f) = \lim_{\Delta f \to 0} \frac{1}{\Delta f} \left\{ \lim_{T \to \infty} \frac{1}{2T} \left[\int_{-T}^{T} x(t,f,\Delta f) \cdot y(t,f,\Delta f) dt - \right. \right.$$

$$\left. \left. -i \int_{-T}^{T} x(t,f,\Delta f) \cdot y^{o}(t,f,\Delta f) dt \right] \right\} \qquad , \qquad (4.1.7)$$

where the function $y^{o}(t,f,\Delta f)$ is equal to the function $y(t,f,\Delta f)$ shifted 90 degrees in phase angle.

The cross-spectral density function is in general a complex function of frequency, consisting of a real part, $C_{xy}(f)$, called coincident or co-spectral density function and an imaginary part, $-Q_{xy}(f)$, called quadrature or quad-spectral density function, i.e.

$$G_{xy}(f) = C_{xy}(f) - iQ_{xy}(f) \qquad . \qquad (4.1.8)$$

Alternatively, the cross-spectral density function can be expressed in polar form as

$$G_{xy}(f) = |G_{xy}(f)| \cdot e^{-i\theta_{xy}(f)} \qquad , \qquad (4.1.9)$$

where the magnitude and the phase angle are related to the co- and quad-spectral density functions by the expressions

$$|G_{xy}(f)| = \left[C_{xy}^{2}(f) + Q_{xy}^{2}(f) \right]^{\frac{1}{2}} \qquad , \qquad (4.1.10)$$

and

$$\theta_{xy}(f) = \arctan \left(\frac{Q_{xy}(f)}{C_{xy}(f)} \right) \qquad . \qquad (4.1.11)$$

A real-valued quantity, which is related to the cross-spectral density function, is the coherence function, defined as

$$\gamma_{xy}^{2}(f) = \frac{|G_{xy}(f)|^{2}}{G_{x}(f) \cdot G_{y}(f)} \qquad . \qquad (4.1.12)$$

The coherence function is a measure of the correlation between the
values of two functions of time and takes values between 0 and 1. When
the coherence function is equal to zero for a certain frequency, f, the
two functions, x(t) and y(t), are said to be incoherent at the frequency
f. When the coherence function is equal to unity for all frequencies,
the two functions are said to be fully coherent.

The graphical representation of the cross-spectral density function
is called cross-spectrum. It consists of the plot of both the magni-
tude and the phase angle of the cross-spectral density function versus
frequency.

Based on the definitions mentioned above, three different methods
for the calculation of the power- and cross-spectral density functions
are available. The recent development of FFT (fast Fourier transform)
techniques made the direct Fourier transform exceedingly advantageous
for the spectral analysis of long time histories. Therefore, the
direct Fourier transform method based on a new FFT technique, as des-
cribed in the following sections, will be used.

4.2 Finite Interval Effect -- Cosine Taper Data Window

Any time history is by definition extended over a finite time inter-
val. Definitions and equations, which are proper for infinite time
series, may be erroneous, when applied to time histories. Therefore,
careful consideration of the finite interval effect has to be made.

The general Fourier transform, $X(f)$, of the time function x(t) is
defined as

$$X(f) = \int_{-\infty}^{\infty} x(t) \cdot e^{-i2\pi ft} dt \qquad , \qquad (4.2.1)$$

while the finite Fourier transform, $X(f,T)$, of the time history $x(t)$, where t lies in the interval $[-T,T]$, is defined as

$$X(f,T) = \int_{-T}^{T} x(t) \cdot e^{-i2\pi ft} dt \qquad . \qquad (4.2.2)$$

Any time history can be considered as produced by a sample function, $x(t)$, multiplied by a window function, $w(t)$, which eliminates all values of $x(t)$ outside the interval $[-T,T]$. The window function that permits all values in the interval $[-T,T]$ to pass undeformed is called the rectangular or boxcar window function and is defined as

$$w(t) = \begin{cases} 1 & |t| \leq T \\ 0 & T \leq |t| \end{cases} \qquad . \qquad (4.2.3)$$

With the use of the rectangular window function, the finite Fourier transform can be alternatively expressed as

$$X(f,T) = \int_{-\infty}^{\infty} x(t) \cdot w(t) \cdot e^{-i2\pi ft} dt \qquad . \qquad (4.2.4)$$

According to the convolution theorem, the finite Fourier transform can also be considered as the convolution of the general Fourier transform, $X(f)$, with the Fourier transform, $W(f,T)$, of the window function, i.e.

$$X(f,T) = \int_{-\infty}^{\infty} X(f - \xi) \cdot W(\xi,T) d\xi \qquad . \qquad (4.2.5)$$

The Fourier transform of the rectangular window function is calculated to be

$$W(f,T) = \int_{-\infty}^{\infty} w(t) \cdot e^{-i2\pi ft} dt = \int_{-T}^{T} e^{-i2\pi ft} dt = \frac{\sin 2\pi ft}{\pi f} \quad . \quad (4.2.6)$$

The rectangular window function and its Fourier transform for positive frequencies are shown in figure 12.

The effect of the rectangular window can be illustrated with the following example. Consider the sinusoidal function $x(t) = \cos 2\pi f_o t$, where f_o is a constant frequency. Its infinite Fourier transform is calculated to be

$$X(f) = \tfrac{1}{2}[\delta(f + f_o) + \delta(f - f_o)] \qquad , \qquad (4.2.7)$$

while its finite Fourier transform in the interval $[-T,T]$ is calculated, according to equation 4.2.5, as

$$X(f,T) = \tfrac{1}{2} \left[\frac{\sin 2\pi(f + f_o)T}{\pi(f + f_o)} + \frac{\sin 2\pi(f - f_o)T}{\pi(f - f_o)} \right] \qquad . \qquad (4.2.8)$$

The functions $X(f)$ and $X(f,T)$ are plotted versus frequency in figure 13 for the range of positive frequencies and for the case when the product $f_o T$ is equal to 5. As can be seen in this figure, the function $X(f)$ has a non-zero value only at the point $f = f_o$, while the function $X(f,T)$ extends over the entire frequency domain and presents positive and negative peaks, called sidelobes.

When $x(t)$ is a wide-band function (i.e. having a wide frequency spectrum), its finite Fourier transform will consist of the superimposed effects of all frequencies, according to equation 4.2.5. Although the negative sidelobes effect will now be much smaller than in the narrow-band function case, a distortion in the spectral estimates is to be expected. Under certain circumstances, it is even possible that negative values of the power spectral density function appear for certain frequencies, which is opposed to the physical significance of this function. This danger is reduced by replacing the rectangular

window function with some other window function, which presents lower sidelobes.

From the existing number of data window functions, which have been suggested and used by different authors, the cosine taper data window function was chosen as most satisfactory for meteorological time histories. The cosine taper data window function deforms one tenth of the data at each end by multiplying these data by a half cosine bell and leaves the rest eight tenths of the data undeformed. This window function is defined in the interval [-T,T] as follows,

$$w(t) = \begin{cases} 0 & T < |t| \\ \frac{1}{2}\left(1 + \cos\frac{10\pi t}{2T}\right) & 0.8T \le |t| \le T \\ 1 & 0 \le |t| < 0.8T \end{cases} \quad . \quad (4.2.9)$$

The Fourier transform of the cosine taper data window function is

$$W(f,T) = \frac{(25 - 12\ f^2 T^2)[\sin(2\pi fT) + \sin(2\pi f0.8T)]}{2\pi f[25 - 4f^2 T^2]} \quad . \quad (4.2.10)$$

Both the cosine taper data window function and its Fourier transform are shown in figure 14. Compared to the rectangular window function, it shows lower sidelobes and, therefore, produces less leakage in the spectral estimates. Nevertheless, the spectral estimates have to be multiplied by a scale factor of 1/0.875, due to the deformation of part of the data.

4.3 The Fast Fourier Transform

4.3.1 Introduction

Consider a real- or complex-valued discrete time sequence, x_k, for k = 0,1,2,...,N-1 which consists of N data points sampled at a

uniform time increment, Δt, so that the total time interval, T, is
equal to $N \cdot \Delta t$. The finite Fourier transform of this time sequence,
as defined by equation 4.2.2, has to be approximated by the discrete
Fourier transform, X_r, defined as follows

$$X_r = \frac{T}{N} \sum_{k=0}^{N-1} x_k e^{-i2\pi \frac{rk}{N}} \quad , \quad r = 0,1,\ldots,N-1 \quad . \quad (4.3.1)$$

This expression can be obtained from equation 4.2.2 by replacing
the time, t, by $\frac{kT}{N}$, the time increment, Δt, by $\frac{T}{N}$ and the frequency, f,
by $\frac{r}{T}$. The discrete Fourier transform consists of N discrete values,
corresponding to N consecutive frequencies, separated from each other
with a frequency increment, Δf, equal to $\frac{1}{T}$.

The computation of the discrete Fourier transform of a complex data
sequence of N points, according to equation 4.3.1, requires N complex
multiplications and additions. For an adequately large number of data
points, this number of operations would consume an enormous amount of
computer time and makes equation 4.3.1 practically useless. A more
efficient method for the computation of the discrete Fourier transform
of long data sequences is the fast Fourier transform, requiring only
$2N\log_2 N$ complex operations, instead of N^2. For $8192 = 2^{13}$ data points
the FFT requires approximately 315 times less computer time than required
by using the equation 4.3.1.

There exist several FFT techniques, varying in their details. A
technique, having the additional advantage of not requiring the bit-
reversal of the final values, will be presented in the following section.

4.3.2 Derivation of the Equations

The highest efficiency of the FFT is obtained, when the number, N,

of data points to be transformed is equal to an integer power of 2. If this is not the case, the number of data can either be truncated to the nearest lower power of 2 by omitting some of the data or reach the nearest higher power of 2 by adding some zero-valued data at the end of the sequence.

Consider a time sequence of N points, where N is equal to 2^P, $p = 2,3,\ldots$, extending over the time interval $[0,T]$. Letting $W = e^{-i2\pi}$ for convenience, the equation 4.3.1 can be rewritten as

$$X_r = \frac{T}{N} \sum_{k=0}^{N-1} x_k W^{\frac{rk}{N}} \quad , \quad r = 0,1,\ldots,N-1 \quad . \quad (4.3.2)$$

The integers k and r can be expressed in the binary number system as

$$k = h_{p-1} \cdot 2^{p-1} + h_{p-2} \cdot 2^{p-2} + \cdots + h_2 \cdot 2^2 + h_1 \cdot 2^1 + h_0 \cdot 2^0 \quad , \quad h_i = 0,1 \quad (4.3.3)$$

and

$$r = j_{p-1} \cdot 2^{p-1} + j_{p-2} \cdot 2^{p-2} + \cdots + j_2 \cdot 2^2 + j_1 \cdot 2^1 + j_0 \cdot 2^0 \quad , \quad j_i = 0,1, \quad (4.3.4)$$

or, according to a different notation, as

$$k = (h_{p-1},\ldots,h_1,h_0) \quad (4.3.5)$$

and

$$r = (j_{p-1},\ldots,j_1,j_0) \quad . \quad (4.3.6)$$

Following this notation, equation 4.3.2 can be written as

$$X(j_{p-1},\ldots,j_1,j_0) = \frac{T}{N} \sum_{k=0}^{N-1} x(h_{p-1},\ldots,h_1,h_0) W^{\frac{rk}{N}} \quad , \quad (4.3.7)$$

or, furthermore,

$$X(j_{p-1},\ldots,j_1,j_0) = \frac{T}{N} \sum_{h_0=0}^{1} \sum_{h_1=0}^{1} \cdots \sum_{h_{p-1}=0}^{1} x(h_{p-1},\ldots,h_1,h_0) W^{\frac{rk}{N}} \quad . (4.3.8)$$

The first step of the FFT begins with the definition of the quantities

N_1, k_1 and r_1, as follows

$$N_1 = \frac{N}{2} = 2^{p-1} \quad , \quad (4.3.9)$$

$$k_1 = k - h_{p-1} \cdot 2^{p-1} = h_{p-2} \cdot 2^{p-2} + \cdots + h_1 \cdot 2^1 + h_0 \cdot 2^0 \quad (4.3.10)$$

and

$$r_1 = \frac{r - j_0}{2} = j_{p-1} \cdot 2^{p-2} + \cdots + j_2 \cdot 2^1 + j_1 \cdot 2^0 \quad . \quad (4.3.11)$$

The exponential term in equation 4.3.8 can be expanded as

$$W^{\frac{rk}{N}} = W^{\frac{(2r_1 + j_0)(k_1 + h_{p-1} 2^{p-1})}{N}} = W^{\frac{r_1 k_1}{N_1}} W^{\frac{j_0 k_1}{N}} W^{\frac{j_0 h_{p-1}}{2}} \quad , (4.3.12)$$

where the term $W^{r_1 h_{p-1}}$ was omitted since it is equal to one. The new quantities A_1 are introduced by the definition

$$A_1(h_{p-2}, \ldots, h_0; j_0) = \sum_{h_{p-1}=0}^{1} x(h_{p-1}, \ldots, h_1, h_0) W^{\frac{j_0 h_{p-1}}{2}} W^{\frac{j_0 k_1}{N}} \quad . \quad (4.3.13)$$

Finally, at the end of the first step of the FFT, equation 4.3.1 takes the following form

$$X(j_{p-1}, \ldots, j_1, j_0) = \frac{T}{N} \sum_{h_0=0}^{1} \sum_{h_1=0}^{1} \cdots \sum_{h_{p-2}=0}^{1} A_1(h_{p-2}, \ldots, h_0; j_0) W^{\frac{r_1 k_1}{N_1}} . (4.3.14)$$

The N values of A_1 can be calculated from the original data directly via equation 4.3.13 and require 2N complex operations. The N values of X_r can be calculated from equation 4.3.14, requiring $N \frac{N}{2}$ complex operations. Consequently, the total number of operations is in the first step reduced from N^2 to $N(\frac{N}{2} + 2)$.

The former approach can be further generalized. At the qth step where $q = 1, 2, \ldots, p-1$, the quantities N_q, k_q, r_q and A_q are introduced as follows

$$N_q = \frac{N_{q-1}}{2} = 2^{p-1} \qquad , \qquad (4.3.15)$$

$$k_q = k_{q-1} - h_{p-q} \cdot 2^{p-q} = h_{p-q-1} \cdot 2^{p-q-1} + \cdots + h_1 \cdot 2^1 + h_o \cdot 2^o \, , \, (4.3.16)$$

$$r_q = \frac{r_{q-1} - j_{q-1}}{2} = j_{p-1} \cdot 2^{p-q-1} + \cdots + j_{q+1} \cdot 2^1 + j_q \cdot 2^o \qquad (4.3.17)$$

and

$$A_q(h_{p-q-1}, \ldots, h_o; j_{q-1}, \ldots, j_o) =$$

$$= \sum_{h_{p-q}=0}^{1} A_{q-1}(h_{p-q}, \ldots, h_o; j_{q-2}, \ldots, j_o) W^{\frac{j_{q-1} h_{p-q}}{2}} W^{\frac{j_{q-1} k_q}{N_{q-1}}} \, . \, (4.3.18)$$

The general expression of the discrete Fourier transform, X_r, at the qth step is by induction obtained in the following form

$$X(j_{p-1}, \ldots, j_1, j_o) =$$

$$= \frac{T}{N} \sum_{h_c=0}^{1} \sum_{h_1=0}^{1} \cdots \sum_{h_{p-q-1}=0}^{1} A_q(h_{p-q-1}, \ldots, h_o; j_{q-1}, \ldots, j_o) W^{\frac{r_q k_q}{N_q}} \, . (4.3.19)$$

When q is equal to p-1, equation 4.3.19 is reduced to

$$X(j_{p-1}, \ldots, j_1, j_o) = \frac{T}{N} \sum_{h_o=0}^{1} A_{p-1}(h_o; j_{p-2}, \ldots, j_o) W^{\frac{r_{p-1} k_{p-1}}{N_{p-1}}} \, . \, (4.3.20)$$

The above formulation implies that the discrete Fourier transform, X_r, of the discrete time history x_k, where $r, k = 0, 1, \ldots, 2^p - 1$ can be computed in p steps, from the consecutive calculation of the quantities A_q. Each of these steps requires 2N complex multiplications and additions, so that the total number of operations is 2pN. Furthermore, at each step q, the quantities A_q can replace the quantities A_{q-1} in the computer memory, so that only N memory positions are required.

4.3.3 A Simple Example

The following example provides a detailed illustration of the FFT approach, as discussed in chapter 4.3.2. A discrete time history, consisting of 8 data points, x_i, where $i = 0,1,\ldots,7$, and extended at the time interval $[0,T]$, is given. Following the binary system notation, the quantities x_i can be expressed as follows

$$
\begin{aligned}
x_0 &= x(0,0,0) & x_4 &= x(1,0,0) \\
x_1 &= x(0,0,1) & x_5 &= x(1,0,1) \\
x_2 &= x(0,1,0) & x_6 &= x(1,1,0) \\
x_3 &= x(0,1,1) & x_7 &= x(1,1,1)
\end{aligned}
\tag{4.3.21}
$$

The discrete Fourier transform of this time history consists of 8 values, X_r, where $r = 0,1,\ldots,7$, which, according to equation 4.3.2, will have the following expressions in terms of the original data values

$$
\begin{aligned}
X_0 &= \frac{T}{8}(x_0 + x_1 + x_2 + x_3 + x_4 + x_5 + x_6 + x_7) \\
X_1 &= \frac{T}{8}(x_0 + x_1 W^{1/8} + x_2 W^{2/8} + x_3 W^{3/8} + x_4 W^{4/8} + x_5 W^{5/8} + x_6 W^{6/8} + x_7 W^{7/8}) \\
X_2 &= \frac{T}{8}(x_0 + x_1 W^{2/8} + x_2 W^{4/8} + x_3 W^{6/8} + x_4 + x_5 W^{2/8} + x_6 W^{4/8} + x_7 W^{6/8}) \\
X_3 &= \frac{T}{8}(x_0 + x_1 W^{3/8} + x_2 W^{6/8} + x_3 W^{1/8} + x_4 W^{4/8} + x_5 W^{7/8} + x_6 W^{2/8} + x_7 W^{5/8}) \\
X_4 &= \frac{T}{8}(x_0 + x_1 W^{4/8} + x_2 + x_3 W^{4/8} + x_4 + x_5 W^{4/8} + x_6 + x_7 W^{4/8}) \\
X_5 &= \frac{T}{8}(x_0 + x_1 W^{5/8} + x_2 W^{2/8} + x_3 W^{7/8} + x_4 W^{4/8} + x_5 W^{1/8} + x_6 W^{6/8} + x_7 W^{3/8}) \\
X_6 &= \frac{T}{8}(x_0 + x_1 W^{6/8} + x_2 W^{4/8} + x_3 W^{2/8} + x_4 + x_5 W^{6/8} + x_6 W^{4/8} + x_7 W^{2/8}) \\
X_7 &= \frac{T}{8}(x_0 + x_1 W^{7/8} + x_2 W^{6/8} + x_3 W^{5/8} + x_4 W^{4/8} + x_5 W^{3/8} + x_6 W^{2/8} + x_7 W^{1/8})
\end{aligned}
\tag{4.3.22}
$$

In the above expression, use has been made of the fact that W^n, where n is an integer, is equal to 1.

The FFT consists of three steps, i.e. the consecutive calculation of A_1, A_2, X according to the equation 4.3.18.

First Step

$$A_1(h_1,h_o;j_o) = \sum_{h_2=0}^{1} x(h_2,h_1,h_o)W^{\frac{j_o h_2}{2}} W^{\frac{j_o k_1}{N}} \tag{4.3.23}$$

$A_1(0,0,0) = x(0,0,0)W^O + x(1,0,0)W^O = x_o + x_4$

$A_1(0,0,1) = x(0,0,0)W^O + x(1,0,0)W^{4/8} = x_o + x_4 W^{4/8}$

$A_1(0,1,0) = x(0,0,1)W^O + x(1,0,1)W^O = x_1 + x_5$

$A_1(0,1,1) = x(0,0,1)W^{1/8} + x(1,0,1)W^{5/8} = x_1 W^{1/8} + x_5 W^{5/8}$

$A_1(1,0,0) = x(0,1,0)W^O + x(1,1,0)W^O = x_2 + x_6$

$A_1(1,0,1) = x(0,1,0)W^{2/8} + x(1,1,0)W^{6/8} = x_2 W^{2/8} + x_6 W^{6/8}$

$A_1(1,1,0) = x(0,1,1)W^O + x(1,1,1)W^O = x_3 + x_7$

$A_1(1,1,1) = x(0,1,1)W^{3/8} + x(1,1,1)W^{7/8} = x_3 W^{3/8} + x_7 W^{7/8} \tag{4.3.24}$

Second Step

$$A_2(h_o;j_1,j_o) = \sum_{h_1=0}^{1} A_1(h_1,h_o;j_o)W^{\frac{j_1 h_1}{2}} W^{\frac{j_1 k_2}{N_1}} \tag{4.3.25}$$

$A_2(0,0,0) = A_1(0,0,0)W^O + A_1(1,0,0)W^O = x_o + x_4 + x_2 + x_6$

$A_2(0,0,1) = A_1(0,0,1)W^O + A_1(1,0,1)W^O = x_o + x_4 W^{4/8} + x_2 W^{2/8} + x_6 W^{6/8}$

$A_2(0,1,0) = A_1(0,0,0)W^O + A_1(1,0,0)W^{4/8} = x_o + x_4 + x_2 W^{4/8} + x_6 W^{4/8}$

$A_2(0,1,1) = A_1(0,0,1)W^O + A_1(1,0,1)W^{4/8} = x_o + x_4 W^{4/8} + x_2 W^{6/8} + x_6 W^{2/8}$

$A_2(1,0,0) = A_1(0,1,0)W^O + A_1(1,1,0)W^O = x_1 + x_5 + x_3 + x_7$

$A_2(1,0,1) = A_1(0,1,1)W^O + A_1(1,1,1)W^O = x_1 W^{1/8} + x_5 W^{5/8} + x_3 W^{3/8} + x_7 W^{7/8}$

$A_2(1,1,0) = A_1(0,1,0)W^{2/8} + A_1(1,1,0)W^{6/8} =$
$\qquad x_1 W^{2/8} + x_5 W^{2/8} + x_3 W^{6/8} + x_7 W^{6/8}$

$A_2(1,1,1) = A_1(0,1,1)W^{2/8} + A_1(1,1,1)W^{6/8} =$
$\qquad x_1 W^{3/8} + x_5 W^{7/8} + x_3 W^{1/8} + x_7 W^{5/8} \tag{4.3.26}$

Third Step

$$X(j_2,j_1,j_o) = \frac{T}{8} \sum_{h_o=0}^{1} A_2(h_o;j_1,j_o) W^{\frac{r_2 k_2}{N_2}} \qquad (4.3.27)$$

$X_o = X(0,0,0) = \frac{T}{8}[A_2(0,0,0)W^o + A_2(1,0,0)W^o] =$

$\quad = \frac{T}{8}(x_o + x_4 + x_2 + x_6 + x_1 + x_5 + x_3 + x_7)$

$X_1 = X(0,0,1) = \frac{T}{8}[A_2(0,0,1)W^o + A_2(1,0,1)W^o] =$

$\quad = \frac{T}{8}(x_o + x_4 W^{4/8} + x_2 W^{2/8} + x_6 W^{6/8} + x_1 W^{1/8} + x_5 W^{5/8} + x_3 W^{3/8} + x_7 W^{7/8})$

$X_2 = X(0,1,0) = \frac{T}{8}[A_2(0,1,0)W^o + A_2(1,1,0)W^o] =$

$\quad = \frac{T}{8}(x_o + x_4 + x_2 W^{4/8} + x_6 W^{4/8} + x_1 W^{2/8} + x_5 W^{2/8} + x_3 W^{6/8} + x_7 W^{6/8})$

$X_3 = X(0,1,1) = \frac{T}{8}[A_2(0,1,1)W^o + A_2(1,1,1)W^o] =$

$\quad = \frac{T}{8}(x_o + x_4 W^{4/8} + x_2 W^{6/8} + x_6 W^{2/8} + x_1 W^{3/8} + x_5 W^{7/8} + x_3 W^{1/8} + x_7 W^{5/8})$

$X_4 = X(1,0,0) = \frac{T}{8}[A_2(0,0,0)W^o + A_2(1,0,0)W^{4/8}] =$

$\quad = \frac{T}{8}(x_o + x_4 + x_2 + x_6 + x_1 W^{4/8} + x_5 W^{4/8} + x_3 W^{4/8} + x_7 W^{4/8})$

$X_5 = X(1,0,1) = \frac{T}{8}[A_2(0,0,1)W^o + A_2(1,0,1)W^{4/8}] =$

$\quad = \frac{T}{8}(x_o + x_4 W^{4/8} + x_2 W^{2/8} + x_6 W^{6/8} + x_1 W^{5/3} + x_5 W^{1/8} + x_3 W^{7/8} + x_7 W^{3/8})$

$X_6 = X(1,1,0) = \frac{T}{8}[A_2(0,1,0)W^o + A_2(1,1,0)W^{4/8}] =$

$\quad = \frac{T}{8}(x_o + x_4 + x_2 W^{4/8} + x_6 W^{4/8} + x_1 W^{6/8} + x_5 W^{6/8} + x_3 W^{2/8} + x_7 W^{2/8})$

$X_7 = X(1,1,1) = \frac{T}{8}[A_2(0,1,1)W^o + A_2(1,1,1)W^{4/8}] =$

$\quad = \frac{T}{8}(x_o + x_4 W^{4/8} + x_2 W^{6/8} + x_6 W^{2/8} + x_1 W^{7/8} + x_5 W^{3/8} + x_3 W^{5/8} + x_7 W^{1/8})$

$$\qquad (4.3.28)$$

The final expressions in the equation 4.3.28 are identical to the expressions in equation 4.3.22. Nevertheless, the required number of operations with the FFT method is 24, while, according to equation 4.3.22, the number of operations would be 64. The order of operations and the elements used at each step of the previous example are illustrated in figure 15.

4.3.4 The FFT Computation

Although a FFT subroutine was available from the V.P.I. & S.U. computer library, it proved most efficient to develop a new program based on the formulation of chapter 4.3.2. The flow chart of this program is presented in figure 16.

A considerable saving in the computer time was obtained by the recursive calculation of the sines and cosines, in which the exponential terms are expanded, instead of recalling the built-in subroutines. The general exponential term is expanded as

$$W^{\frac{rk}{N}} = e^{-i2\pi\frac{rk}{N}} = \cos\frac{2\pi rk}{N} - i\cdot\sin\frac{2\pi rk}{N} \quad , \quad rk = 0,1,\ldots,N-1 \quad , \quad (4.3.29)$$

while the sines and cosines can also be expanded as

$$\cos\frac{2\pi rk}{N} = \cos\frac{2\pi(rk-1)}{N} \cos\frac{2\pi}{N} - \sin\frac{2\pi(rk-1)}{N} \sin\frac{2\pi}{N}$$

and

$$\sin\frac{2\pi rk}{N} = \cos\frac{2\pi(rk-1)}{N} \sin\frac{2\pi}{N} + \sin\frac{2\pi(rk-1)}{N} \cos\frac{2\pi}{N} \quad . \quad (4.3.30)$$

According to the expressions 4.3.30, all sines and cosines required can be calculated with simple operations from the initial values of $\cos\frac{2\pi}{N}$ and $\sin\frac{2\pi}{N}$. Furthermore, since all sines and cosines are simply related to the sines and cosines in the first quadrant, the expressions 4.3.30 need to be used only for values of rk equal to $0,1,\ldots,\frac{N}{4} - 1$.

4.4 Spectral Calculations in Each Block of Data

The FFT technique, as discussed in chapter 4.3, was developed for complex data sequences. When applied to real time histories, such as the records of atmospheric measurements, it permits the simultaneous computation of the Fourier transforms of two of these real time histories.

Given the two real discrete time histories, x_k and y_k, where $k = 0,1,\ldots,N-1$, a new complex sequence, z_k, can be generated as follows

$$z_k = x_k + iy_k \quad , \quad k = 0,1,\ldots,N-1 \quad . \quad (4.4.1)$$

If Z_r, $r = 0,1,\ldots,N-1$, is the discrete Fourier transform of z_k and Z_r^* its complex conjugate, it has been proved (see for instance reference 1), that the discrete Fourier transforms of the time histories x_r and y_r can be respectively calculated as

$$X_r = \frac{1}{2}[Z_r + Z_{N-r}^*] \quad , \quad r = 0,1,\ldots,\frac{N}{2} \quad (4.4.2)$$

and

$$Y_r = \frac{1}{2i}[Z_r - Z_{N-r}^*] \quad , \quad r = 0,1,\ldots,\frac{N}{2} \quad (4.4.3)$$

It has to be mentioned that the finite Fourier transform of a real time history has independent values only in the first half of the frequency domain, namely for frequencies up to the so called Nyquist frequency $\frac{N}{2T}$. The values of the Fourier transform in the second half of the frequency domain are simply the complex conjugates of respective values in the first half, i.e.

$$X_r = X^*_{N-r} \quad , \quad r = \frac{N}{2}, \frac{N}{2} + 1, \ldots, N \quad . \quad (4.4.4)$$

Taking advantage of the relations 4.4.2 and 4.4.3, the discrete Fourier transforms of two of the quantities T, u, v and w at a time are simultaneously calculated for each block of 8192 data points. The block-spectral density function estimates will be calculated with use of the expressions 4.1.1 and 4.1.4, appropriately modified for discrete time histories.

Let X_r^n and Y_r^n, $r = 0, 1, \ldots, \frac{N}{2}$, be the discrete Fourier transforms of the nth block of the blocked time histories x_k and y_k, $k = 0, 1, \ldots, N-1$. The block-power spectral density function estimate, $G_x^n(f_r)$, is then calculated as

$$G_x^n(f_r) = \frac{2}{T}|X_r^n|^2 \quad , \quad (4.4.5)$$

and the block-cross-spectral density function estimate, as

$$G_{xy}^n(f_r) = \frac{2}{T} X_r^{n*} Y_r^n \quad , \quad (4.4.6)$$

where $r = 0, 1, \ldots, \frac{N}{2}$ and $n = 1, 2, \ldots, M$.

The estimates of the coincidence and quadrature spectral density functions for each block can be independently calculated as

$$C_{xy}^n(f_r) = \frac{2}{T}[Re(X_r^n) \; Re(Y_r^n) - Im(X_r^n) \; Im(Y_r^n)] \quad (4.4.7)$$

and

$$-Q_{xy}^n(f_r) = \frac{2}{T}[Re(X_r^n) \; Im(Y_r^n) + Im(X_r^n) \; Re(Y_r^n)] \quad . \quad (4.4.8)$$

All block-spectral estimates need further to be multiplied by the scale factor 1/0.875, due to the cosine taper data window.

4.5 Smoothing of the Spectral Estimates

The block-spectral estimates, G_x^n and G_{xy}^n, as calculated in chapter 4.4, follow chi-square distributions of 2 degrees of freedom with mean values the respective spectral density functions, G_x or G_{xy}, and standard deviations equal to the respective mean values (see reference 1). This implies that the average systematic error of the estimate will be equal to 100%, which is quite unacceptable. Consistent estimates of the spectral density function can be obtained by smoothing the block estimates. A combined smoothing technique, of first smoothing over the ensemble of estimates (or segment averaging) and the smoothing over appropriate frequency intervals will be used to produce appreciably accurate spectral estimates. The combined smoothing is performed for the power spectral estimates and for the co- and quad-spectral estimates, which are of main interest.

Let G represent any of the quantities G_x, C_{xy} and Q_{xy}. The ensemble smoothing consists in averaging all block spectral estimates, G^n, so that the respective sample spectral estimates, $\overline{G}$, are obtained, i.e.

$$\overline{G}(f_r) = \frac{1}{M} \sum_{n=1}^{M} G^n(f_r) \quad , \quad r = 0,1,\ldots,\frac{N}{2} - 1 \quad . \quad (4.5.1)$$

The frequency smoothing consists in averaging all sample spectral estimates over a frequency interval $[f_{r+1}, f_{r+\ell}]$ and assign the average values to the center frequency $f_{r+\frac{\ell+1}{2}}$. Therefore, each value of the smoothed spectral estimates, $\hat{G}$, stands for ℓ values of the raw spectral estimates, $\overline{G}$, and is generated according to the expression

$$\hat{G}(f_{r+\frac{\ell+1}{2}}) = \frac{1}{\ell} \sum_{m=1}^{\ell} \overline{G}(f_{r+m}) \qquad . \qquad (4.5.2)$$

The nonuniform distribution of energy in the spectra requires that the frequency intervals for frequency smoothing are longer at the high frequency regions, where less power is present. The proposed frequency smoothing provides 46 values of the smoothed spectral estimates out of 4096 values of the raw spectral estimates. The calculation of these values and their distribution in the spectrum are obtained from the following expressions

$$q = 1,\ldots,4 \quad , \quad \ell = 1$$

$$\hat{G}(f_r) = \overline{G}(f_r) \qquad \qquad , \ r = q \qquad \qquad , \ (4.5.3)$$

$$q = 5,\ldots,15 \quad , \quad \ell = 4$$

$$\hat{G}(f_{r+2.5}) = \frac{1}{4} \sum_{m=1}^{4} \overline{G}(f_{r+m}) \qquad , \ r = 4(q-4) \qquad , \ (4.5.4)$$

$$q = 16,\ldots,24 \quad , \quad \ell = 16$$

$$\hat{G}(f_{r+8.5}) = \frac{1}{16} \sum_{m=1}^{16} \overline{G}(f_{r+m}) \qquad , \ r = 16(q-13) \quad , \ (4.5.5)$$

$$q = 25,\ldots,33 \quad , \quad \ell = 64$$

$$\hat{G}(f_{r+32.5}) = \frac{1}{64} \sum_{m=1}^{64} \overline{G}(f_{r+m}) \qquad , \ r = 64(q-22. \quad , \ (4.5.6)$$

$$q = 34,\ldots,46 \quad , \quad \ell = 256$$

$$\hat{G}(f_{r+128.5}) = \frac{1}{256} \sum_{m=1}^{256} \overline{G}(f_{r+m}) \quad , \ r = 256(q-31) \ . \ (4.5.7)$$

As discussed before, the estimates of the smoothed power, $\hat{G}_x$, coincidence, $\hat{C}_{xy}$, and quadrature, $\hat{Q}_{xy}$, spectral density functions are directly calculated with the use of the expressions 4.5.1,...,4.5.7. The smoothed estimates of the remaining spectral quantities, as defined

in chapter 4.1, have still to be computed. The magnitude, $|\hat{G}_{xy}(f)|$, and the phase angle, $\hat{\theta}_{xy}(f)$, of the smoothed cross-spectral density estimate are respectively calculated as

$$|\hat{G}_{xy}(f)| = [\hat{C}^2_{xy}(f) + \hat{Q}^2_{xy}(f)]^{\frac{1}{2}} \qquad (4.5.8)$$

and

$$\hat{\theta}_{xy}(f) = \arctan \frac{\hat{Q}_{xy}(f)}{\hat{C}_{xy}(f)} \qquad , \qquad (4.5.9)$$

while the smoothed estimate, $\hat{\gamma}^2_{xy}(f)$, of the coherency function is calculated as

$$\hat{\gamma}^2_{xy}(f) = \frac{|\hat{G}_{xy}(f)|^2}{\hat{G}_x(f)\,\hat{G}_y(f)} \qquad . \qquad (4.5.10)$$

4.6 Plotting of the Spectra

In this report, the product of the spectral density function at a certain frequency and the corresponding frequency itself is plotted versus the natural logarithm of the frequency. This type of presentation of the spectra provides a more detailed picture of the spectral functions in the higher frequency region where much less power is present with comparison to the low frequency region. In addition, this way of spectral plotting provides for a method of fast checking of the spectral estimates.

The variances and covariances of a pair of mean-free time histories are related to the power and coincidence spectral density functions respectively (see reference 1) by the relations

$$\overline{x^2} = \int_0^\infty G_x(f)\, df \qquad (4.6.1)$$

and

$$\overline{xy} = \int_0^\infty C_{xy}(f)df \qquad . \qquad (4.6.2)$$

By simply transforming the integrand quantities, one may rewrite the above relations as

$$\overline{x^2} = \int_0^\infty f \cdot G_x(f) \ d(\ln f) \qquad (4.6.3)$$

and

$$\overline{xy} = \int_0^\infty f \cdot C_{xy}(f) \ d(\ln f) \qquad . \qquad (4.6.4)$$

Therefore, the accuracy of the spectral estimates can be checked by comparing the respective values of the variances and covariances, as calculated with procedures described in chapter III, to the areas under the curves obtained by plotting the product of the frequency and the power or coincidence spectral density function values at this frequency versus the natural logarithm of this frequency.

CHAPTER V

DISCUSSION OF THE RESULTS

The objective of this thesis is to provide an efficient method
for the measurement and the analysis of atmospheric turbulence data
and specifically to explain the procedures used for the statistical
and spectral analysis of the data. Therefore, the discussion is based
on one complete set of results obtained from the analysis of the data
recorded at one specific run with one of the anemometer systems. From
the several records of data which were available at the time when this
thesis was written the data of run number 1 were selected. These data
were obtained on August 20, 1973, with the TSI #1193 anemometer at the
100-foot level of the 250-foot meteorological tower located at NASA
Wallops Island Flight Center. Calibration specifications for the TSI
#1193 anemometer are provided in figures 7, 8, 9, 10 and 11 and in
table I. For the mean velocity and mean probe-yaw angle of run 1,
shown in table IV, it can be seen from the figures 11 and 10 respec-
tively that the expected error in the calculation of the magnitude
of the velocity is of the order of 1 percent while the expected error
in the calculation of the velocity components does not exceed 4 percent.

The data-record consists of 475,136 data points, recorded at a
time increment of 0.005 seconds over a total time interval of approxi-
mately 39 minutes and 35 seconds. As discussed in section 3.3, it is
divided into 58 blocks consisting of 8192 data points each, extending

52

over a time interval of approximately 41 seconds. The block-mean values
for the velocity components in the sensor oriented coordinate system,
their standard deviations, the velocity magnitude and the probe-yaw
angle are shown in table II. By inspecting the variation of these quan-
tities over the total number of blocks, one may observe a random rather
than systematic varying distribution. Only for the last four blocks
the mean wind seems to change slightly in magnitude as well as direction
but without any considerable change in its frequency composition. The
total number of reverse arrangements for the block-means of the above
quantities is also shcwn in table II. One can see that all the calcu-
lated values for the number of reverse arrangements lie within the limits
of assumed stationarity as discussed in section 3.4. Therefore, it
was decided to consider the data of run 1 as being stationary and, hence,
to proceed with the statistical and spectral analysis.

The block-means of the temperature and the velocity components in
the mean-wind oriented coordinate system are shown in table III. It can
be seen from this table that the vertical and lateral components take
values much smaller than the values of the longitudinal component, which
confirms that the mean wind is nearly horizontal, and nearly parallel to
the axis of the probe. The sample-mean values of the temperature, the
velocity components in the mean wind direction, the magnitude and phase
angle of the velocity vector and all variances and covariances, obtained
by averaging the respective block-mean values, are shown in table IV.
As shown in this table, the calculated value of the sample probe-yaw
angle is very small (approximately 1.34 degrees), which is a good indi-

cation for the accuracy of the measurements. This mean wind is coming
from a south-eastern direction, namely directly from the Atlantic Ocean
without any considerable upstream obstacle distortion.

It has to be emphasized at this point that the values of the vari-
ances and covariances depend on the length of the block-time interval
considered, due to the change in the block-mean values which are sub-
tracted from the instantaneous values. As discussed in section 4.6,
the variances and covariances represent the area under a spectral curve.
This area obviously depends on the frequency interval considered. For
instance, it has been generally accepted that the complete power spectrum
of the longitudinal wind component has a form similar to the one shown
in figure 17, as calculated by Van der Hoven from measurements at Brook-
haven. This spectrum extends over a wide range of frequencies and pre-
sents two major peaks. The peak at the low-frequency region (at a period
of approximately 100 hours) corresponds to periodic passage of cold or
warm fronts, while the peak at the high-frequency region (at a period of
the order of 1 minute) corresponds to the turbulent fluctuations of the
wind. It is the latter part of the velocity spectrum, often called the
"gust velocity" spectrum, which is of interest in the study of turbulence.
The region of the spectrum between the two peaks, called the "mesometeor-
ological gap" contains very little power, due to the fact that no normal
physical process can produce velocity fluctuations with frequencies
lying in this range.

Therefore, the values of variances and covariances are consistent
and comparable to each other, only when they are calculated from data-

blocks extending over time intervals large enough to determine the spectrum down to frequencies near the mesometeorological gap, usually of the order of one cycle per hour. This, of course, would require data-samples extending over intervals of the order of several hours. For a given fixed data-sample, the block-time length can be increased by dividing the sample into a smaller number of blocks. This method has the disadvantage that it provides less accurate values for the sample-variances and covariances, since they are calculated as the average of a smaller number of block-values.

The block-time length effect can be well illustrated with the use of the turbulence intensities, defined as the ratios of the standard deviations of the velocity components in the mean wind oriented coordinate system and the velocity magnitude. The turbulence intensities calculated from the data of run 1 for the block time lengths of approximately 41, 328 and 1188 seconds are shown in table V. It can be seen from this table that the values of the turbulence intensities increase considerably as the block-time length is increased, especially in the case of the lateral velocity component.

The block-time length is also of great importance for the power and cross-spectra, since it determines the lower frequency for which a spectral density fu_tion can be estimated from a given sample of data. Consider a sample of data consisting of M blocks of N data points each, sampled at a time increment Δt. Then the block-time length is equal to $N \cdot \Delta t$, while the total sample-time length will be equal to $M \cdot N \cdot \Delta t$. The smooth spectral estimates, as discussed in chapter IV, can be obtained

for the frequency range between the lowest frequency (or fundamental frequency), $1/N \cdot \Delta t$ and the Nyquist frequency (or folding frequency), $1/2 \cdot \Delta t$. Since the number of data per block, N, is held fixed equal to 8192 due to the FFT needs, the only way of estimating the spectra in lower frequency regions is to increase the time increment, Δt, i.e. to consider selectively only one part of the data points, separated from each other with a longer time increment, Δt. As a result of the fixed sample-time length, the number of blocks, M, has to be adequately decreased, with the consequence of decreasing the effectiveness of the ensemble smoothing.

The smooth spectral estimates in the frequency range from approximately 0.0244 hertz up to 100 hertz, are calculated by considering all data points, namely taking $\Delta t = 0.005$ seconds and M = 58. Spectral estimates for lower frequencies down to 0.0030 hertz are obtained by considering one data-point out of eight, i.e. by taking $\Delta t = 0.040$ seconds and, as a consequence, M = 7. An attempt of estimating spectral values for frequencies as low as 0.00084 hertz by taking $\Delta t = 0.145$ seconds and M = 2 (i.e. considering only one every 29 data points) was abandoned, as producing unacceptably high distorted spectral estimates as a result of the poor ensemble smoothing.

The power spectra of the longitudinal, the lateral and the vertical velocity components and the temperature are shown in figures 18, 19, 20 and 21 respectively. It can be seen in these figures that the power spectral estimates show a considerably small amount of scatter, expecially for frequencies higher than approximately 0.1 hertz. At the

lower frequency region, there exists higher scatter of the spectral

values, due primarily to the absence or inefficiency of the frequency

smoothing, as discussed in section 4.5. It can also be seen that spec-

tral values estimated from data sampled at time increments equal to

0.005 and 0.040 seconds are in general consistent, while increasing the

time increment to 0.145 seconds provides highly distorted values. The

form of the curves that can be fitted to the calculated spectral values

for the velocity components is in general monotonously decreasing, which

confirms that the estimated spectra lie in the gust velocity region. The

spectral curves approach zero at some frequency higher than 100 hertz.

Some high power spectral values, not shown in the above figures, were

calculated for frequencies close to 100 hertz but were discarded as

resulting from resolution errors. It has to be recalled at this point

that all frequencies higher than 100 hertz were removed from the original

data with the use of sharp low-pass electronic filters.

The estimated values of the magnitude of the cross-spectral density

function, the co-spectral density function and the coherence function

between the longitudinal and the vertical velocity components are shown

in figures 22, 23 and 24 respectively. These estimates are in general

less smooth than the power spectral estimates, due to the higher err r

involved in the calculations between two time histories. Of specific

interest is figure 24, since it indicates that the longitudinal and the

vertical velocity component fluctuations are completely incoherent for

all frequencies below a cut-off frequency of approximately 5 hertz.

Nevertheless, these fluctuations are considerably coherent for higher

frequencies, with an average value of the coherence function approximately equal to 0.6.

The checking of the accuracy of the spectral estimates, as suggested in section 4.6, was performed for all the above cases with satisfactory results.

CHAPTER VI

CONCLUSION AND RECOMMENDATIONS

Concluding the discussion that has been made in the previous chapters of this thesis, one could summarize what was achieved as follows.

Highly accurate measurements are necessary for the detailed description of the wind flow in the atmospheric boundary layer. The data obtained from these measurements have also to be in an appropriate form in order to provide accurate estimates of the required statistical and spectral quantities. To meet these requirements, a complete instrumentation system was designed and a new data-analysis method was developed.

The TSI 1080 three-dimensional split-film anemometer system was selected for the measurement of the instantaneous values of the wind-velocity vector and the temperature. It provides seven output voltages from which the velocity components in the sensor-oriented coordinate system and the temperature can be calculated. The general calibration procedure, which was suggested by TSI, was proved to be complicated and inaccurate and, therefore, a new co   e calibration procedure had to be developed. This calibration was based on the recognized fact that the anemometer gives the most accurate results when the probe operates with its axis parallel to the direction of the mean-wind vector and the sensors directed into the wind.

All measurements that were necessary for the calibration were performed at the Quality Verification and Calibration Facility at NASA

Wallops Flight Center. The entire procedure was streamlined into a standard form, allowing a quick and efficient calibration of the large number of anemometers used in this research program. Based on this calibration, a computer program was developed, which converts the output voltages of the anemometers into the actual velocity components and the temperature. The accuracy of the obtained quantities was checked and found satisfactory.

Six probes were mounted at the elevations of 30, 50, 100, 150, 200 and 250 feet on the 250-foot meteorological tower located at Wallops Island on the Atlantic coast. All probes could be rotated so that their axis could be placed closely parallel to the mean wind direction. A new complete data-acquisition system was designed and fixed in an instrumentation trailer, which enabled easy transportation and protection of the system. At each run of the system, the output voltages from all six anemometers were simultaneously recorded on analog magnetic tapes. Later, each analog tape was played back and the analog signals from each anemometer were digitized, sampled at a rate of one data-point every 0.005 seconds and recorded on a digital magnetic tape. Due to its complexity, the data-acquisition system requires elaborate calibration checks to insure its proper operation. The time duration of each data-sample is approximately 40 minutes, as imposed by the maximum capacity of the analog tapes. It has been attempted to increase the sample time by using a lower speed of the analog tape-recorder, but this resulted in unacceptably high noise-levels in the recorded signals.

Each of the above digital magnetic tapes contains a record of the

seven output voltages of one TSI anemometer at one run of the system.
With the use of the program "CONVERSION", as shown in the appendix,
a new magnetic tape was generated, containing a record of the three
velocity components in the sensor oriented coordinate system and the
temperature. Each time history consists of approximately 480,000 data
points, separated from each other with a time interval of 0.005 seconds.

Consistent estimates of the statistical and spectral quantities
could be obtained only if certain averaging procedures would be applied
to the data. Therefore, each time history was divided into a number
of data-blocks, so that all desired quantities would be calculated as
averages of the respective block-values. The number of data-points in
each block was fixed and equal to 8192, as imposed by the fast Fourier
transform needs and the capacity of the available computer. The entire
analysis was based on the assumption that the measured time histories
were stationary, which implies that all statistical quantities do not
vary significantly over the total sample time interval. This assump-
tion was checked with the use of the program "STATIONARITY". This
program provides the block-mean values and the block-standard deviations
of the velocity components and the temperature as well as the results
of a statistical test which detects monotonic trends of the above quan-
tities. Each data-record was further processed, only if the results of
the inspection of the statistical block-values and the trend test would
ensure stationarity within reasonable limits of confidence.

The velocity components in the sensor-oriented coordinate system
do not possess any physical meaning. Therefore, a coordinate transfor-

mation into a coordinate system connected with the mean wind direction was necessary. This transformation provided the longitudinal, lateral and vertical velocity components, which could give a good description of the properties of the wind velocities. The new velocity components were calculated and together with the temperature recorded on a new digital magnetic tape with the use of the computer program "MEAN-WIND". This program also provides the variances and covariances of the above four time histories as well as the turbulence intensities. As already mentioned, each time history has been divided into a number of blocks and all sample-quantities were calculated as the averages of the block-values.

One of the main objectives of this thesis was to provide a method for the calculation of reasonably accurate measurements of the power and cross-spectral density functions of all three velocity components and the temperature, expecially in the high frequency range between 0.1 and 100 hertz. Such a high frequency range is necessary for the understanding of the turbulent stresses, turbulent transport phenomena and turbulent dissipation. Spectral estimates for lower frequencies down to 0.003 hertz were also calculated, but with lower accuracy due to the limited time length of each data-sample.

It was recognized that the finite record-length of the data used, would produce a certain amount of distortion in the spectral estimates. Therefore, the cosine taper data window was used to reduce this effect. The power, cross-, co- and quad-spectral density function estimates and the coherence function estimate were calculated with the direct Fourier

transform method. A new fast Fourier transform technique was developed

and used to enable fast and effective computations. This FFT technique

possesses the addidional advantage of not requiring any bit-reversal

operation. A recursive computation of the necessary sines and cosines

was also used to further reduce the computation time.

First, a set of raw spectral estimates were obtained for each

block of 8192 data-points. Each block-spectral estimate consists of

4096 discrete values. Then all block-spectral values corresponding

to each frequency were averaged to produce the sample-spectral estimates,

consisting also of 4096 discrete values. Finally, the sample-spectral

values were averaged over appropriate frequency intervals to produce

the smooth spectral function estimates, consisting of 46 spectral values

each. The frequency intervals were arranged in such a way, that the

consequent smooth spectral values would be separated by an approximately

constant distance, when plotted versus a logarithmic frequency scale.

It was also decided to represent the spectral estimates by plotting the

smooth spectral density functions multiplied by the respective frequency

versus the natural logarithm of the frequency. This way, a clear repre-

sentation of the spectra in the high frequency region was obtained,

although very small power is present in this region. A fast way of

checking the accuracy of the spectral curves was possible by comparing

the areas under these curves to the respective values of variances and

covariances. The smooth spectral estimates are in general much more

reliable than the raw spectral estimates, since they are almost free of

scatter which may occur in a specific sample but is not due to an

existing physical process. The smooth estimates obtained according to the methods discussed, are considered to be reliable for use in most applications. All computations that were necessary in order to obtain the smooth spectral estimates of the three velocity components and the temperature, were performed with the use of the program "SPECTRA", also shown in the appendix. This program can be used in any sufficiently large modern digital computer.

The discussion in this thesis was confined on one single record of data, obtained with one anemometer system at the 100-foot level of the meteorological tower. The main concern was to develop and check the proposed method for the measurement and the statistical analysis of atmospheric turbulence. As soon as several complete sets of measurements from all six anemometers at the different elevations of the meteorological tower are available, this method can be used to provide sufficient material for a documented discussion on several important aspects of the turbulence in the atmospheric boundary layer.

At the time this thesis was written, a number of modifications and extensions of the above method were conceived but were not executed due to the lack of time and the limitations of the computing facilities at NASA Wallops Flight Center. Nevertheless, these modifications and extensions are presented here so that they can be used in the continuation of this research project.

1. Increase of the number of data per block. A final modification of the computer program used for spectral calculations enabled the reduction of the amount of computer memory required, so that a number of

16,384 data points could be simultaneously handled with the IBM 370
computer. Therefore, the number of data per block can be increased from
8,192 = 2^{13} to 16,384 = 2^{14}. This modification will increase the fre-
quency interval for which spectral estimates can be obtained to the
frequency range between approximately 0.0122 and 100 hertz and is also
expected to improve the accuracy of all spectral estimates.

     Calculation of the auto- and cross-correlation functions. As
discussed in section 4.1, the auto-correlation function and the cross-
correlation function form Fourier transform pairs with the power and the
cross-spectral density functions respectively. Therefore, the correla-
tion functions, $R_x(\tau)$ and $R_{xy}(\tau)$, can be calculated as the inverse
Fourier transforms of the spectral density function estimates, $\hat{G}_x(f)$
and $\hat{G}_{xy}(f)$, respectively.

When auto- and cross-correlation functions are calculated from
spectral estimates, obtained from finite discrete time histories, cer-
tain considerations have to be made in order to avoid erroneous results.
Details on these considerations and computational recipes can be found
in the references 1 and 16.

     3. Calculation of the integral scales of turbulence. The integral
scale lengths of turbulence characterize the maximum distance of two
points whose velocity fluctuations are correlated. Once the auto-cor-
relation functions are calculated, as discussed in the previous section,
simple integrations can provide the Eulerian integral time scales of
turbulence in the mean wind direction. Then, by assuming the validity
of Taylor's hypothesis, the integral scale lengths of turbulence in

the mean wind direction can also be obtained. These scales are an

estimate of the physical size of the turbulent eddies in the direction

of the mean wind at the different tower levels.

4. Calculation of the cross-spectra and cross-correlations between

the velocity components and the temperature at different altitudes.

These quantities can be easily calculated by combining the data obtained

from the anemometers located at different elevations on the meteorological

tower. The study of the variation of these quantities with height can

provide significant information about the vertical momentum and heat

flux as well as the vertical scales of the turbulence.

REFERENCES

1. Bendat, J.S. and A.G. Piersol, "Random Data: Analysis and Measure-
    ment Procedures", Wiley-Interscience, New York 1971.

2. Bergland, G.D., "A Guided Tour of the Fast Fourier Transform",
    IEEE Spectrum, Vol. 6 pp. 41-52, July 1969.

3. Bingham, C., M.D. Godfrey and J.W. Tukey, "Modern Techniques of
    Power Spectrum Estimation", IEEE Transactions on Audio and
    Electroacoustics, Vol. AU-15, No. 2, June 1967.

4. Blackadar, A.K., H.A. Panofsky and F. Fiedler, "Investigation of
    the Turbulent Wind Field Below 500 Feet Altitude at the Eastern
    Test Range, Florida", NASA CR-2438, June 1974.

5. Blackman, R.B. and J.W. Tukey, "The Measurement of Power Spectra",
    Dover Publications, New York, 1958.

6. Busch, N.E. and H.A. Panofsky, "Recent Spectra of Atmoshperic
    Turbulence", Quarterly Journal of the Royal Meteorological
    Society, Vol. 94, April 1968.

7. Carl, D.M., T.C. Tarbell and H.A. Panofsky, "Profiles of Wind
    and Temperature from Towers over Homogeneous Terrain", Journal
    of the Atmospheric Sciences, Vol. 30, pp. 788-794, 1973.

8. Champagne, F.H., C.A. Sleicher and O.H. Wehrmann, "Turbulence
    Measurements with Inclined Hot Wires", Journal of Fluid Mechanics,
    Vol. 28, pp. 153-175, 1967.

9. Cooley, J.W. and J.W. Tukey, "An Algorithm for the Machine Cal-
    culation of Complex Fourier Series", Mathematics of Computer,
    Vol. 19, pp. 297-301, April 1965.

10. Hinze, J.O., "Turbulence", McGraw-Hill Book Co., Inc., New York,
    1959.

11. IUCRM Symposiu Proceedings, Part I, "Waves and Turbulence in
    Stable Layers and their Efeects on EM Propagation", Boundary-
    Layer Meteorology, Vol. 4, April 1973.

12. Kaimal, J.C., J.C. Wyngaard, Y. Izumi and O.R. Coté, "Spectral
    Characteristics of Surface-Layer Turbulence", Quarterly Journal
    of the Royal Meteorological Society, Vol. 98, pp. 563-589, 1972.

13. Lumley, J.L. and H.A. Panofsky, "The Structure of Atmospheric Turbulence", John Wiley and Sons, Inc., 1964

14. Monin, A.S., "The Atmospheric Boundary Layer", Ann. Rev. of Fl. Mech., Vol 2, 1970.

15. Olin, J.G. and R.B. Kiland, "Split-Film Anemometer Sensor for Three-Dimensional Velocity-Vector Measurements", Symposium on Aircraft Wake Turbulence, Seattle, September 1970.

16. Otnes, R.K. and L. Enochson, "Digital Time Series Analysis", John Wiley and Sons, Inc., New York, 1972.

17. Panofsky, H.A., "The Atmospheric Boundary Layer Below 150 Meters", Ann. Rev. of Fl. Mech., Vol. 6, 1974

18. Plate, E.J., "Aerodynamic Characteristics of Atmospheric Boundary Layers", AEC Critical Review Series, 1971.

19. Schlichting, H., "Boundary Layer Theory", McGraw-Hill Book Co., 1968.

20. Teunissen, H.W., "Characteristics of the Mean Wind and Turbulence in the Planetary Boundary Layer", U.S. Dept. of Commerce AD 722047, 1970.

21. Thermo-Systems, Inc., "Operating and Service Manual for Total Vector Velocity System", Saint Paul, Minnesota, 1970.

22. Tieleman, H.W., K.P. Fewell and H.L. Wood, "An Evaluation of the Three-Dimensional Split-Film Anemometer for Measurements of Atmospheric Turbulence", VPI-E-73-9, March 1973.

23. Tieleman, H.W. and W.W.L. Chen, "Statistical Analysis of Low Level Atmospheric Turbulence", VPI-E-74-3, January 1974.

24. Van Atta, C.W., "Sampling Techniques in Turbulence Measurements", Ann. Rev. of Fl. Mech., Vol. 6, 1974.

25. Vinnichenco, N.K., N.Z. Pinus, S.M. Shmeter and G.N. Shur, "Turbulence in the Free Atmosphere", Consultants Bureau, New York-London, 1973.

26. Wyngaard, J.C. and O.R. Coté, "The Budgets of Turbulent Kinetic Energy and Temperature Variance in the Atmospheric Surface Layer", J. of Atmosph. Sc., Vol. 28, March 1971.
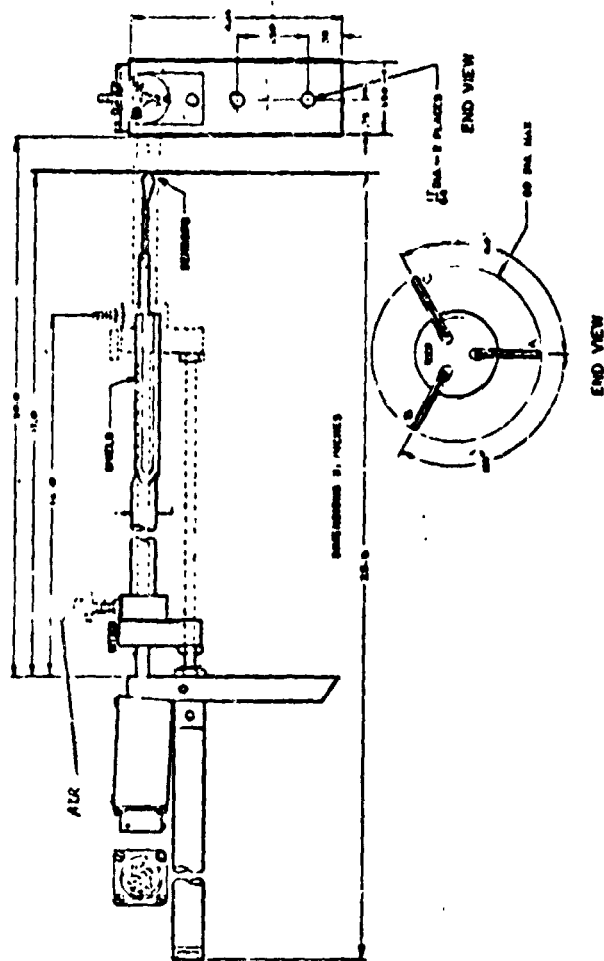
Figure 1: Schematic Drawing of the TSI 1296E Probe.
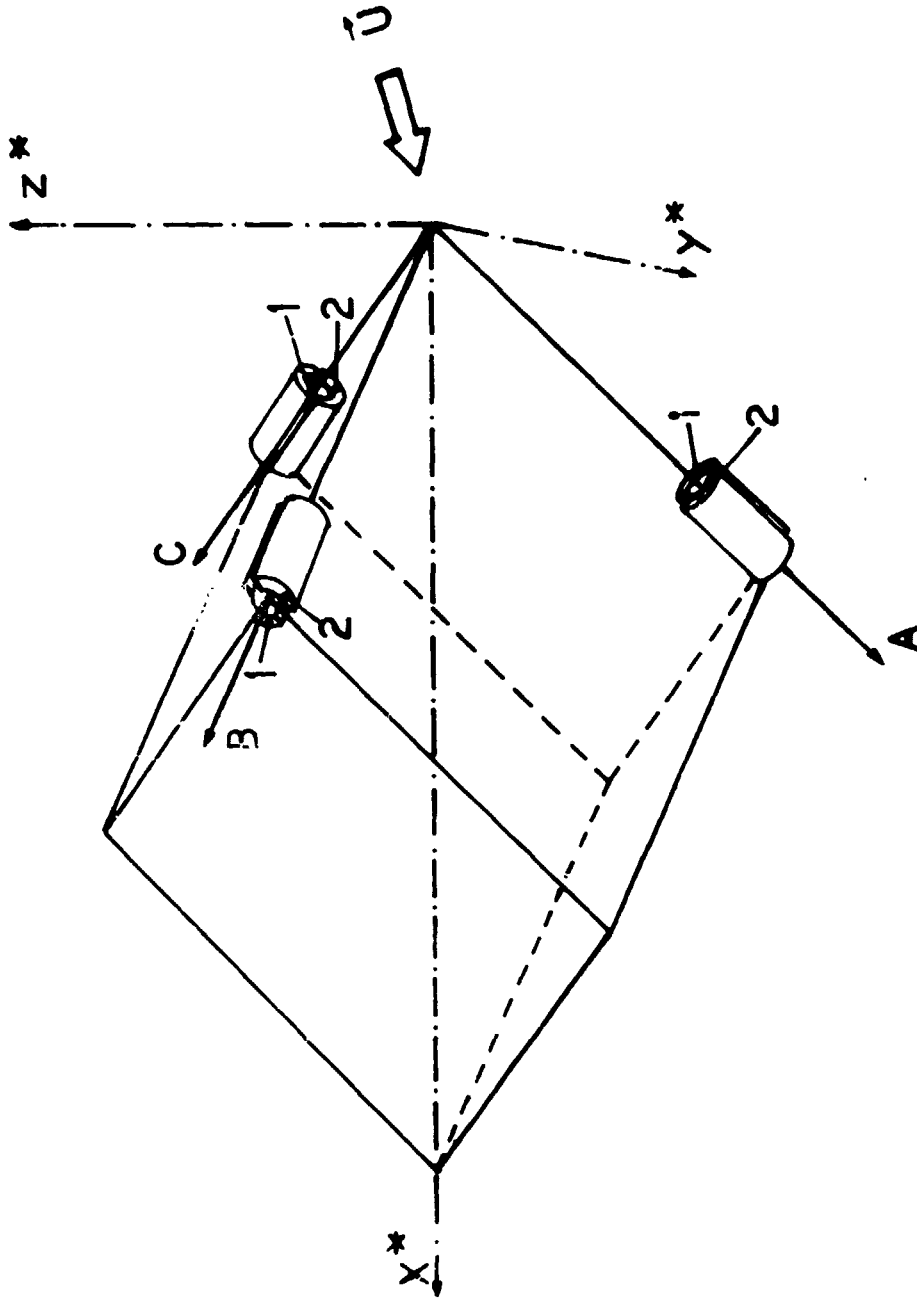
Figure 2: Schematic Diagram of the Sensor Oriented Coordinate System, ABC, and the Probe Oriented Coordinate System, x*y*z*.
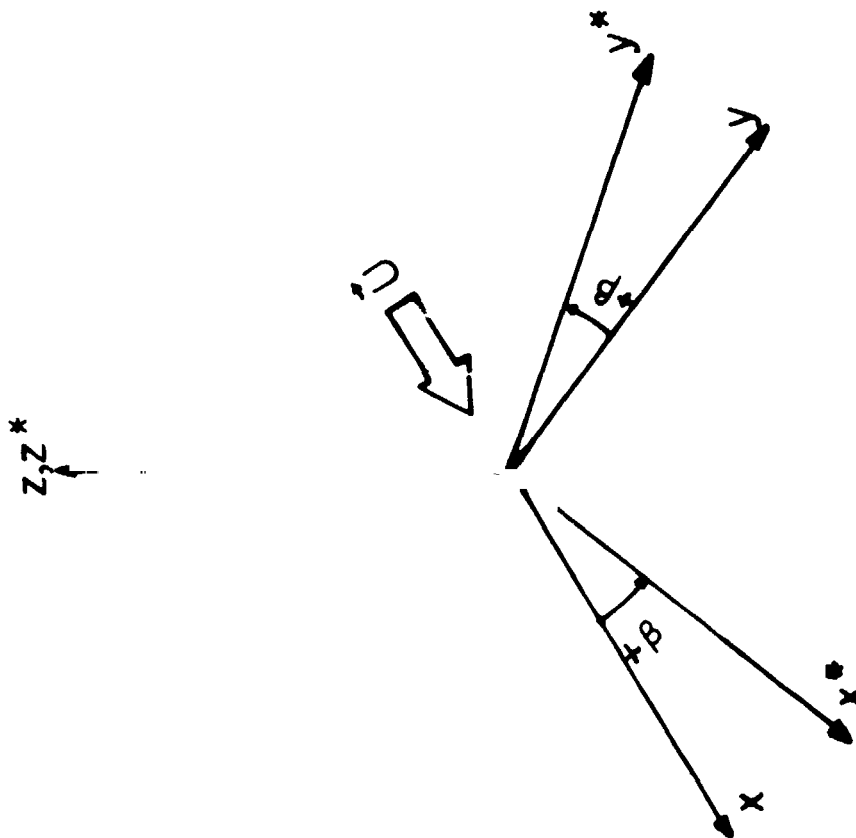
Figure 3: Schematic Diagram of the Probe Oriented Coordinate System, x*y*z*, and the Mean Wind Oriented Coordinate System, xyz, with the Probe-Yaw Angle, β, and the Mean Wind Vector, Ū.
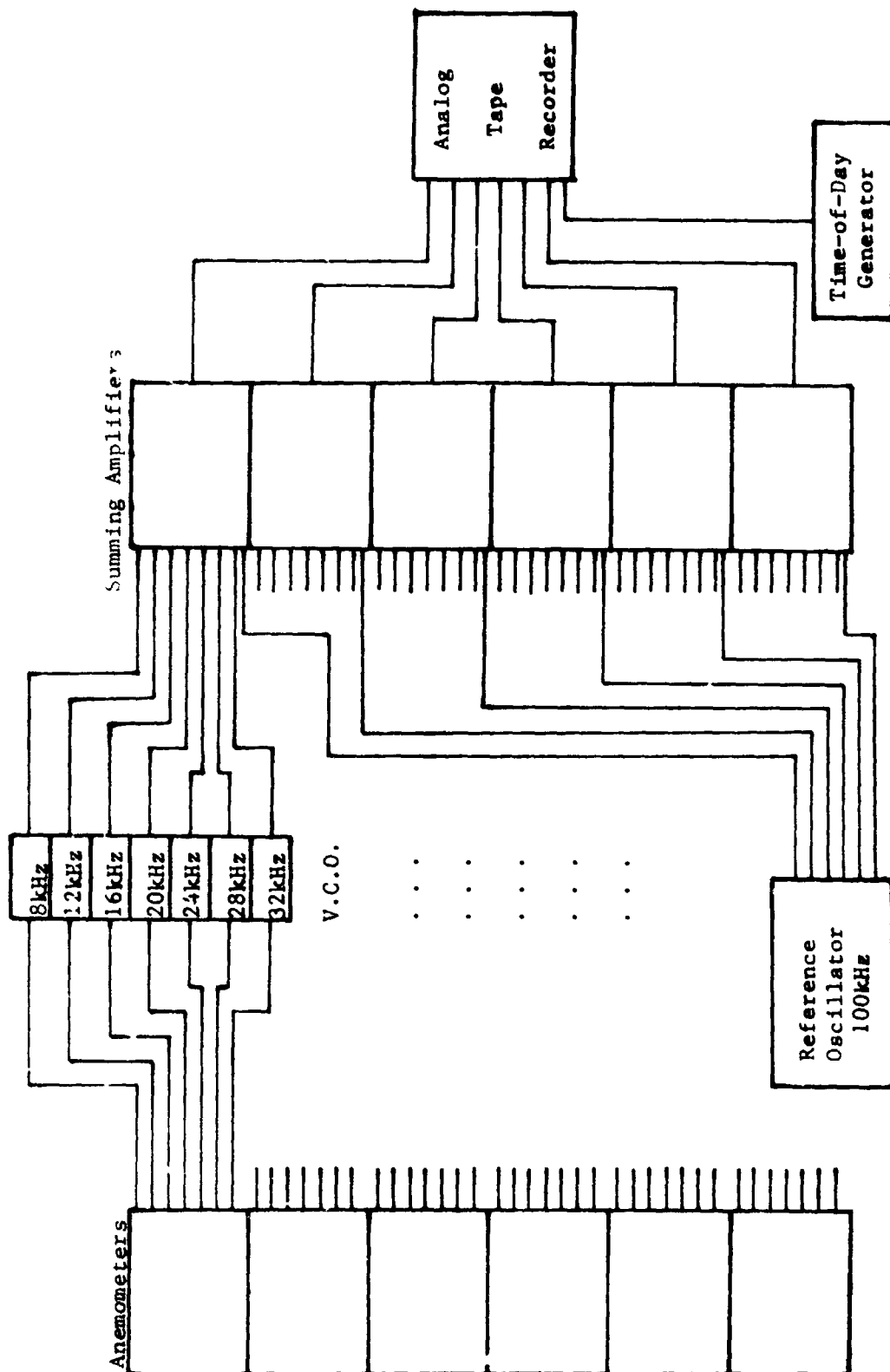
Figure 4: Multiplexing and Analog Recording System.
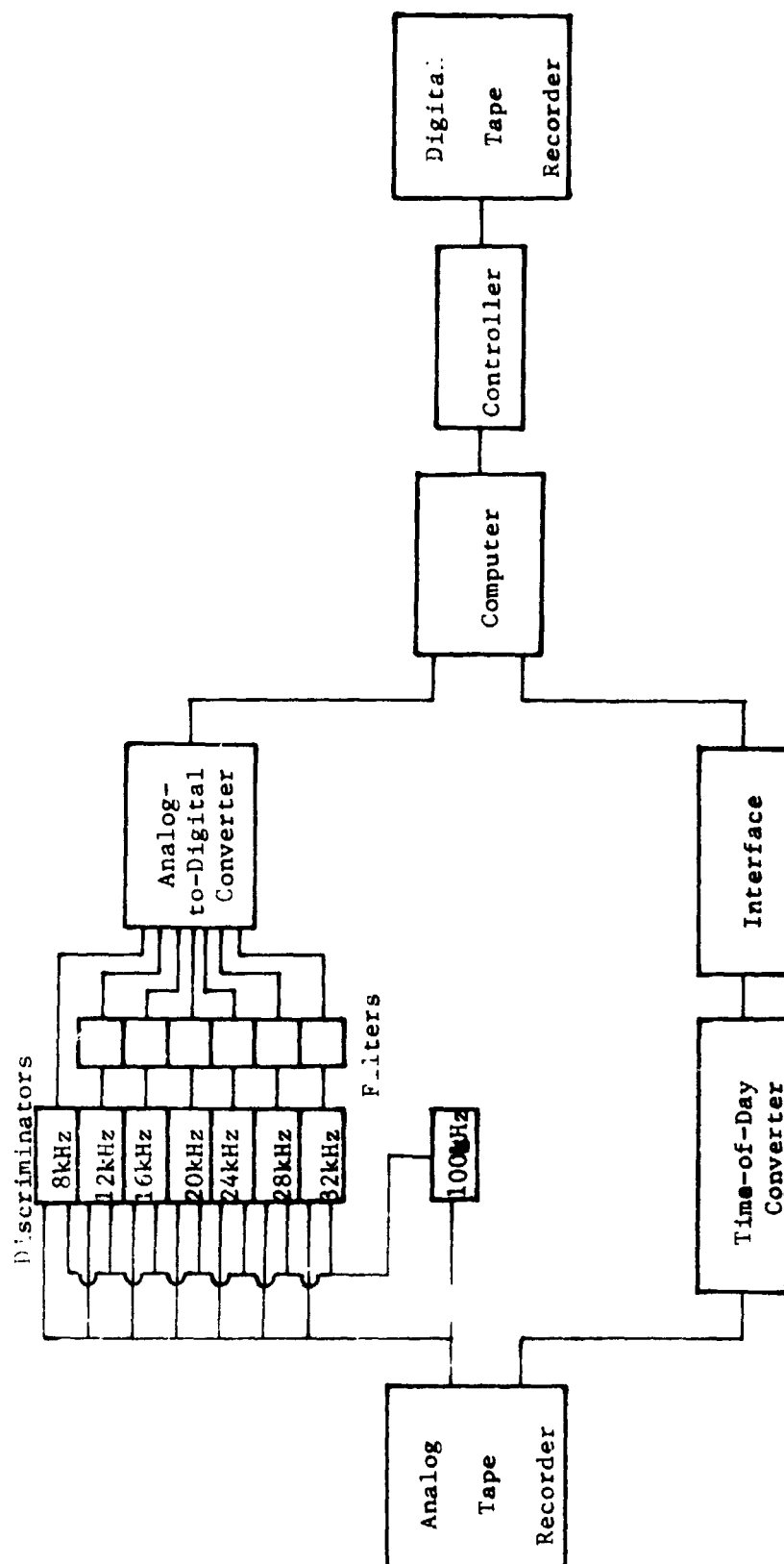
Figure 5: Demultiplexing, Digitizing and Digital Recording System.
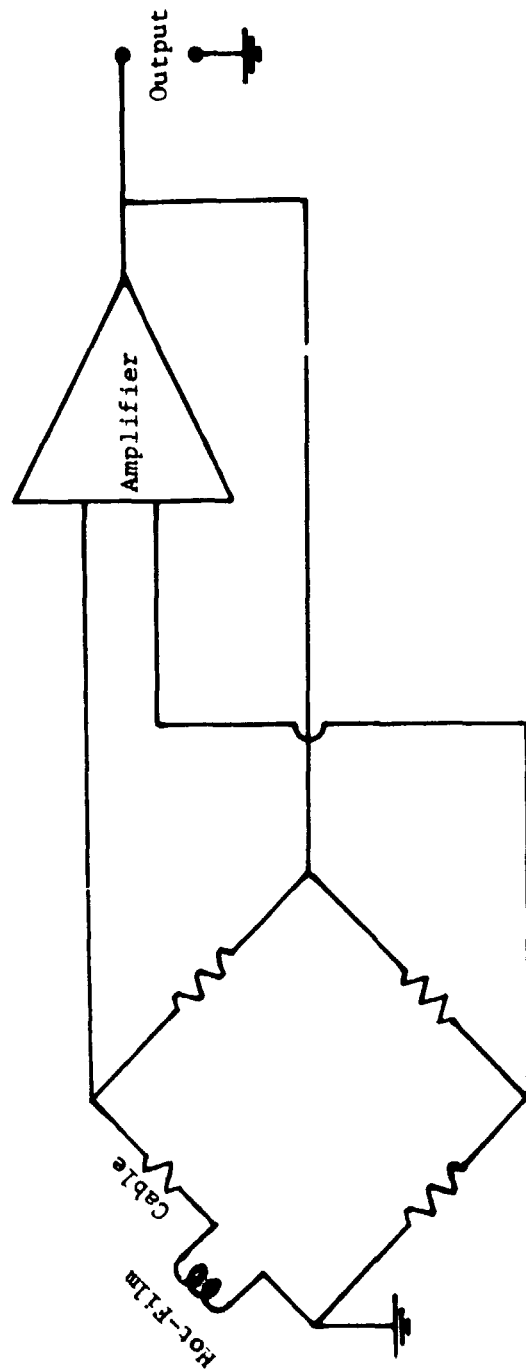
Figure 6: Schematic Diagram of a Constant-Temperature Anemometer Circuit.
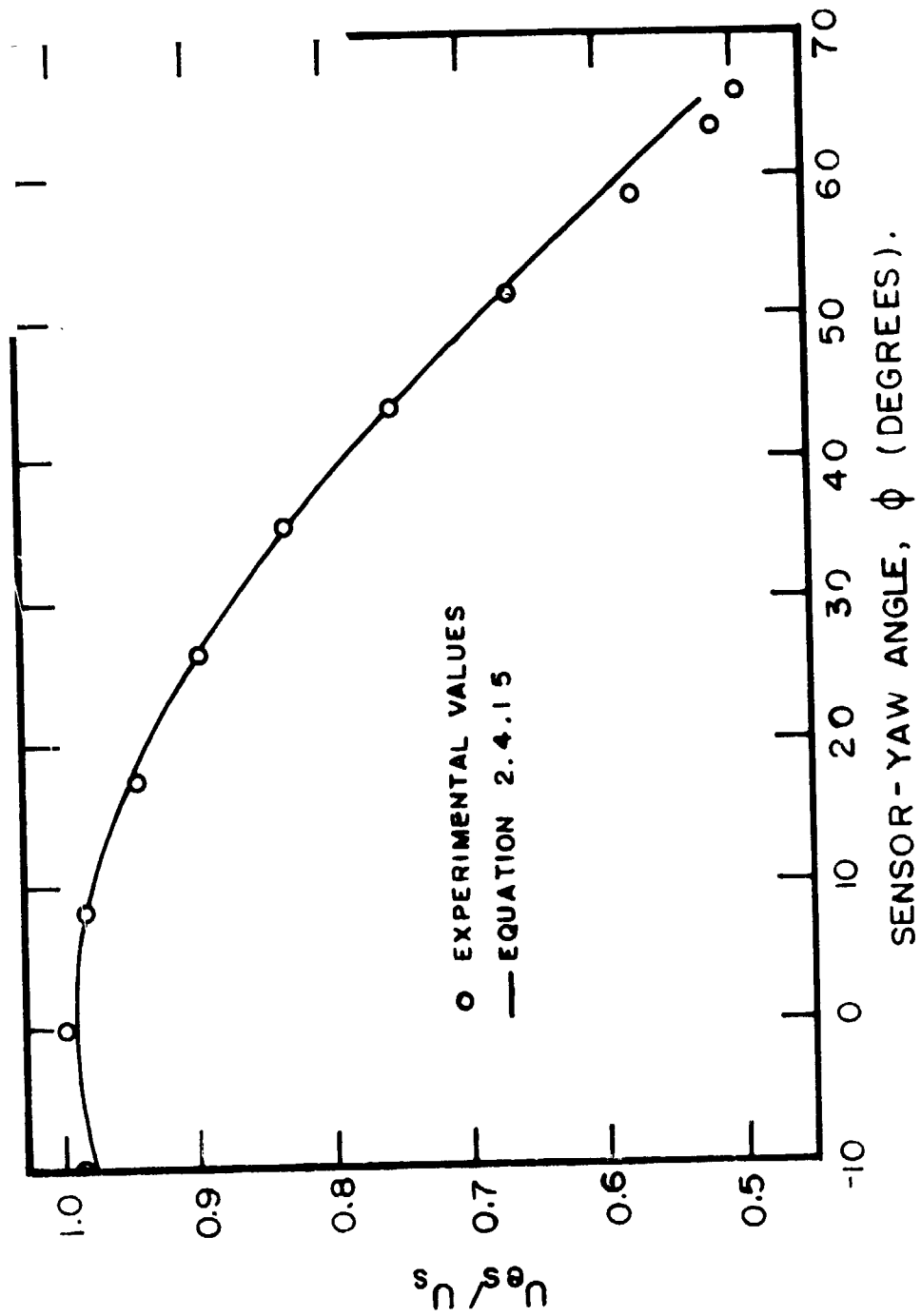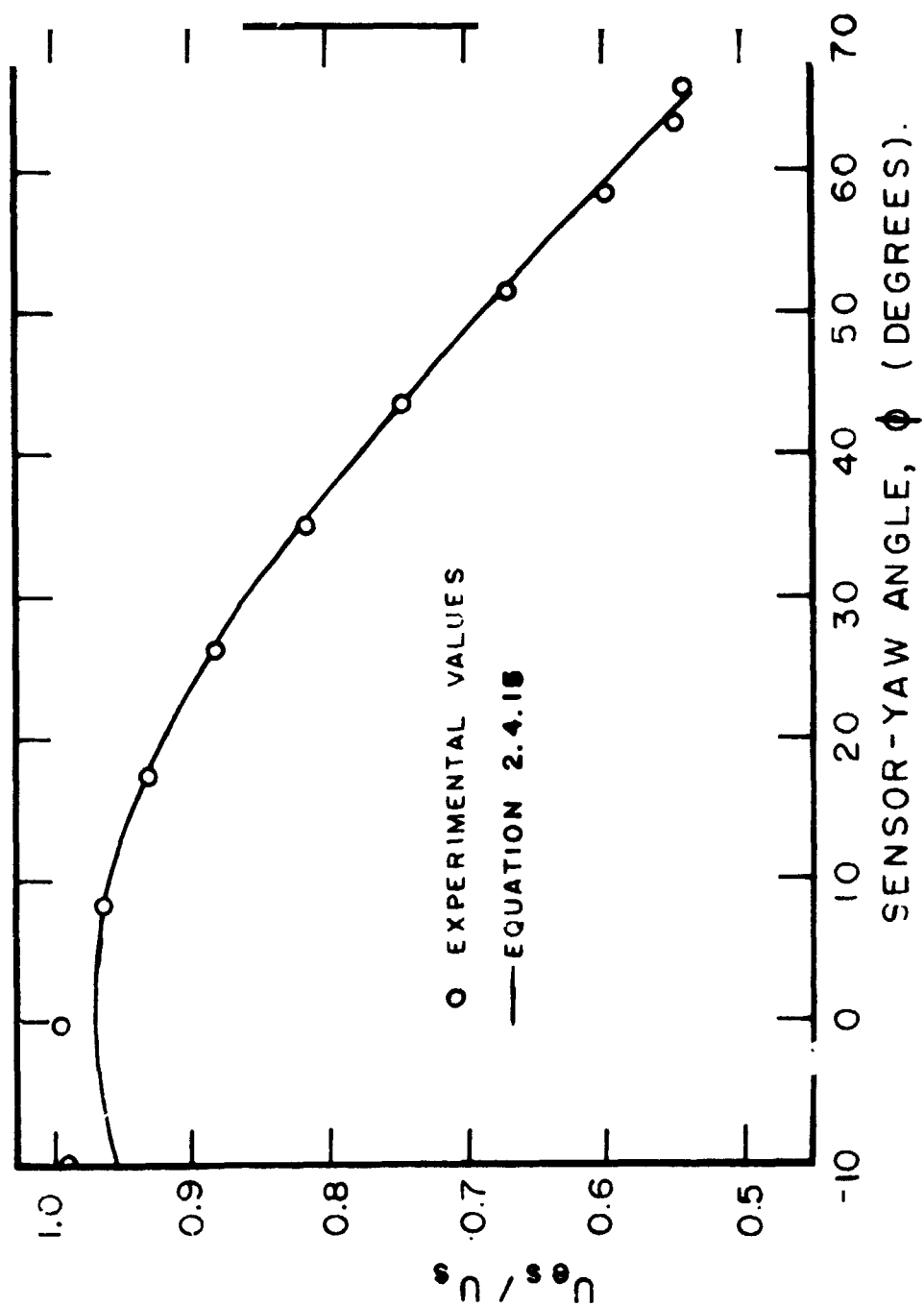
Figure 7. Calibration Curve for U_{es}/U_s vs. ϕ, Sensor E #1192.

Figure ? Calibration Curve for U_{es}/U_s vs. ϕ, Sensor C #1193.
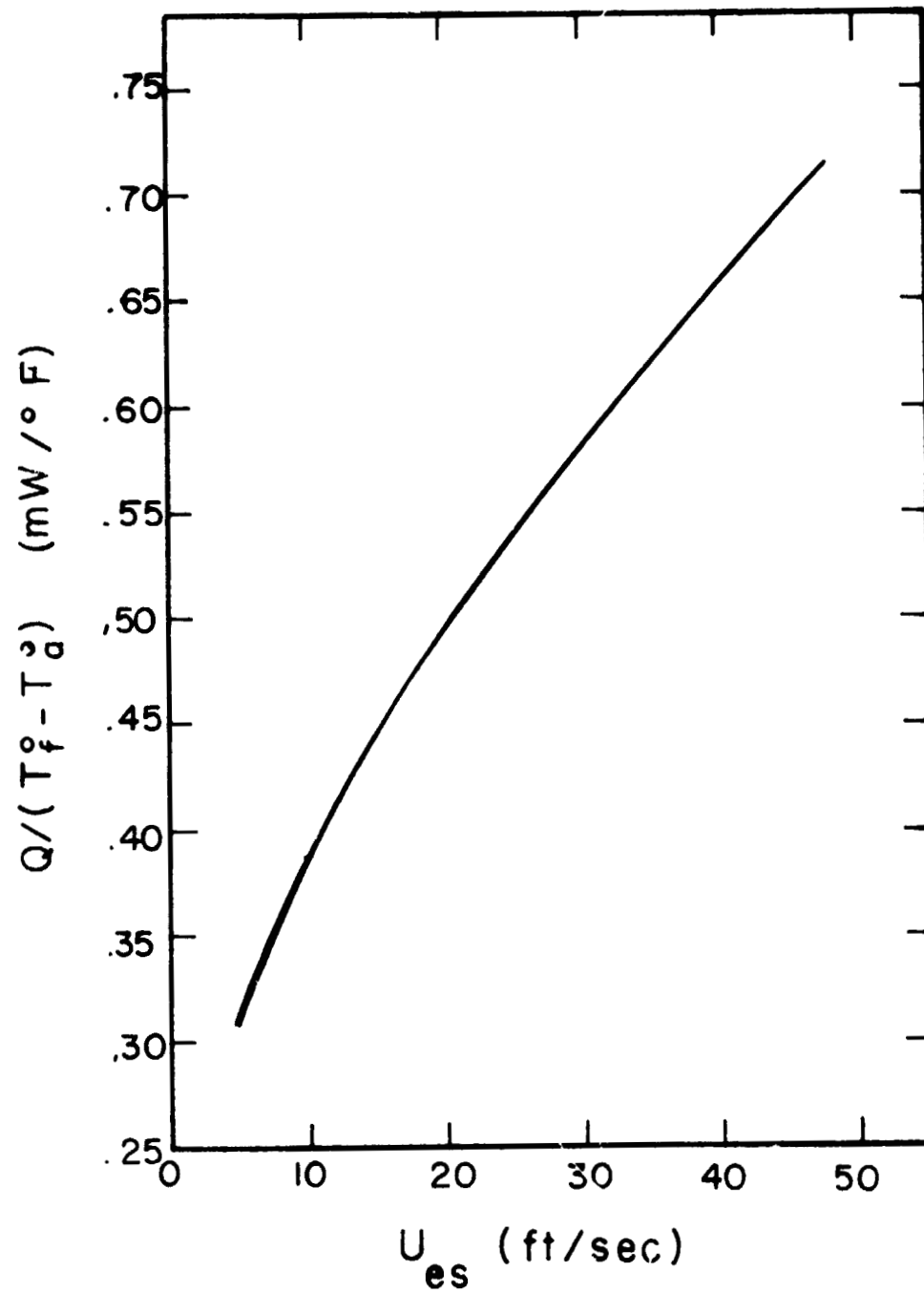
Figure 9: Calibration Curve for $Q/(T_f^o - T_a^o)$ vs. U_{es}, #1193.
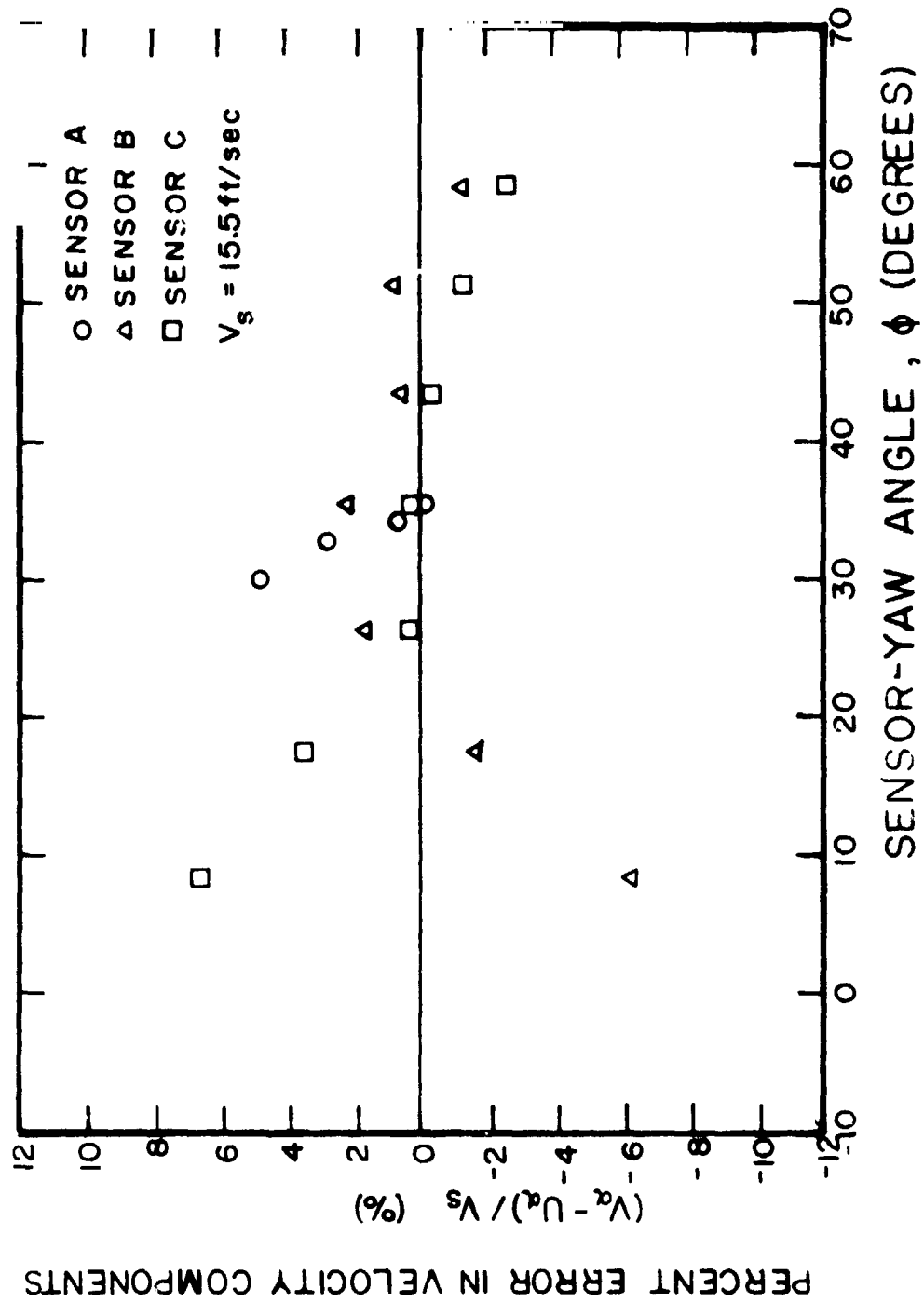
Figure 10. Error in Velocity Components vs. Sensor-Yaw Angle #1193.
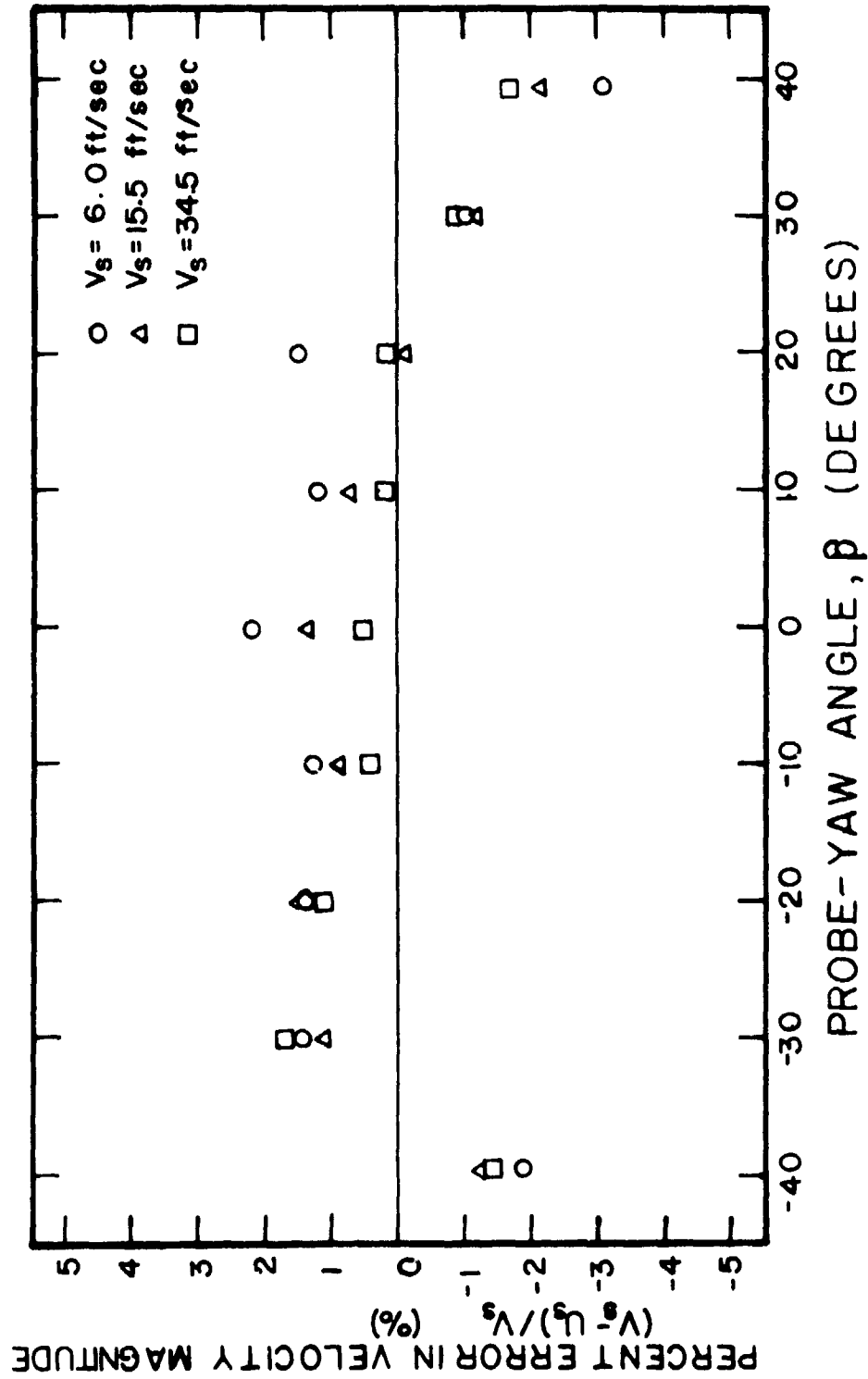
Figure 11· Error in Velocity Magnitude vs. Probe Yaw Angle, β, #1193.
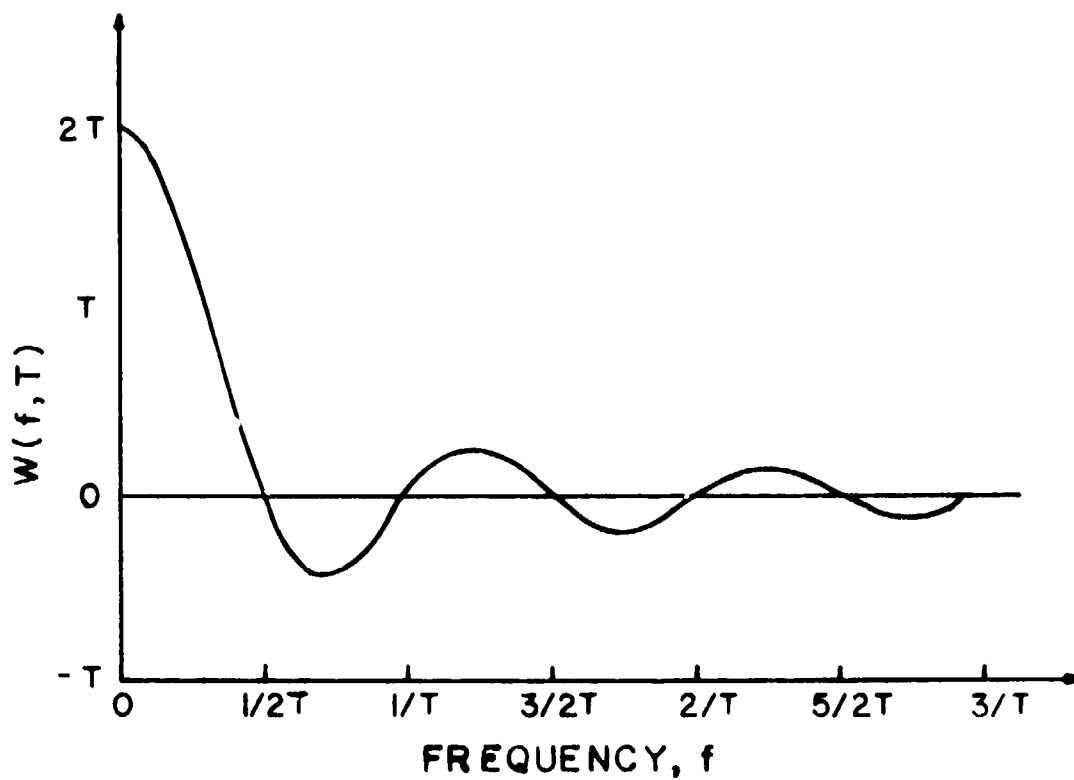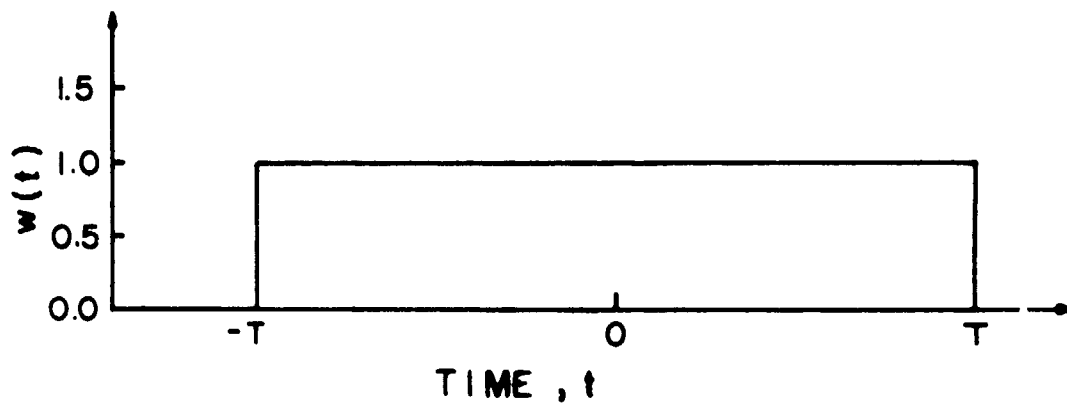
Figure 12:   The Rectangular Window Function (Top)
            and its Fourier Transform (Bottom)
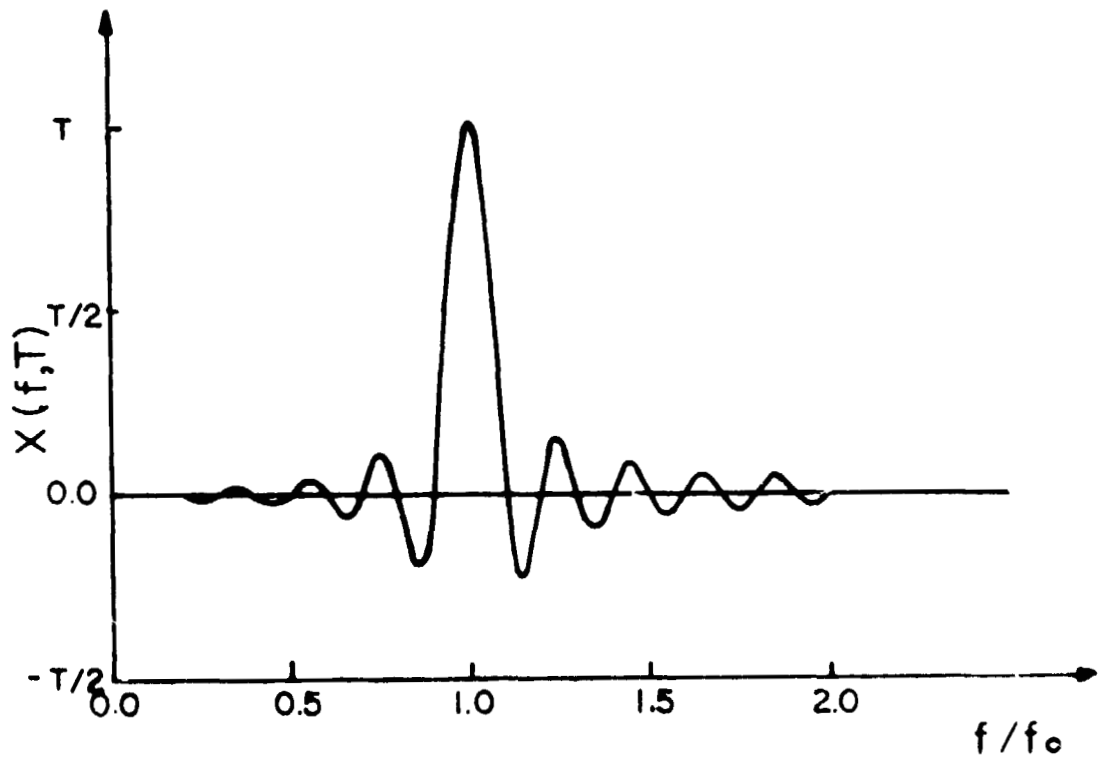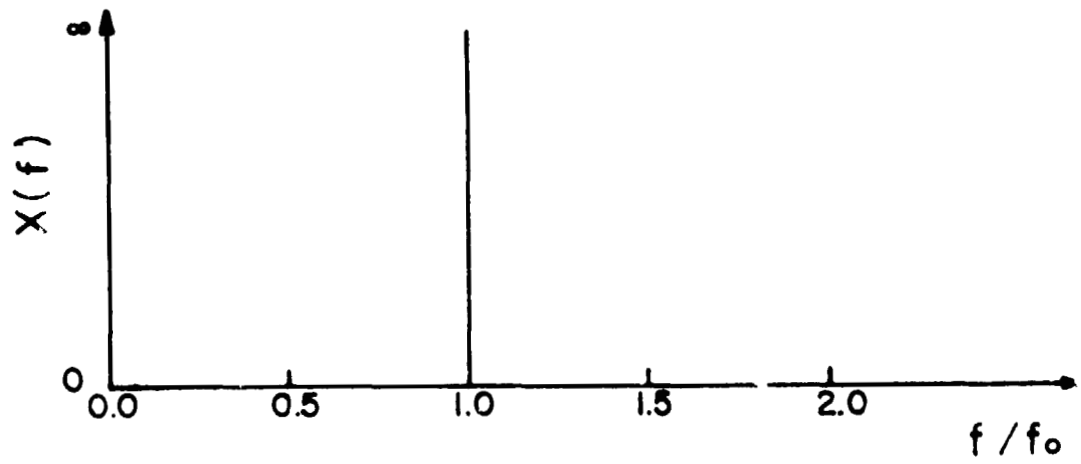
Figure 13: The Infinite (Top) and the Finite (Bottom)
Fourier Transform of the Sinusoidal Function
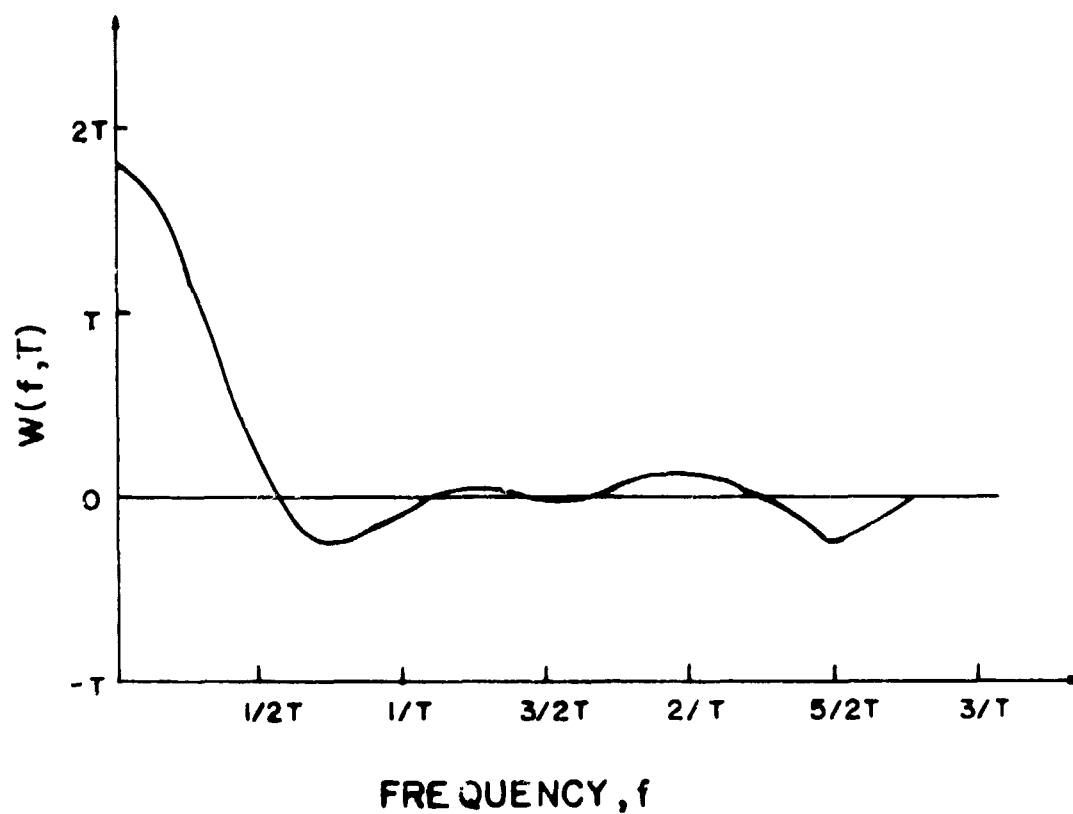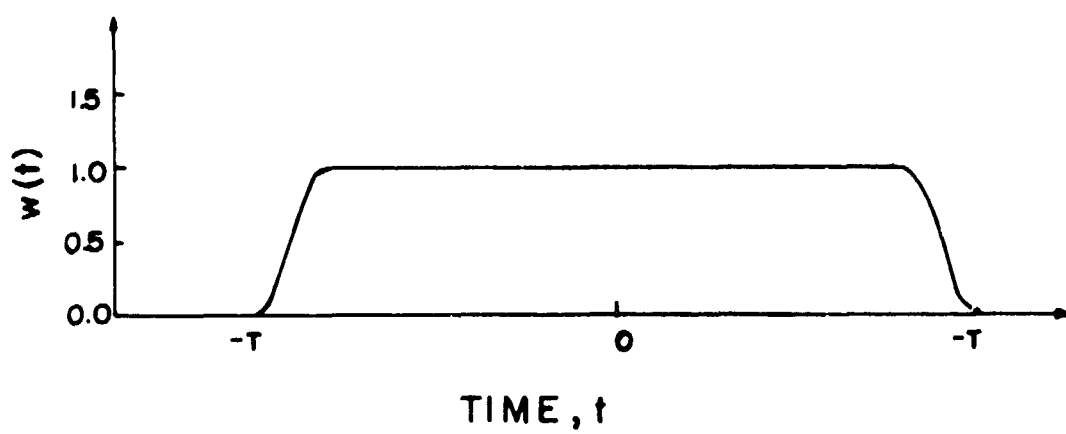
Figure 14: The Cosine Taper Data Window Function (Top) and its Fourier Transform (Bottom).
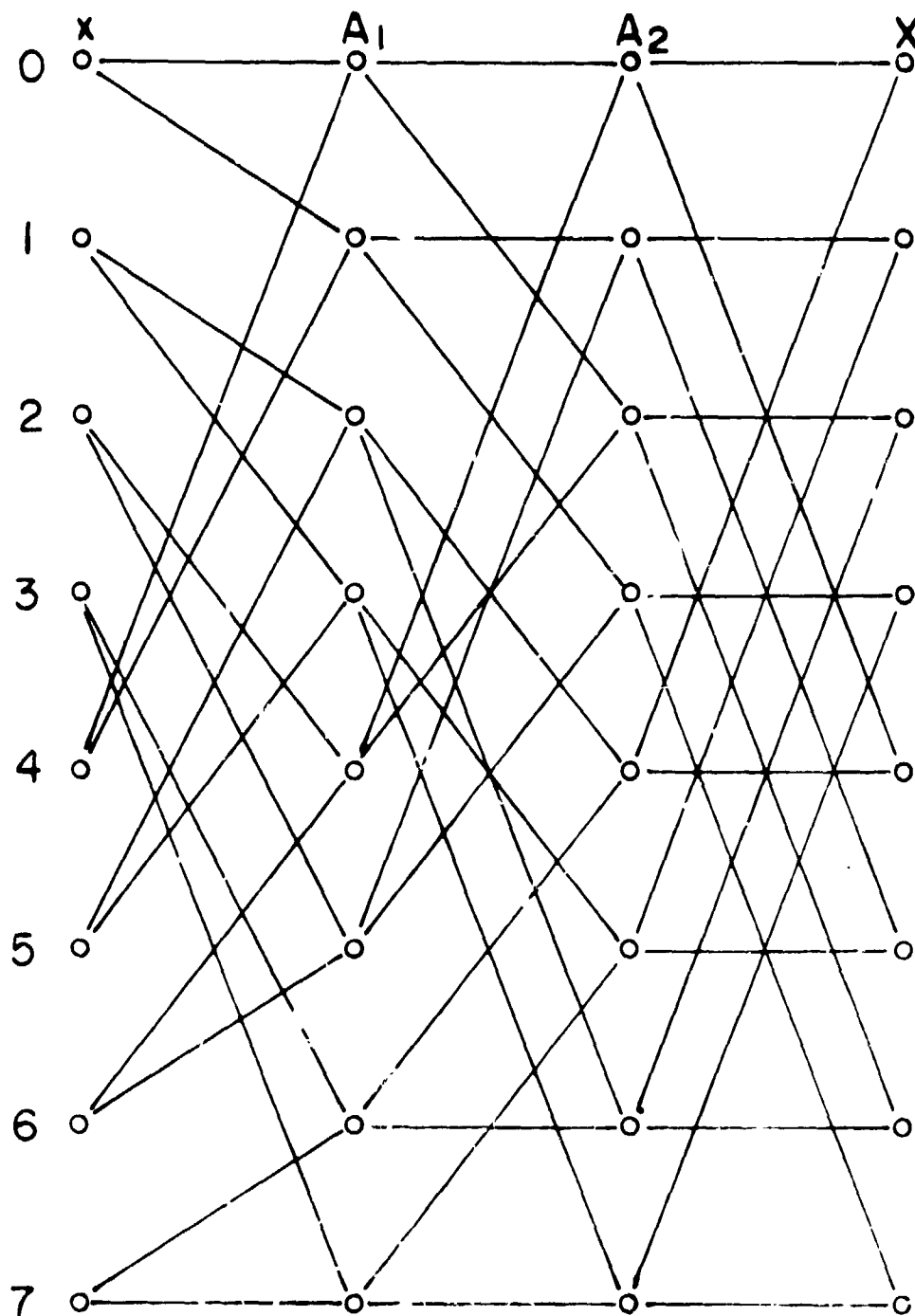
Figure 15: FFT Steps for a Time History of 8 Points.

Figure 16: Flow Chart Diagram of the FFT FORTRAN Program.

C - 2
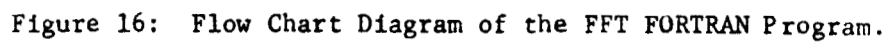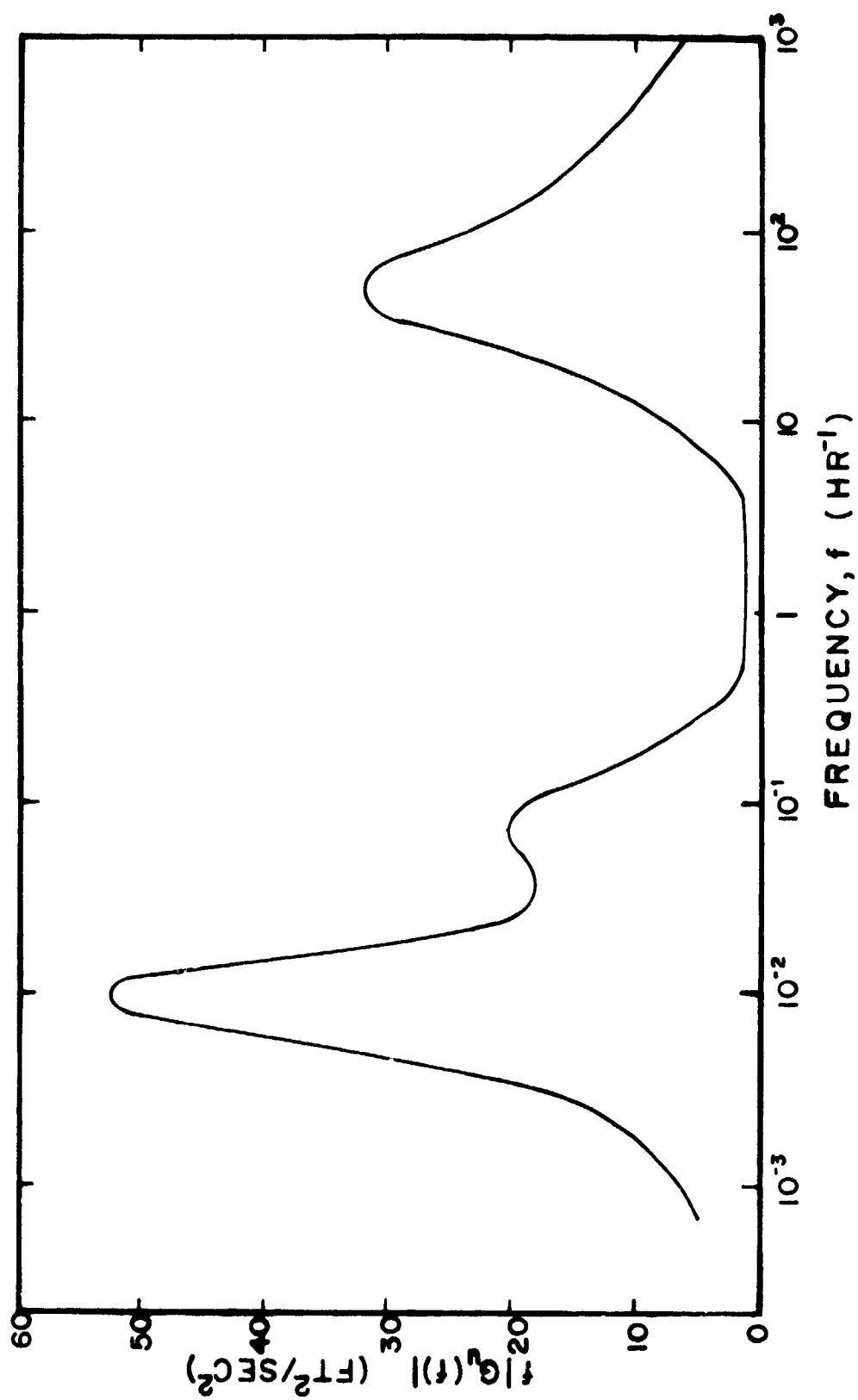
Figure 17: Van der Hoven's Power Spectrum of the Longitudinal Velocity Component.
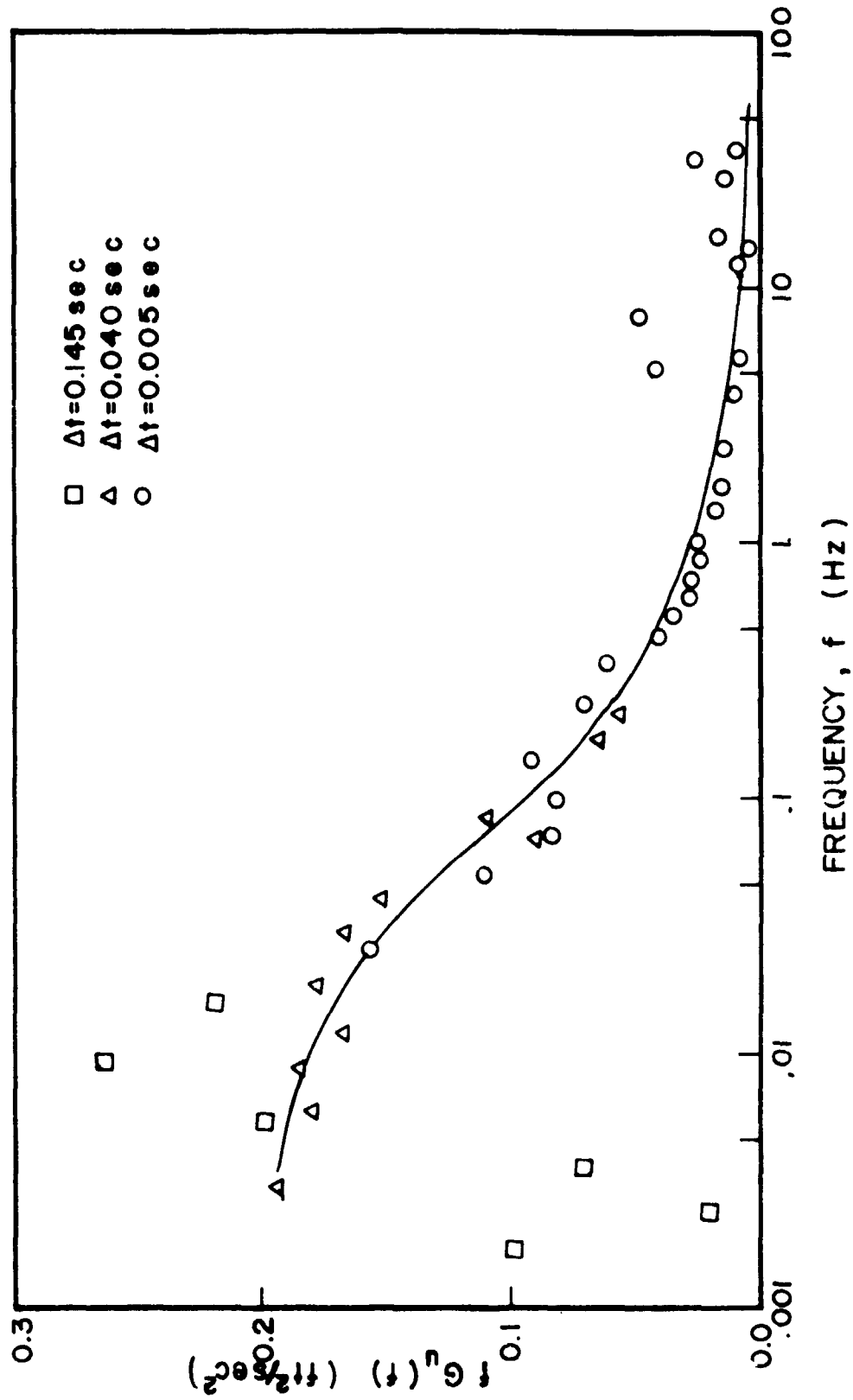
Figure 18: Power Spectrum of the Longitudinal Velocity Component.
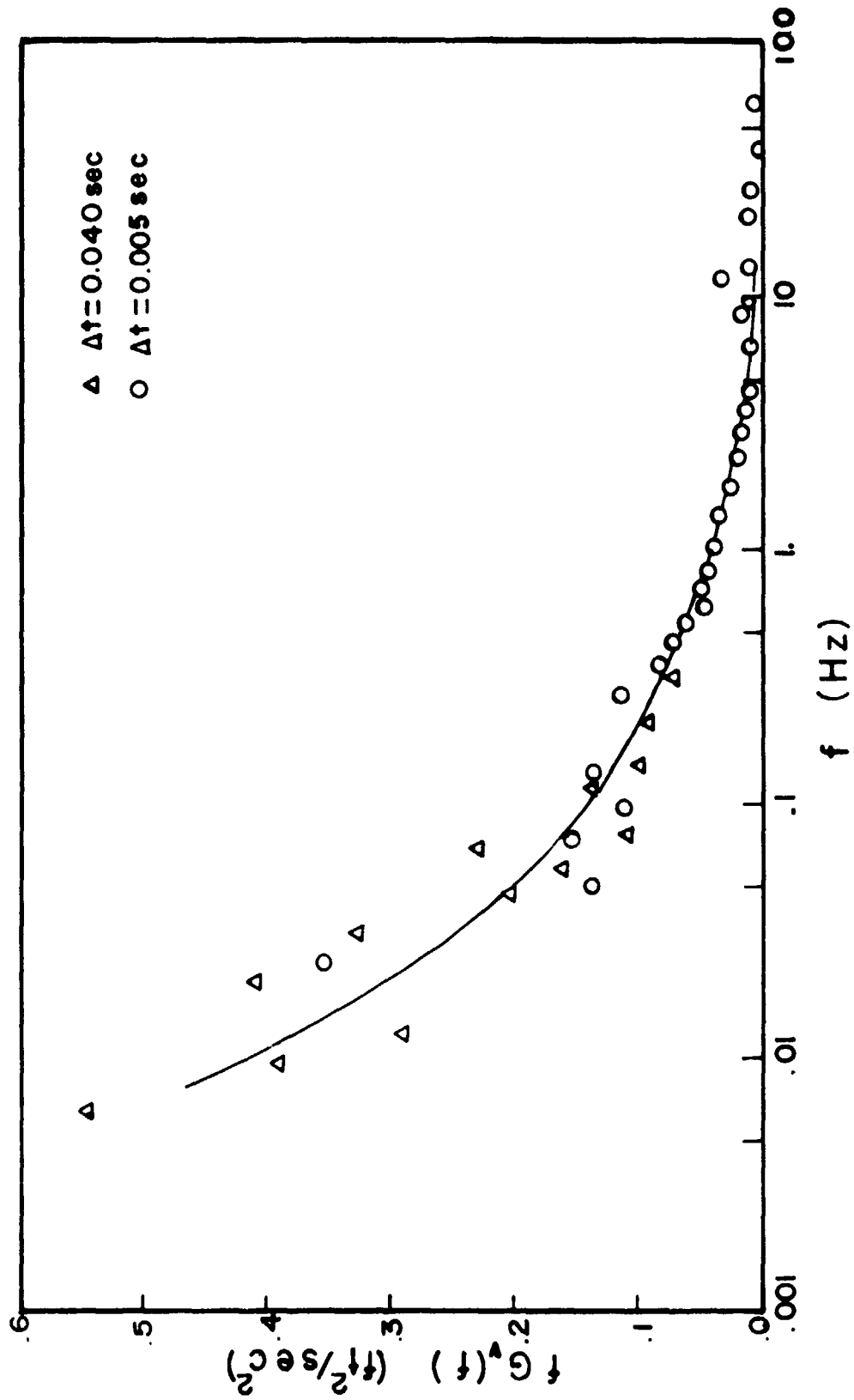
Figure 19. Power Spectrum of the Lateral Velocity Component.
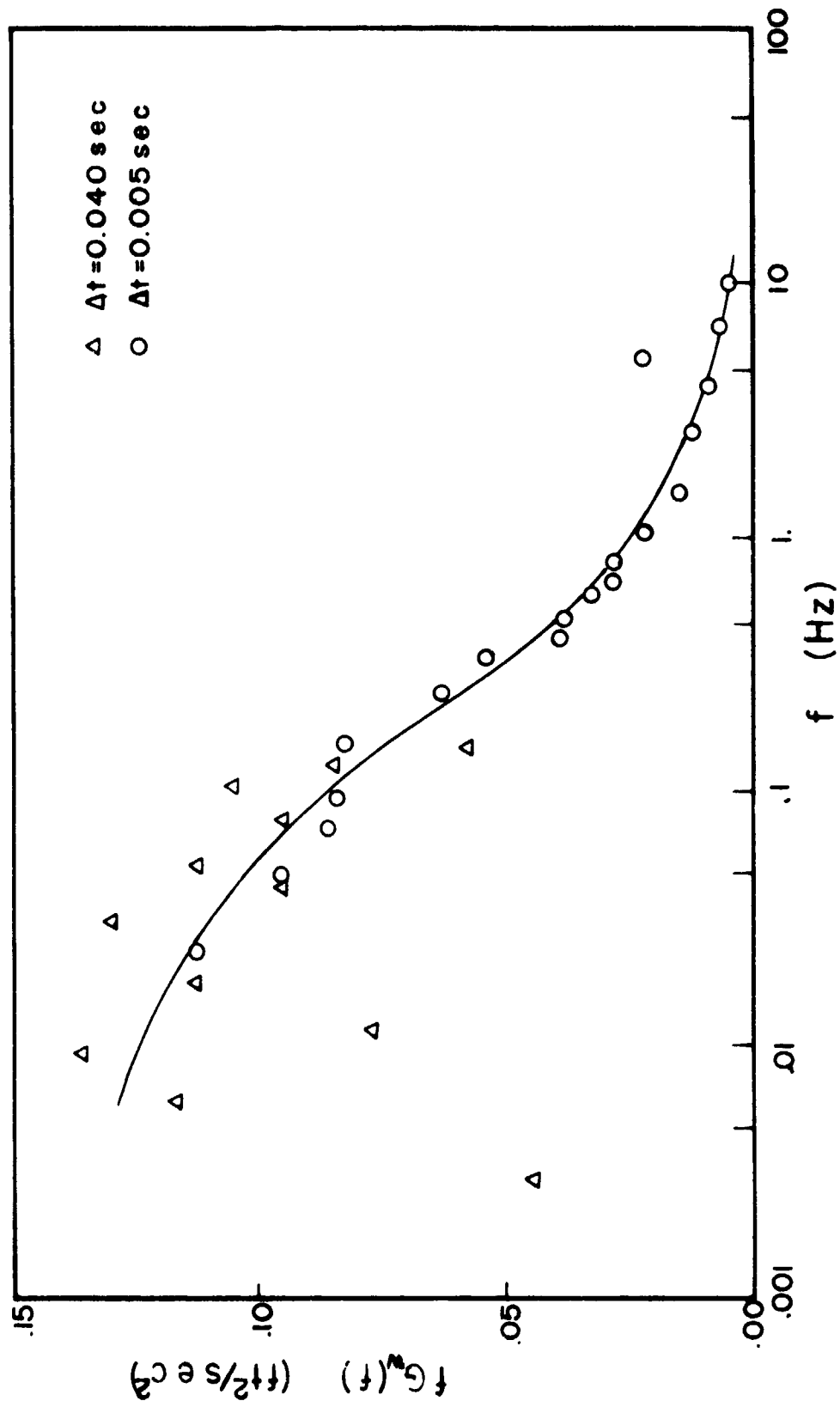
Figure 20: Power Spectrum of the Vertical Velocity Component.
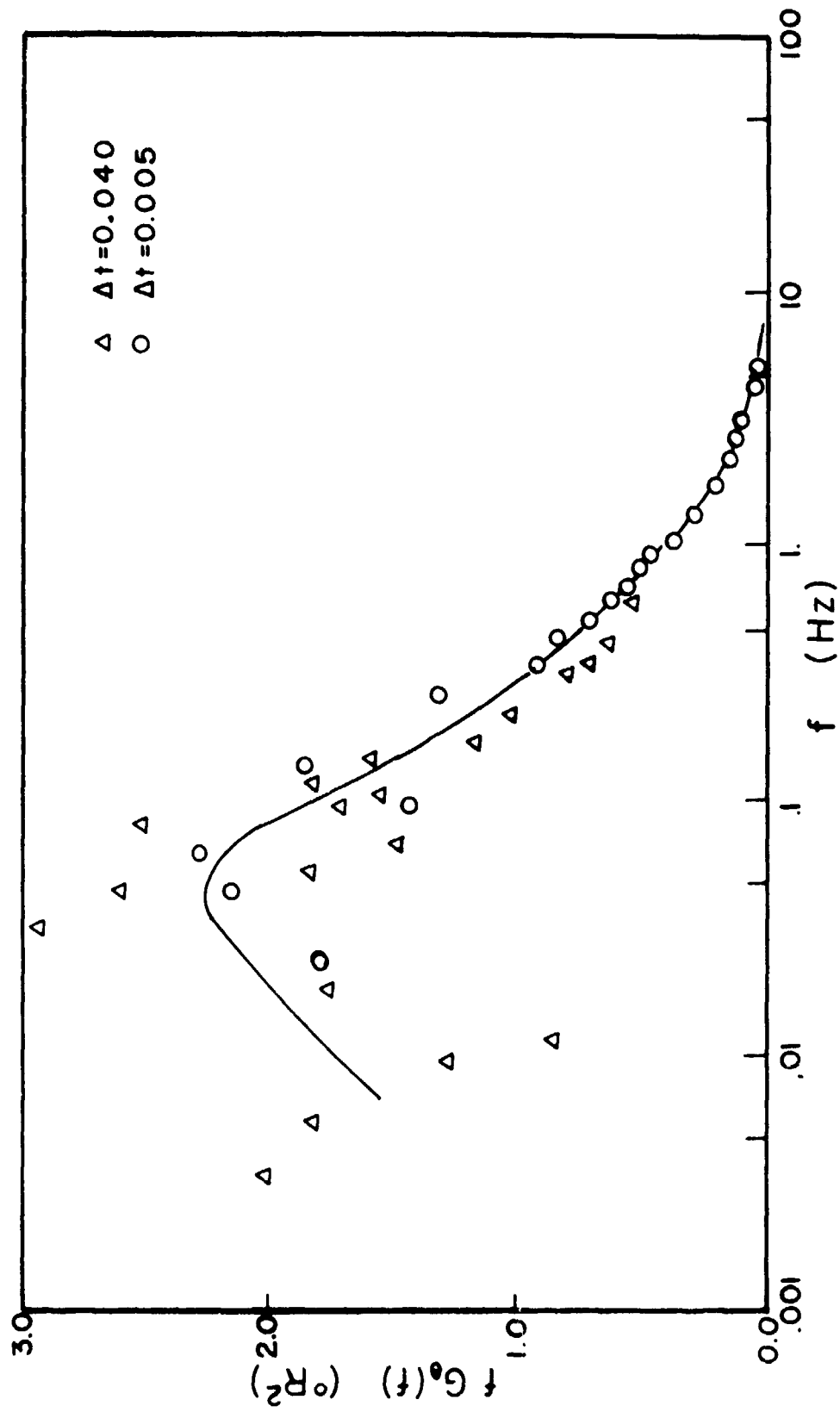
Figure 21. Power Spectrum of the Temperature.
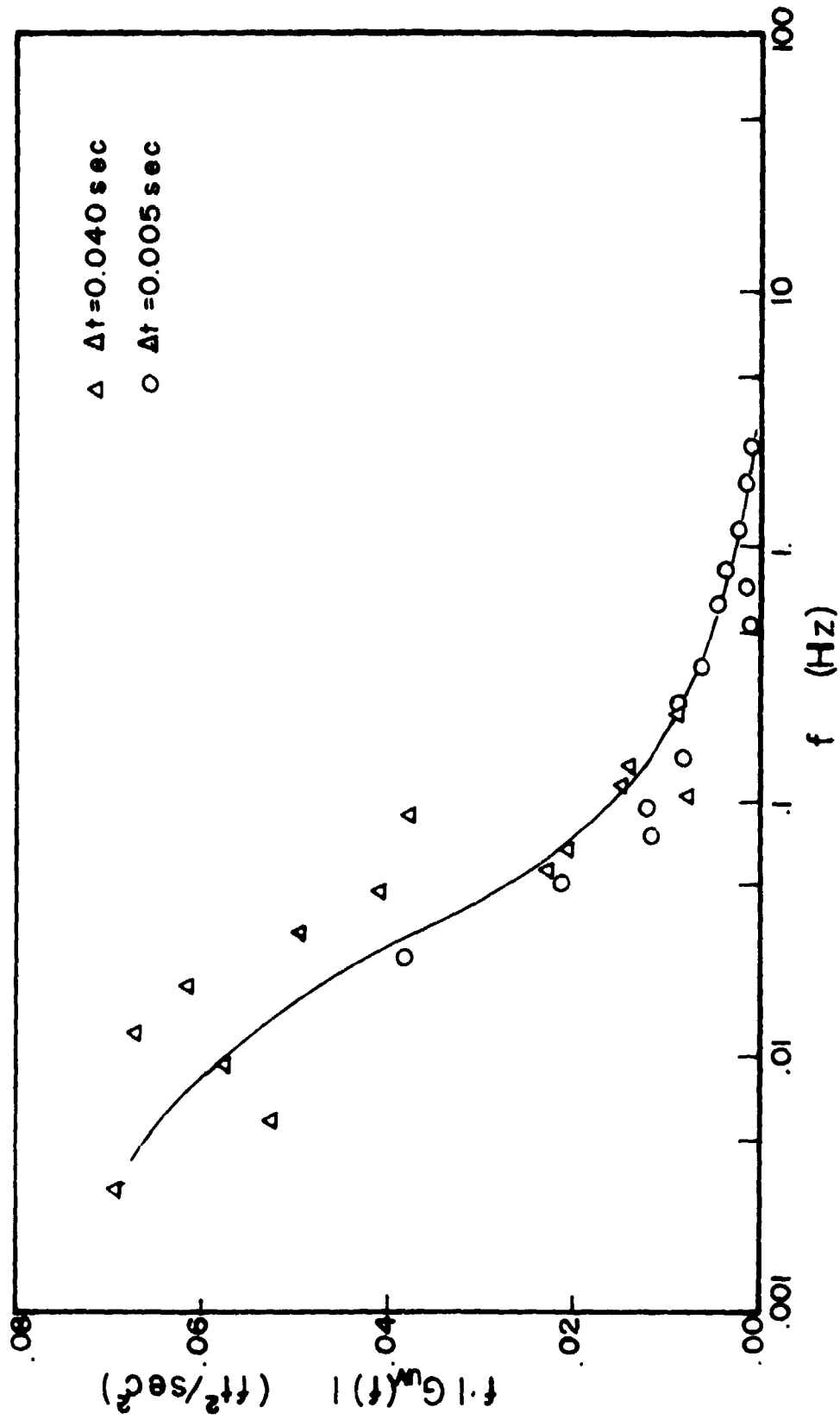
Figure 22: Cross-Spectrum of the Longitudinal and the Vertical Velocity Components.
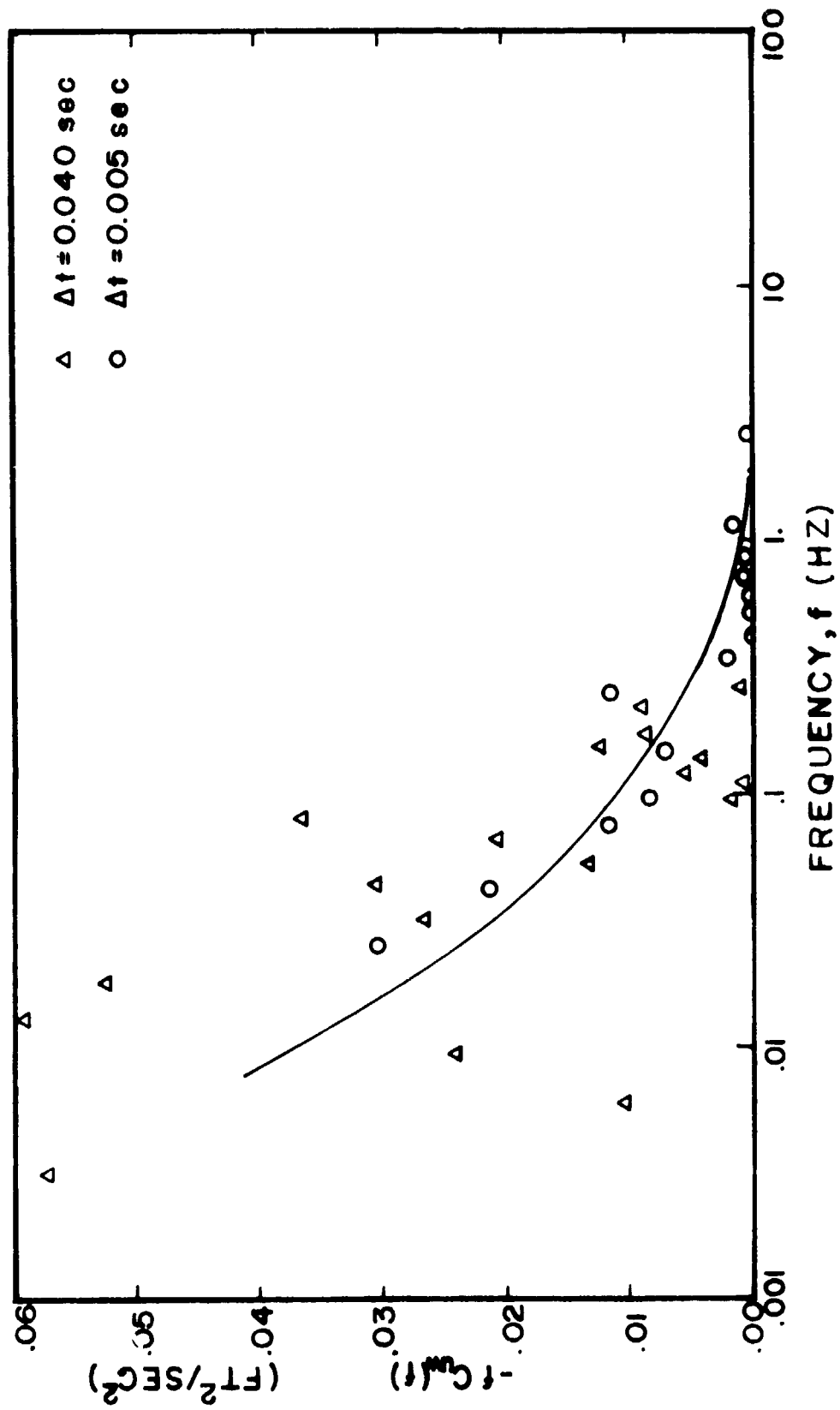
Figure 23: Co-Spectrum of the Longitudinal and the Vertical Velocity Components.
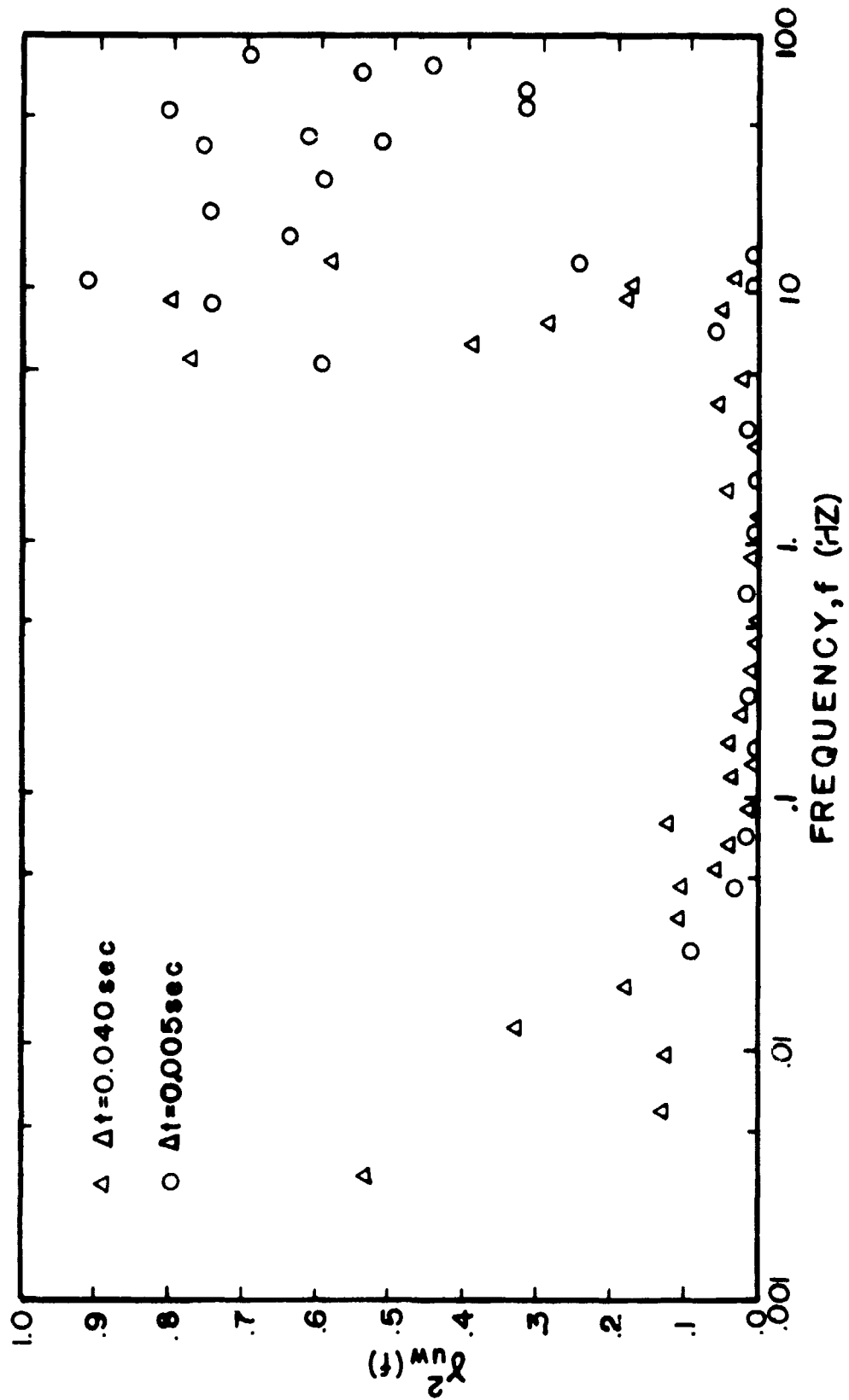
Figure 24: Coherence Function of the Longitudinal and the Vertical Velocity Components.

TABLE I. CALIBRATION CONSTANTS OF THE TSI #1193 ANEMOMETER

Sensor	Film	T_a^o	T_f^o	T_f^{cold}	R_f^{cold}	α_f^{cold}	T_c^m	R_c^m	K	k	C	R
A	1	76	633	73.5	43.81	0.001087	77	7.33	2.0804	-	-	
	2	76	633	73.5	44.49	0.001074	77	7.31	2.1540			0.99217
B	1	76	521	73.5	42.74	0.001254	77	7.39	2.0793	0.12	1.01010	
	2	76	521	73.5	42.89	0.001273	77	7.26	2.2088			1.05738
C	1	76	516	73.5	49.55	0.001256	77	7.37	2.0289	0.16	1.03093	
	2	76	516	73.5	42.94	0.001295	77	7.28	2.1748			0.98214

$$0.52 < Q \quad , \quad D = 0.1299 \quad , \quad n = 0.44$$
$$0.38 < Q < 0.52 \quad , \quad D = 0.1723 \quad , \quad n = 0.35$$
$$Q < 0.38 \quad , \quad D = 0.1761 \quad , \quad n = 0.33994$$

$$k_{av} = 2.08645$$

$$C_{T1} = 29.35 \quad , \quad C_{T2} = 20.77$$

TABLE 11. BLOCK-MEAN VALUES OF THE VELOCITY COMPONENTS IN THE SENSOR ORIENTED COORDINATE SYSTEM, THEIR STANDARD DEVIATIONS, THE VELOCITY MAGNITUDE AND THE PROBE-YAW ANGLE (RUN 1, 100-FOOT LEVEL)

Block Number	Velocity Components			Standard Deviations of the Velocity Components			Velocity Magnitude	Probe-Yaw Angle
n	$\overline{U}_A^n$(fps)	$\overline{U}_B^n$(fps)	$\overline{U}_C^n$(fps)	$\sqrt{u_A^{2n}}$(fps)	$\sqrt{u_B^{2n}}$(fps)	$\sqrt{u_C^{2n}}$(fps)	$\overline{U}^n$(fps)	ϱ^n(deg)
1	8.61	8.41	7.83	0.704	0.799	0.377	14.36	-1.65
2	8.50	7.51	7.58	0.591	0.695	0.349	13.64	0.23
3	7.95	7.93	6.81	0.744	0.653	0.481	13.14	-3.44
4	8.20	7.69	7.50	0.906	0.796	0.790	13.51	-0.58
5	9.05	5.54	8.11	0.492	0.489	0.376	13.54	8.69
6	8.22	7.76	7.75	0.760	1.685	0.910	13.70	0.02
7	9.35	7.67	8.63	0.633	0.892	0.560	14.85	2.62
8	8.61	7.48	7.59	0.680	0.564	0.488	13.69	0.33
9	7.68	8.21	7.77	0.515	0.787	0.673	13.67	-1.33
10	7.73	7.30	8.58	1.305	0.780	0.527	13.66	3.79
11	9.19	7.20	9.08	0.485	0.458	0.332	14.80	5.16
12	9.39	6.60	9.37	0.639	0.935	0.553	14.82	7.63
13	8.09	5.75	9.99	0.871	0.699	0.517	14.08	12.28
14	8.70	6.21	9.94	0.495	0.626	0.514	14.60	10.42
15	8.28	6.73	9.24	0.628	0.616	0.418	14.12	7.23
16	8.25	6.67	8.64	0.594	0.511	0.576	13.68	5.83
17	8.19	6.37	9.59	0.996	0.794	0.641	14.13	9.28
18	9.01	6.72	9.30	0.497	0.743	0.550	14.58	7.21
19	8.09	6.89	9.12	0.586	0.494	0.812	14.53	6.24
20	7.81	6.19	8.82	0.791	0.777	0.770	13.31	8.02
21	7.72	6.98	8.62	0.814	0.926	0.921	13.52	4.93
22	7.51	7.72	7.75	0.883	0.750	0.530	13.27	0.09
23	8.30	7.55	7.28	0.541	0.466	0.270	13.37	-0.03
24	8.22	7.74	7.70	0.558	0.608	0.743	13.67	-0.
25	8.58	6.00	8.77	0.695	0.816	0.491	13.65	8.
26	8.22	6.01	8.98	0.621	0.558	0.657	13.57	8.

TABLE II. (Continued)

Block Number	Velocity Components			Standard Deviations of the Velocity Components			Velocity Magnitude	Probe-Yaw Angle
n	$\bar{U}_A^n$(fps)	$\bar{U}_B^n$(fps)	$\bar{U}_C^n$(fps)	$\sqrt{\overline{u_A^{2n}}}$(fps)	$\sqrt{\overline{u_B^{2n}}}$(fps)	$\sqrt{\overline{u_C^{2n}}}$(fps)	$\bar{U}^n$(fps)	ε^n(deg)
27	7.29	8.44	7.08	0.746	1.078	1.763	13.21	-4.18
28	7.18	8.32	5.86	0.621	0.629	0.470	12.45	-8.03
29	8.12	8.07	6.28	0.644	0.741	0.521	13.05	-5.57
30	7.47	8.33	6.63	0.792	1.045	0.583	13.01	-5.33
31	8.79	9.00	7.17	0.702	0.559	0.591	14.48	-5.15
32	9.07	8.63	6.90	0.703	0.550	0.438	14.29	-4.93
33	8.53	8.32	7.46	0.908	0.729	0.965	14.05	-2.48
34	8.90	7.29	8.32	0.452	0.390	0.554	14.20	2.94
35	9.07	7.63	8.04	0.619	0.723	0.531	14.32	1.16
36	8.76	7.19	7.84	0.587	1.090	0.412	13.78	1.91
37	7.81	7.69	7.65	0.804	0.573	0.560	13.36	-0.13
38	8.53	6.69	8.38	0.570	1.022	0.682	13.70	5.01
39	8.43	5.97	7.63	0.766	1.176	0.546	12.84	5.25
40	7.88	5.51	8.38	0.570	1.022	0.682	12.76	9.15
41	8.51	6.39	8.84	0.767	0.971	0.940	13.84	7.23
42	8.05	5.70	8.42	0.819	0.700	0.619	12.97	8.57
43	7.91	5.89	7.88	0.512	0.540	0.419	12.62	6.43
44	8.00	6.08	7.87	0.491	0.559	0.457	14.77	5.71
45	8.40	6.24	8.40	0.484	0.684	0.518	13.42	6.54
46	7.93	4.29	9.08	0.657	0.795	0.692	12.79	15.41
47	7.52	5.72	7.83	0.563	0.639	0.636	12.27	6.99
48	8.60	5.76	8.96	0.838	0.788	0.635	13.69	9.54
49	8.30	8.46	8.03	883	0.854	0.987	14.31	-1.21
50	8.04	8.89	8.31	53	0.894	1.078	14.59	-1.62
51	7.94	7.67	8.58	3	1.380	0.683	13.99	2.64
52	9.97	8.32	9.04	0.731	0.833	0.668	15.82	1.85
53	9.43	8.21	8.95	0.678	0.546	0.566	15.37	1.95

TABLE II. (Continued)

Block Number	Velocity Components			Standard Deviations of the Velocity Components			Velocity Magnitude	Probe-Yaw Angle
n	$\bar{U}_A^n$(fps)	$\bar{U}_B^n$(fps)	$\bar{U}_C^n$(fps)	$\sqrt{u_A^{2n}}$(fps)	$\sqrt{u_B^{2n}}$(fps)	$\sqrt{u_C^{2n}}$(fps)	$\bar{U}^n$(fps)	β^n(deg)
54	9.43	10.24	7.90	0.627	1.311	1.231	16.01	-5.95
55	9.00	12.31	6.25	0.932	0.895	0.679	16.48	-15.08
56	9.73	13.51	5.34	0.613	0.499	0.514	17.48	-19.30
57	10.00	13.24	5.55	0.652	0.479	0.544	1⁷.⁵0	-18.13
58	9.60	12.64	6.71	1.049	1.066	0.722	17.23	-14.08

Total Number of Reverse Arrangements for the Variation of the Block-Quantities

	745	743	908	765	771	642	767	912

TABLE III. BLOCK-MEAN VALUES OF THE VELOCITY COMPONENTS
IN THE MEAN WIND ORIENTED COORDINATE SYSTEM
AND THE TEMPERATURE (RUN 1, 100-FOOT LEVEL)

Block Number	Temperature	Velocity Components		
n	$\overline{T}^n (°F)$	$\overline{u}^n (fps)$	$\overline{v}^n (fps)$	$\overline{w}^n (fps)$
1	82.14	14.34	0.75	0.40
2	85.22	13.61	0.26	0.78
3	85.67	13.08	1.09	0.47
4	83.44	13.50	0.45	0.49
5	80.73	13.32	-1.72	1.70
6	81.67	13.69	0.31	0.38
7	82.20	14.82	-0.33	0.98
8	85.88	13.66	0.24	0.88
9	80.65	13.65	0.64	0.25
10	83.21	13.64	-0.58	0.17
11	81.99	14.74	-0.98	0.86
12	82.76	14.68	-1.62	1.14
13	81.99	13.82	-2.67	0.18
14	81.43	14.41	-2.30	0.51
15	81.24	14.04	-1.45	0.23
16	82.08	13.63	-1.07	0.49
17	81.20	13.99	-1.95	0.18
18	81.36	14.48	-1.49	0.82
19	81.48	14.45	-1.24	0.80
20	82.39	13.22	-1.55	0.25
21	81.23	13.49	-0.85	0.06
22	83.07	13.26	0.29	0.19
23	89.02	13.34	0.50	0.72
24	84.26	13.66	0.35	0.41
25	82.53	13.52	-1.64	0.98
26	82.27	13.44	-1.78	0.60
27	79.82	13.14	1.27	0.38
28	80.50	12.28	2.03	0.08
29	86.61	12.93	1.57	0.77
30	82.65	13.92	1.51	0.01
31	85.08	14.37	1.64	0.57
32	86.93	14.17	1.56	1.06
33	84.41	14.01	0.94	0.52
34	84.43	14.17	-0.40	0.89
35	84.31	14.29	0.05	1.01
36	84.46	13.74	-0.14	1.01
37	85.67	13.36	0.34	0.11
38	81.97	13.65	-0.88	0.81

TABLE III.   (Continued)

Block Number	Temperature	Velocity Components		
n	$\overline{T}^n(°F)$	$\overline{u}^n(fps)$	$\overline{v}^n(fps)$	$\overline{w}^n(fps)$
39	81.15	12.74	−0.87	−1.33
40	83.32	12.61	−1.73	−0.97
41	81.78	13.75	−1.42	−0.72
42	81.06	12.84	−1.63	−0.81
43	82.08	12.54	−1.12	−0.84
44	81.58	12.70	−0.97	−0.84
45	81.92	13.34	−1.21	−0.88
46	84.78	12.37	−3.10	−1.01
47	81.80	12.20	−1.21	−0.60
48	81.22	13.51	−1.95	−1.02
49	82.57	14.30	0.64	−0.04
50	80.22	14.56	0.75	0.46
51	81.03	13.98	−0.32	0.25
52	84.12	15.79	−0.14	−1.05
53	84.07	15.36	−0.16	−0.69
54	81.28	15.88	2.03	−0.30
55	77.92	15.80	4.66	0.23
56	77.31	16.36	6.16	−0.25
57	77.20	16.49	5.83	−0.49
58	77.33	16.61	4.58	0.06

TABLE IV.   SAMPLE MEANS, VARIANCES AND COVARIANCES OF THE TEMPERATURE
AND THE VELOCITY COMPONENTS IN THE MEAN WIND ORIENTED
COORDINATE SYSTEM (58 BLOCKS, RUN 1, 100-FOOT LEVEL)

Sample Means	Sample Variances	Sample Covariances
$\bar{u} = 13.90$ fps	$\overline{u^2} = 0.475$ $(\text{fps})^2$	$\overline{uv} = 0.063$ $(\text{fps})^2$
$\bar{v} = 0.00$ fps	$\overline{v^2} = 0.753$ $(\text{fps})^2$	$\overline{uw} = -0.102$ $(\text{fps})^2$
$\bar{w} = -0.53$ fps	$\overline{w^2} = 0.391$ $(\text{fps})^2$	$\overline{u\theta} = 0.178$ $\text{fps} \cdot {}^\circ\text{R}$
$\bar{U} = 13.91$ fps	$\overline{\theta^2} = 6.46$ $({}^\circ\text{R})^2$	$\overline{vw} = 0.060$ $(\text{fps})^2$
$\beta = 1.34$ degrees		$\overline{v\theta} = -0.111$ $\text{fps} \cdot {}^\circ\text{R}$
$\bar{T} = 82.44$ ${}^\circ\text{F}$		$\overline{w\theta} = -0.390$ $\text{fps} \cdot {}^\circ\text{R}$

TABLE V. TURBULENCE INTENSITIES FOR DIFFERENT BLOCK TIME LENGTHS
(RUN 1, 100-FOOT LEVEL)

T(sec)	$\sqrt{\overline{u^2}}/\overline{U}$	$\sqrt{\overline{v^2}}/\overline{U}$	$\sqrt{\overline{w^2}}/\overline{U}$
~41	0.0495	0.0624	0.0450
~328	0.0648	0.1101	0.0527
~1188	0.0871	0.1455	0.0556

APPENDIX

LISTING OF FORTRAN PROGRAMS

```
C
C     ******************** CONVERSION ******************************C
C     ----------------------------------------------------------------
C     CALCULATION OF THE TEMPERATURE AND THE VELOCITY COMPS FROM
C     THE VOLTAGES.
C     ----------------------------------------------------------------
      INTEGER VOLT(7,418),TEMPU
      REAL K,KAV,KS,NHIGH,NMID,NLOW
      DIMENSION TFO(3),RFCOLD(3,2),AFCOLD(3,2),RCMEAS(3,2)
      DIMENSION DRC(3,2),RFO(3,2),TF(3,2),CF(3,2)
      DIMENSION E(3,2),S(3),K(3,2),KS(3),HT(3),PHI(3),PHID(3),
     1(3),UES(3),C(3)
      DIMENSION V(3,2,418),UCOMP(3,418),TEMP(418)
      PI=3.14159265*
      READ(5,5)NOPROB
      WRITE(6,23)NOPROB
      READ(5,1)(TFO(I),I=1,3),TAU
      READ(5,2)TFCOLD,((RFCOLD(I,J),J=1,2),I=1,3)
      READ(5,3)((AFCOLD(I,J),J=1,2),I=1,3)
      READ(5,2)TCMEAS,((RCMEAS(I,J),J=1,2),I=1,3)
      READ(5,11)((K(I,J),J=1,2),I=1,3)
      READ(5,27)HHIGH,HLOW,DHIGH,DMID,DLOW,AHIGH,NMID,NLOW
      READ(5,29)KAV,(KS(I),I=1,3),((C(I),I=2,3)
      READ(5,28)(R(I),I=1,3)
      READ(5,31) CT1,CT2
      READ (5,301) P, TAMB, TCABLE, ITAPE
    1 FORMAT(4F8.2)
    2 FORMAT(F5.1,6F10.3)
    3 FORMAT(6F10.8)
    5 FORMAT(I4)
   11 FORMAT(6F8.4)
   23 FORMAT(1H1,20X,'PROBE SERIAL NO',I3//)
   27 FORMAT(6F8.5)
```

```
25 FORMAT(3F10.6)
27 FORMAT(5F10.6)
31 FORMAT(2F8.2)
301 FORMAT (3F8.3,I1)
C------------------------------------------------------------------------C
C     CALCULATION OF CORR. FACTORS FROM TEMPERATURES
C------------------------------------------------------------------------C
      DO 50 I=1,3
      DO 50 J=1,2
      DRC(I,J)=RCMEAS(I,J)*(1.+(TAO-TCMEAS))/(390.1+TCMEAS))*(TAO-TCABLE)
     1/(390.1+TAO)
      RFO(I,J)=RFCOLD(I,J)*(1.+AFCOLD(I,J)*(TFO(I)-TFCOLD))
      TF(I,J)=TFO(I)+DRC(I,J)/(AFCOLD(I,J)*RFCOLD(I,J))
      CF(I,J)=(1.+DRC(I,J)/RFO(I,J))*(TFO(I)-TAO)/(TF(I,J)-TAMB)
50 CONTINUE
      WRITE(6,333) TAMB,TCABLE,P
333 FORMAT(20X,'TAMB=',F7.2,10X,'TCABLE=',F7.2,10X,'P=',F7.2//)
      NDTBK=418
      NOBLK=1149
      DO 500 KKK=1,NOBLK
      DO 600 I=1,NDTBK
600 READ(10,6) (VOLT(J,I),J=1,7)
5 FORMAT(7A2)
      TEMP(J)=VOLT(1,J)
      V(1,1,J)=VOLT(2,J)
      V(2,1,J)=VOLT(4,J)
      V(3,1,J)=VOLT(6,J)
      V(1,2,J)=VOLT(3,J)
      V(1,2,J)=VOLT(5,J)
      V(3,2,J)=VOLT(7,J)
C------------------------------------------------------------------------C
C     CALCULATION OF COOLING VELOCITIES
```

```
C------------------------------------------------------------------------C
      DO 100 JJJ=1,NDTBK
      TEMP(JJJ)=CT1*TEMP(JJJ)*.004882+CT2
      DO 12 I=1,3
      DO 12 J=1,2
 12   E(I,J)=.009764*V(I,J,JJJ)+3.
      DO 17 I=1,3
      HT(I)=(K(I,1)*CF(I,1)*E(I,1)**2+K(I,2)*CF(I,2)*E(I,2)**2)/(TFO(I)-
     1TAO)
      IF(HT(I)-HHIGH)14,14,13
 13   UES(I)=(HT(I)/DHIGH)**(1./NHIGH)
      GO TO 17
 14   IF(HT(I)-HLOW)16,16,15
 15   UES(I)=(HT(I)/DMID)**(1./NMID)
      GO TO 17
 16   UES(I)=(HT(I)/DLOW)**(1./NLOW)
 17   CONTINUE
C------------------------------------------------------------------------C
C     CALCULATIONS OF ANGLES,SIGNS,VELOCITY COMPONENTS.
C------------------------------------------------------------------------C
      US=SQRT((UES(1)**2+UES(2)**2+UES(3)**2)/KAV)
      U=US*(TEMP(JJJ)+460.)*.0564528/P
      DO 25 I=2,3
      S(I)=(1.-(C(I)*UES(I)/US)**2)/(1.-KS(I))
 25   IF(S(I).LE.0.0) S(I)=.000
      S(1)=1.-S(2)-S(3)
      IF(S(1).LE.0.0) S(1)=.000
      DO 34 I=1,3
      S(I)=SQRT(S(I))
 34   IF(S(I).GT.1.0) S(I)=1.000
      IF(E(1,1)-R(1)*E(1,2)).LT.0.0) S(2)=-S(2)
      IF(E(2,1)-R(2)*E(2,2)).LT.0.0) S(3)=-S(3)
```

```
      IF((R(3,1)-R(3)*R(3,2)).LT...0) S(1)=-S(1)
      DO 26 I=1,3
      PHI(I)=ARSIN(S(I))
      PHID(I)=180.*PHI(I)/PI
   26 UCOMP(1,JJJ)=U*S(I)
  100 CONTINUE
      IF (ITAPE.EQ.1) GO TO 302
      DO 49 I=1,NDTBK
   49 WRITE(17) TEMP(I),(UCOMP(J,1),J=1,3)
  302 WRITE(6,602) KKK
  602 FORMAT(5X,'THE TEMPERATURE AND VELOCITY COMPS. FOR BLOCK',I5)
      DO 101 I=1,401,100
  101 WRITE(6,102) TEMP(I),(UCOMP(J,1),J=1,3)
  102 FORMAT(10X,4F14.6)
  500 CONTINUE
      STOP
      END
```

```
C     ********************* STATIONARITY  *********************
C     ---------------------------------------------------------
C     CALCULATION OF THE MEAN VALUES,YAW ANGLES AND STANDARD
C     DEVIATIONS IN EACH BLOCK.
C     CALCULATION OF THE SAMPLE MEAN TEMPERATURE AND THE SAMPLE
C     MEAN WIND MAGNITUDE AND YAW ANGLE.
C     APPLICATION OF THE STATISTICAL TEST FOR STATIONARITY.
C     ---------------------------------------------------------
      DIMENSION U(4,8192),UBBK(58,4),UBKT(58),UBTOTL(4),BETA1(58)
      DIMENSION DEG(58),E1(3,3),UMEAN(3),VAR(58,4),STDEV(58,4)
      DIMENSION TEST(58,8),REVARR(58,8),TOTREV(8)
C     ---------------------------------------------------------
C     NOBLK=NUMBER OF BLOCKS
C     NDTBK=DATBK=NUMBER OF DATA IN EACH BLOCK
C     IB=THE BLOCK NUMBER
C     NTS=NUMBER OF TIME SERIES
C     ---------------------------------------------------------
      NTS=4
      NDTBK=3192
      NOBLK=58
      BLKND=NOBLK
      IB=1
 5000 DO 7 I=1,NDTBK
    7 READ(10) U(4,I),U(1,I),U(1,I),U(2,I),U(3,I)
C     ---------------------------------------------------------
C     CALCULATION OF BLOCK MEANS.
C     UBBK(IB,J)=MEAN VALUE IN EACH BLOCK,IP=1,2,...,NOBLK, J=1,2,...,4
C     ---------------------------------------------------------
      DO 11 J=1,NTS
   11 UBBK(IB,J)=0.0
      I=1
   12 DO 13 J=1,NTS
```

```
13 UBBK(IB,J)=UBBK(IB,J)+U(J,I)
   IF(I .EQ. NDTBK) GO TO 14
   I=I+1
   GO TO 12
14 DATBK=NDTBK
   DO 15 J=1,NTS
15 UBBK(IB,J)=UBBK(IB,J)/DATBK
   UBKT(IB)=SQRT(UBBK(IB,1)**2+UBBK(IB,2)**2+UBBK(IB,3)**2)
C
C ----------------------------------------------------------------
C    CALCULATION OF THE PROBE YAW ANGLE FOR EACH BLOCK.
C ----------------------------------------------------------------
C
   BETAI(IB) = ATAN(-1.22475*(UBBK(IB,2)-UBBK(IB,3))/(UBBK(IB,1)
  1+UBBK(IB,2)+UBBK(IB,3)))
   DEG(IB)=(180.0/3.14159)*BETAI(IB)
C
C ----------------------------------------------------------------
C    CALCULATION OF THE STANDARD DEVIATIONS FOR EACH BLOCK.
C ----------------------------------------------------------------
C
   DO 16 K=1,NTS
16 VAR(IB,K)=0.0
   DO 19 I=1,NDTBK
   DO 18 K=1,NTS
18 VAR(IB,K)=VAR(IB,K)+U(K,I)*U(K,I)
   DO 19 K=1,NTS
   VAR(IB,K)=VAR(IB,K)/DATBK-UBBK(IB,K)*UBBK(IB,K)
19 STDEV(IB,K)=SQRT(ABS(VAR(IB,K)))
   IF (IB .EQ. NCBLK) GO TO 3000
   IB=IB+1
   GO TO 5000
3000 CONTINUE
   WRITE (6,100)
100 FORMAT(1H1,1X,'BK NO',2X,'MEAN V(A)',2X,'MEAN V(B)',2X,'MEAN V(C)'
  1,3X,'MAGNITUDE',2X,'MEAN TEMP',2X,'BLK ANG',2X,'STD DEV VA',2X,
```

```
      2'STD DEV V3',2X,'STD DEV VC',2X,'STD DEV T'//)
      DO 101 IB=1,NOBLK
  101 WRITE(6,102) IB,UBBK(IB,1),UBBK(IB,2),UBBK(IB,3),UAKT(IB),UBBK(IB,
     14),DEG(IB),STDEV(IB,1),STDEV(IB,2),STDEV(IB,3),STDEV(IB,4)
  102 FORMAT(3X,I2,2X,F9.3,3(3X,F9.3),2X,F9.3,3X,F6.2,4(3X,F9.3))
C-----------------------------------------------------------------------C
C     CALCULATION OF THE SAMPLE MEAN VELOCITY COMPS. AND TEMPERATURE
C-----------------------------------------------------------------------C
      DO 20 J=1,NTS
   20 UBTOTL(J)=0.0
      J=1
   21 DO 22 IB=1,NOBLK
   22 UBTOTL(J)=UBTOTL(J)+UBBK(IB,J)
      IF(J .EQ. NTS) GO TO 24
      J=J+1
      GO TO 21
   24 DO 23 J=1,NTS
   23 UBTOTL(J)=UBTOTL(J)/BLKNO
C-----------------------------------------------------------------------C
C     CALCULATION OF THE SAMPLE MEAN VELOCITY MAGNITUDE,THE SAMPLE
C     PROBE YAW ANGLE AND THE MEAN WIND COMPS. IN THE MEAN WIND
C     DIRECTION ORIENTED COORDINATE SYSTEM.
C-----------------------------------------------------------------------C
      VTOTL1=SQRT(UBTOTL(1)**2+UBTOTL(2)**2+UBTOTL(3)**2)
      BETOL1 = ATAN(-1.22475*(UBTOTL(2)-UBTOTL(3))/(UBTOTL(1)+UBTOTL(2)
     1+UBTOTL(3)))
      BEDEG=(180.0/3.14159)*BETOL1
      TI(1,1)=0.57735*COS(BETOL1)
      TI(1,2)=0.57735*SIN(BETOL1)
      TI(1,3)=-0.81650
      TI(2,1)=0.57735*COS(BETOL1)-0.70711*SIN(BETOL1)
      TI(2,2)=0.57735*SIN(BETOL1)+0.70711*COS(BETOL1)
```

```
      E1(2,3)=0.40824
      E1(3,1)=0.57735*CGS(BETOL1)+0.70711*SIN(BETOL1)
      E1(3,2)=0.57735*SIN(BETOL1)-0.70711*COS(BETOL1)
      E1(3,3)=0.43824
      DO 43 I=1,3
43    UMEAN(I)=0.0
      DO 45 I=1,3
      DO 45 J=1,3
45    UMEAN(I)=UMEAN(I)+E1(J,I)*UPTOTL(J)
      WRITE(6,46)(UBTOTL(J),J=1,NTS)
46    FORMAT('1','SAMPLE MEAN VEL COMPS =',3F12.6,5X,'SAMPLE MEAN TEMP =
     1',F12.6//)
      WRITE(6,47)VTOTL1,BETOL1,3EDEG
47    FORMAT(//'MEAN VEL MAGN =',F12.6,10X,'MEAN VEL YAW ANGLE =',F11.8
     2,'RAD  =',F11.8,' DEGREES'//)
      WRITE(6,48)(UMEAN(I),I=1,3)
48    FORMAT('LONGITUD. MEAN WIND COMP =',F12.6,5X,'LATERAL MEAN WIND C
     3OMP =',F12.6,5X,'VERTICAL MEAN WIND COMP =',F12.6///)
C------------------------------------------------------------------C
C     CALCULATION OF THE TOTAL NUMBER OF REVERSE ARRANGEMENTS
C     FOR THE VELOCITY COMPS.,THE MEAN VELOCITY MAGNITUDE AND
C     YAW ANGLE AND THE STANDARD DEVIATIONS
C------------------------------------------------------------------C
      NSTD=8
      NTEST=NOBLK-1
      DO 50 IB=1,NOBLK
      DO 51 I=1,3
51    TEST(IB,1)=UBEK(IB,1)
      TEST(IB,4)=UBKT(IB)
      TEST(IB,5)=DEG(IB)
      DO 50 I=6,5
      K=I-5
```

```
 50 TEST(I5,I)=STDEV(I6,K)
    DO 194 I3=1,NOBLK
    DO 194 I=1,NSTD
194 REVARP(I3,I)=0.0
    I3=1
    K=I8+1
195 DO 197 II=1,NSTD
    DO 197 JJ=K,NOBLK
    IF(TEST(I8,II).GT.TEST(JJ,II))GO TO 196
    GO TO 197
196 REVARR(I8,II)=REVARR(I8,II)+1.0
197 CONTINUE
    IF (I8 .EQ. NTEST) GO TO 198
    I8=I8+1
    K=I8+1
    GO TO 195
198 CONTINUE
    DO 190 J=1,NSTD
    TOTREV(J)=0.0
    DO 190 I8=1,NTEST
190 TOTREV(J)=TOTREV(J)+REVARR(I8,J)
    WRITE(6,201) (TOTREV(J),J=1,NSTD)
201 FORMAT(//10X,'TOTAL NO. OF REV. ABS.= ',8F10.1)
    STOP
    END
```

```
C     ************************  MEAN-WIND  ***********************C
C-------------------------------------------------------------------
C     TRANSFORMATION FROM THE SENSOR ORIENTED COORDINATE SYSTEM TO
C     THE MEAN WIND ORIENTED COORDINATE SYSTEM.
C     CALCULATION OF THE SAMPLE VARIANCES AND COVARIANCES
C     AND THE TURBULENCE INTENSITIES.
C-------------------------------------------------------------------
      DIMENSION U(4),V(4,8192),E1(4,4),COV(58,4,4),SCOV(4,4)
      DIMENSION XSUM(4),XBAR(58,4),VCOMP(3),TBINT(3)
      NTS=4
      NDTBK=8192
      NOBLK=58
      BLKNO=NOBLK
      DATBK=NDTBK
C-------------------------------------------------------------------
C     INPUT - MEAN PROBE YAW ANGLE IN RADIANS.
      READ(5,2)BETOL1
    2 FORMAT(F15.10)
C-------------------------------------------------------------------C
      DO 3 I=1,NTS
      DO 3 J=1,NTS
    3 E1(I,J)=0.0
      E1(1,1)=0.57735*COS(BETOL1)
      E1(1,2)=0.57735*SIN(BETOL1)
      E1(1,3)=-0.81650
      E1(2,1)=0.57735*COS(BETOL1)-0.70711*SIN(BETOL1)
      E1(2,2)=0.57735*SIN(BETOL1)+0.70711*COS(BETOL1)
      E1(2,3)=0.40824
      E1(3,1)=0.57735*COS(BETOL1)+0.70711*SIN(BETOL1)
      E1(3,2)=0.57735*SIN(BETOL1)-0.70711*COS(BETOL1)
      E1(3,3)=0.40824
      E1(4,4)=1.0
```

```
      IB=1
1000  DO 1 I=1,NDTBK
    1 READ(10) V(4,I),V(1,I),V(2,I),V(3,I)
      DO 45 K=1,NDTBK
      DO 46 I=1,NTS
      U(I)=0.0
      DO 46 J=1,NTS
   46 U(I)=U(I) + E1(J,I)*V(J,K)
      DO 45 I=1,NTS
   45 V(I,K)=U(I)
C------------------------------------------------------------C
C     CALCULATION OF THE BLOCK MEANS & SUBTRACTION FROM ALL DATA
C     POINTS IN EACH BLOCK.
C------------------------------------------------------------C
      DO 31 I=1,NTS
   81 XSUM(I)=0.0
      DO 82 J=1,NTS
      DO 82 K=1,NDTBK
   82 XSUM(J)=XSUM(J) + V(J,K)
      DO 83 I=1,NTS
   83 XBAR(IB,I)=XSUM(I)/DATBK
      DO 84 J=1,NTS
      DO 84 I=1,NDTBK
   84 V(J,I)=V(J,I)-XBAR(IB,J)
      DO 9 I=1,NDTBK
    9 WRITE(11) V(4,I),V(1,I),V(2,I),V(3,I)
C------------------------------------------------------------C
C     CALCULATION OF BLOCK VARIANCES & COVARIANCES.
C------------------------------------------------------------C
      DO 16 K=1,NTS
      DO 16 J=1,NTS
   16 COV(IB,K,J)=0.0
```

```
      I=1
   17 DO 18 K=1,NTS
      DO 18 L=1,NTS
   18 COV (IB,K,L)=COV(IB,K,L)+V(K,I)*V(L,I)
      IF(I .EQ. NDTBK) GO TO 191
      I=I+1
      GO TO 17
  191 DO 19 K=1,NTS
      DO 19 L=1,NTS
   19 COV(IB,K,L)=COV(IB,K,L)/DATBK
 1002 WRITE(6,1003)IB,(XBAR(IB,J),J=1,4),(COV(IB,J,J),J=1,4)
 1003 FORMAT(1X,I5,8F15.6)
      IF (IB .EQ. NOBLK) GO TO 3000
      IB=IB+1
      GO TO 1000
 3000 CONTINUE
C----------------------------------------------------------------C
C     CALCULATION OF THE SAMPLE VARIANCES AND COVARIANCES        C
C     SCOV=SAMPLE VARIANCES AND COVARIANCES                      C
C----------------------------------------------------------------C
      DO 25 K=1,NTS
      DO 25 J=1,NTS
   25 SCOV(K,J)=0.0
      IB=1
   26 DO 27 K=1,NTS
      DO 27 L=1,NTS
   27 SCOV(K,L)=SCOV(K,L)+COV(IB,K,L)
      IF(IB .EQ. NOBLK) GO TO 28
      IB=IB+1
      GO TO 26
   28 DO 29 K=1,NTS
      DO 29 L=1,NTS
```

```
29  SCUV(K,L)=SCOV(K,L)/BLKN.
    WRITE(6,30)
30  FORMAT('1','CORRELATED VARIABLES',9X,'SAMPLE VARIANCES + COVARIANC
   1ES'//)
    DO 31 I=1,4
    DO 31 J=1,4
31  WRITE(6,32)I,J,SCOV(I,J)
32  FORMAT(1X,8X,I1,' - ',I1,20X,F10.5)
C  ---------------------------------------------------------C
C  CALCULATION OF THE SAMPLE MEAN VELOCITY COMPONENTS AND
C  THE TURBULENCE INTENSITIES.
C  ---------------------------------------------------------C
    DO 33 I=1,3
33  VCOMP(I)=0.0
    DO 35 I=1,3
    DO 34 IB=1,NOBLK
34  VCOMP(I)=VCOMP(I)+XBAR(IB,I)
35  VCOMP(I)=VCOMP(I)/BLKNO
    WRITE(6,36)(VCOMP(I),I=1,3)
36  FORMAT(///'SAMPLE MEAN VEL COMPS = ',3F15.5///)
    VTUTL1=SQRT(VCOMP(1)**2+VCOMP(2)**2+VCOMP(3)**2)
    DO 37 I=1,3
37  TRINT(I)=SQRT(ABS(SCOV(I,I)))/VTUTL1
    WRITE(6,38)(TRINT(I),I=1,3)
38  FORMAT(//'TURBULENCE INTENSITIES =',3F15.7)
    STOP
    END
```

```
C      *********************** SPECTRA *********************
C      ---------------------------------------------------
C      CALCULATION OF POWER SPECTRA,CROSS SPECTRA,CO- AND QUAD-SPECTRA,
C      COHERENCY AND PHASE ANGLE OF REAL TIME SERIES.
C      ---------------------------------------------------
C
       DIMENSION SP1(4097),SP2(4097),CSP(4097),QSP(4097)
       DIMENSION C(2049),X(8192),Z(2048)
       DIMENSION PS11(46),PS22(46),CS12(46),QS12(46)
       DIMENSION AMP12(46),COH12(46),PHS(46),DEGPS(46)
       DIMENSION PNOM1(46),PNOM2(46),CSNOM(46),QSNOM(46)
       DIMENSION CROS(46),CRSNM(46),CRS(10)
       DIMENSION FREQ(46),FLOG(46)
       COMPLEX*8 E,X,Z
C      ---------------------------------------------------
C      NDTBK=NUMBER OF DATA POINTS IN EACH BLOCKED TIME SERIES
C      NOBLK=NUMBER OF BLOCKS USED IN THE SPECTRAL ESTIMATE.
C      NTS=NUMBER OF TIME SERIES TO BE PROCESSED
C      KOUNT=CONTROL NUMBER DEPENDING ON THE TIME SERIES BEEN ANALYZED
C      ---------------------------------------------------
       NDTBK=8192
       NDATBK=NDTBK
       NHALF=NDTBK/2
       HALFN=NHALF
       NHF=NHALF+1
       NOBLK=56
       NDBLK=NOHLK
       NTS=3
       KOUNT=1
       DT=0.005
       PI=3.14159
       XJORD=823
       NIVIS=NOBLK
```

```
C
C   CALCULATION OF THE FREQUENCIES THAT WILL BE USED IN THE SMOOTH
C   SPECTRA.
C   MAVE=NUMBER OF SPECTRAL VALUES AS A RESULT OF COMBINED SMOOTHING
C   DF=THE LOWEST FREQUENCY THAT CAN BE ESTIMATED.
C   DNYQ=THE NYQUIST FREQUENCY.
C
      MAVE=46
      NP=46
      CN=MAVE
      DF=1.0/(DATBK*DT)
      DNYQ=1.0/(2.0*DT)
      DO 66 I=1,4
      P=I
   66 FREQ(I)=P*DF
      DO 61 I=5,15
      Q=I
   61 FREQ(I)= (4.0*(Q-4.0) + 2.5)*DF
      DO 62 I=16,24
      Q=I
   62 FREQ(I)=(16.0*(Q-13.0) +8.5)*DF
      DO 63 I=25,33
      Q=I
   63 FREQ(I)= (64.0*(Q-22.0) +32.5)*DF
      DO 64 I=34,46
      Q=I
   64 FREQ(I)= (256.0*(Q-31.0) +128.5)*DF
      DO 27 I=1,NP
   27 FLOG(I)=ALOG(FREQ(I))
C
C   DATA READING FROM TAPE
C
```

```
      DO 104 I=1,NHF
      SP1(I)=0.0
      SP2(I)=0.0
      CSP(I)=0.0
      QSP(I)=0.0
  104 IB=1
 4000 GO TO (1,2,3), KCUNT
C-------------- U AND W -----------------------------------
    1 DO 10 I=1,NDTBK
      READ(10) T,U,V,W
   10 X(I)=CMPLX(U,W)
      GO TO 1000
C-------------- T AND W -----------------------------------
    2 REWIND 10
    4 DO 20 I=1,NDTRK
      READ(10) T,U,V,W
   20 X(I)=CMPLX(T,W)
      GO TO 1000
C-------------- U AND V -----------------------------------
    3 REWIND 10
    5 DO 30 I=1,NDTRK
      READ(10) T,U,V,W
   30 X(I)=CMPLX(U,V)
 1000 CONTINUE
C---------------------------------------------------------
C   APPLICATION OF THE COSINE TAPER DATA WINDOW.
C---------------------------------------------------------
  144 DO 15 I=1,MOUND
      P=I
      U=0.5*(1.0-COS(PI*P/DIVIS))
   15 X(I)=X(I)*U
      DO 17 I=1,MOUND
```

```fortran
      K=I+7672
      P=I
      H=0.5*(1.0-COS(PI*(DATBK-P)/DIVIS))
17    X(K)=X(K)*H
C-----------------------------------------------------------------
C     CALCULATION OF THE FOURIER TRANSFORM OF A COMPLEX SEQUENCE.
C-----------------------------------------------------------------
C
      CALL FFT (X)
C-----------------------------------------------------------------
C     CALCULATION OF THE BLOCK SPECTRAL ESTIMATES.
C     SEGMENT AVERAGING.
C-----------------------------------------------------------------
      URE=REAL(X(1))
      UIM=0.0
      VRE=AIMAG(X(1))
      VIM=0.0
      SPA=2.0*DT*(URE**2 + UIM**2)/DATBK
      SPB=2.0*DT*(VRE**2 + VIM**2)/DATBK
      SPC=2.0*DT*(URE*VRE + UIM*VIM)/DATBK
      SPD=2.0*DT*(URE*VIM - UIM*VRE)/DATBK
      SP1(1)=SP1(1) + SPA
      SP2(1)=SP2(1) + SPB
      CSP(1)=CSP(1) + SPC
      QSP(1)=QSP(1) + SPD
98    DO 103 I=2,NHF
      K=NDTBK-I+2
      URE = REAL(( X ( I ) + X (K) )/2.0)
      UIM =AIMAG(( X ( I ) - X (K) )/2.0)
      VRE =AIMAG(( X ( I ) + X (K) )/2.0)
      VIM =-REAL(( X ( I ) - X (K) )/2.0)
      SPA=2.0*DT*(URE**2 + UIM**2)/DATBK
      SPB=2.0*DT*(VRE**2 + VIM**2)/DATBK
```

```
      SPC=2.0*DT*(URE*VRE + UIM*VIM)/DATHK
      SPD=2.0*DT*(URE*VIM - UIM*VRE)/DATHX
      SP1(I)=SP1(I) + SPA
      SP2(I)=SP2(I) + SPB
      CSP(I)=CSP(I) + SPC
      QSP(I)=QSP(I) + SPD
  103 IF (IB .EQ. NOBLK) GO TO 6000
      IB=IB+1
      GO TO (1,4,5), KOUNT
 6000 CONTINUE
      DO 109 I=1,NHF
      SP1(I)=SP1(I)/(BLKNO*0.875)
      SP2(I)=SP2(I)/(BLKNO*0.875)
      CSP(I)=CSP(I)/(BLKNO*0.675)
  109 QSP(I)=QSP(I)/(BLKNO*0.875)
      DO 113 I=1,10
  113 CRS(I) = SQRT(CSP(I)**2 + QSP(I)**2)
C-----------------------------------------------------
C   FREQUENCY SMOOTHING.
C-----------------------------------------------------
      DO 22 I=5,NP
      PS11(I)=0.0
      PS22(I)=0.0
      CS12(I)=0.0
   22 QS12(I)=0.0
      DO 71 K=2,5
      J=K-1
      PS11(J)=SP1(K)
      PS22(J)=SP2(K)
      CS12(J)=CSP(K)
   71 QS12(J)=QSP(K)
      L=5
```

```
      MA=3
      M4=4
      K=5
   24 DO 23 I=L,MA
      PS11(K)=PS11(K)+SP1(I)
      PS22(K)=PS22(K)+SP2(I)
      CS12(K)=CS12(K)+CSP(I)
   23 QS12(K)=QS12(K)+QSP(I)
      IF (K .EQ. 15) GO TO 25
      K=K+1
      L=L+M4
      MA=MA+M4
      GO TO 24
   25 CONTINUE
      DO 42 J=5,15
      PS11(J)=PS11(J)/4.0
      PS22(J)=PS22(J)/4.0
      CS12(J)=CS12(J)/4.0
   42 QS12(J)=QS12(J)/4.0
      L=50
      MB=65
      M16=16
      K=16
   52 DO 53 I=L,MB
      PS11(K)=PS11(K)+SP1(I)
      PS22(K)=PS22(K)+SP2(I)
      CS12(K)=CS12(K)+CSP(I)
   53 QS12(K)=QS12(K)+QSP(I)
      IF (K .EQ. 24) GO TO 54
      K=K+1
      L=L+M16
      MB=MB+M16
```

```
      GO TO 52
   54 CONTINUE
      DO 43 J=16,24
      PS11(J)=PS11(J)/16.0
      PS22(J)=PS22(J)/16.0
      CS12(J)=CS12(J)/16.0
   43 QS12(J)=QS12(J)/16.0
      L=194
      MC=257
      M64=64
      K=25
   55 DO 56 I=L,MC
      PS11(K)=PS11(K)+SP1(I)
      PS22(K)=PS22(K)+SP2(I)
      CS12(K)=CS12(K)+CSP(I)
   56 QS12(K)=QS12(K)+QSP(I)
      IF (K .EQ. 33) GO TO 57
      K=K+1
      L=L+M64
      MC=MC+M64
      GO TO 55
   57 CONTINUE
      DO 44 J=25,33
      PS11(J)=PS11(J)/64.0
      PS22(J)=PS22(J)/64.0
      CS12(J)=CS12(J)/64.0
   44 QS12(J)=QS12(J)/64.0
      L=770
      MC=1026
      MC56=250
      K=34
   58 DO 59 I=L,MC
```

```
      PS11(K)=PS11(K)+SP1(I)
      PS22(K)=PS22(K)+SP2(I)
      CS12(K)=CS12(K)+CSP(I.
   59 QS12(K)=QS12(K)+QSP(I)
      IF (K .EQ. 46) GO TO 60
      K=K+1
      L=L+M256
      MD=MD+M256
      GO TO 58
   60 CONTINUE
      DO 45 J=34,46
      PS11(J)=PS11(J)/256.0
      PS22(J)=PS22(J)/256.0
      CS12(J)=CS12(J)/256.0
   45 QS12(J)=QS12(J)/256.0
      DO 114 I=1,NP
  114 CROS(I)=SQRT(CS12(I)**2 + QS12(I)**2)
      DO 264 I=1,NP
      AMP12(I)=CS12(I)+CS12(I) + QS12(I)*QS12(I)
  265 PHS(I) = + ATAN(QS12(I)/CS12(I))
      DO 266 I=1,NP
      COH12(I)=AMP12(I)/(PS11(I)*PS22(I))
  266 DEGPS(I)=180.0*PHS(I)/(2.0*PI)
      DO 28 I=1,NP
      PNOM1(I)=FREQ(I)*PS11(I)
      PNOM2(I)=FREQ(I)*PS22(I)
      CRSNM(I) =FREQ(I)*CROS(I)
      CSNOM(I)=FREQ(I)*CS12(I)
   28 QSNOM(I)=FREQ(I)*QS12(I)
C-------------------------------------------------
C     OUTPUT STATEMENTS.
C-------------------------------------------------
```

```fortran
      GO TO (75,75,75,77),KCOUNT
75    WRITE(6,85)
85    FORMAT(30X,'U  AND  W  VELOCITY COMPONENTS'//)
      GO TO 95
76    WRITE(6,86)
86    FORMAT(30X,'TEMPERATURE  AND  R  VELOCITY COMPONENT')
      GO TO 95
77    WRITE(6,87)
87    FORMAT(30X,'U  AND  V  VELOCITY COMPONENTS'//)
95    CONTINUE
      WRITE(6,106)
106   FORMAT(1X,9X,'FREQUENCY',2X,'POWER SPECTR 1',2X,'POWER SPECTR 2',6
     1X,'COSPECTRUM',4X,'QUADSPECTRUM',2X,'CROSS-SPECTRUM',6X,'COHERENCY
     2',5X,'PHASE ANG (DEG)'/)
      DO 107 I=1,NP
107   WRITE(6,108)FREQ(I),PS11(I),PS22(I),CS12(I),QS12(I),CRLS(I),COHI2(
     3I),DEGPS(I)
108   FORMAT(1X,8F16.5)
      WRITE(6,203)
203   FORMAT(//15X,'LOG OF FREQ',2X,'FREQ MULT SPEC 1',2X,'FREQ MULT SPE
     4C 2',2X,'FREQ MULT COSPEC',2X,'FREQ MULT QUADSPEC',2X,'FREQ MULT C
     6ROSS SPEC'/)
      DO 204 I=1,NP
204   WRITE(6,205)FLOG(I),PNOM1(I),PNOM2(I),CSNOM(I),QSNOM(I),CRSNM(I)
205   FORMAT(1X,6X,6F18.5)
      IF (KOUNT .EQ. NTS) GO TO 2006
      KOUNT=KOUNT+1
      DO 110 I=1,NHF
      SP1(I)=0.0
      SP2(I)=0.0
      CSP(I)=0.0
110   QSP(I)=0.0
```

124

```
GO TO 4000
3000 CONTINUE
STOP
END
```

```fortran
      SUBROUTINE FFT (X)
C
C     FAST FOURIER TRANSFORM OF A COMPLEX SEQUENCE.
C
      IMPLICIT REAL*4(A-H,P-Z)
      COMPLEX*8 E,X,Z
      DIMENSION C(2049),X(8192),Z(2048)
C
C     N  = TOTAL NO. OF DATA
C     NS = STAGE NO .
C     NJ = TOTAL NO. OF ADDITION ( AND SUBTRACTION ) STEPS IN EACH STAGE
C     NJ = TOTAL NO. OF ADDITIONS ( OR SUBT. ) IN ONE ADDITION STEP
C     IA = STARTING NO. OF EACH ADDITION STEP
C     NT = ENDING NO. OF EACH ADDITION STEP
C     J  = ADDITION STEP NO. IN EACH STAGE
C     I  . KA = SUBSCRIPT OF NEW X IN EACH STAGE
C
      N=8192
      NN=N/2
      NM=NN/2
      KK=NN+1
      MM=NM+1
      CALL COSINE (N,NN,NM,C)
      NS=1
      AJ=NN
      NU=1
    1 RI=N/2
      IA=1
      NT=NM
      DO 71 L=1,NN
      KA=L+NN
   71 Z(L)=X(L,)
```

```
C------------------------------------------C
      MA=MM
      NB=1
      KA=KK
      DO 2 J=1,NJ
      NA=NA-NU
      NB=NB+NU
      IF (J-NI) 41,42,43
   41 E=CMPLX(C(NA),-C(NB))
      GO TO 42
   43 E=CMPLX(-C(NA),-C(NB))
   42 DO 9 I=IA,NT
      IF (J.LE.NI) GO TO 81
      IC=I-NM
      IB=I+NN
      KA=KA+1
      K=KA+NU
      X(KA)=Z(IC)+X(IB)
      X(K )=(Z(IC)-X(IB))*E
      GO TO 9
   81 IC=MM-I
      IB=IC+NN
      KA=KA-1
      K=KA-NU
      IF (J.EQ.NI) GO TO 82
      X(KA)=(X(IC)-X(IB))*E
      GO TO 83
   82 X(KA)=X(IC)-X(IB)
   83 X(K )=X(IC)+X(IB)
    9 CONTINUE
      IA=IA+NU
      NT=NT+NU
```

```
      IF (J.NE.NI) GO TO 22
      NA=MM+NU
      NB=1-NU
      KA=NN
      GO TO 2
   22 KA=K
    2 CONTINUE
C-------------------------------------C
      IF (NJ.EQ.2) GO TO 11
      NU=2**NS
      NS=NS+1
      NJ=NI
      GO TO 1
   11 DO 21 I=1,NN
      IB=I+NN
      E=X(I)+X(IB)
      X(IB)=X(I)-X(IB)
   21 X(I)=E
      RETURN
      END
```

```
      SUBROUTINE COSINE (R,NL,NL,C)
C-----------------------------------------------------------------C
C     RECURSIVE CALCULATION OF COSINES NEEDED FOR THE EXPONENTIALS.  C
C-----------------------------------------------------------------C
      DIMENSION C(2049)
      TN=NN
      ANG=3.1415927/TN
      INT8=N/8
      CS=COS (ANG)
      SN=SIN (ANG)
      C(1)=1.
      II=NM+1
      C(II)=0.
      DO 39 J=1,INT8
      JI=J+1
      JJ=NM+2-J
      C(JI)=C(J)*CS-C(JJ)*SN
      JM=NM+1-J
   39 C(JM)=C(J)*SN+C(JJ)*CS
      RETURN
      END
```